Picosecond Time-Resolved Photothermalization Process in Liquid Phase(Dissertation_全文)

AUTHOR(S):

Okazaki, Toshiya

Picosecond Time-Resolved Photothermalization Process in Liquid Phase

Toshiya Okazaki

Department of Chemistry

Graduate School of Science

Kyoto University

1999.

Contents

1. General introduction

The mechanism of the thermalization process after photoexcitation of molecules is very interesting to many researchers in various fields. For example, plastic products around you contain UV absorbers to prevent the polymer degradation. Plastics used in outdoor applications are exposed to the harmful solar radiation between 290 and 400 nm. Imperfections in a polymer chain or certain functional groups, such as a carbonyl group, can absorb the UV radiation. The absorbed energy can lead to photochemical reactions, and polymer degradation can occur rather than dissipation of the energy in a nonharmful form. To protect polymers from photochemical degradation, UV absorbers which absorb most of the harmful radiation are added. The excited states of this UV absorbers must rapidly relax in a manner that converts the excitation energy into heat that is not chemically damaging to the polymer. In other words, a very rapid thermalization is required for UV absorbers. These UV absorbers have been used not only as sunscreens for plastics, but also in other applications (polishes, skin protection etc.).

On the contrary, thermalization is a redundant process for using the light emitting from excited states. Light-emitting diode (LED) is expected for the light source in the next generation. One of the biggest problem for application of LED is to protect the thermalization process by the recombination of the exciton produced by electric excitation. Hence it is very important to study the thermalization mechanism as well as the light emitting process in this field.

In the present thesis, thermalization process of molecules in liquid phase is studied. It plays a important role in many chemical reactions. [1-3] In this case, thermalization process is usually discussed by associating the vibrational relaxation process. A pioneering work on the vibrational relaxation in liquid phase has been carried out by Kaiser and coworkers since 1970's. [4-16] For example, the vibrational relaxation process of anthracene was studied by photoexciting CH-stretching mode using infrared picosecond pulses (fwhm=5 ps). [13] After photoexcitation of the CH-stretching mode, the resulting change of the vibrational population was monitored by a second visible pulse, which promoted the molecule to the S_1 state. The fluorescence intensity originating from the S_1 state was recorded as a function of delay time between the pump and probe pulses. By using the several visible pulses with different wavelength, the different vibrational level can be probed. The rise times

of all the fluorescence signals were very fast, within the temporal resolution of their system (2 ps). This fact tells us that the intramolecular relaxation in the S_0 state of anthracene completes within 2 ps. The fluorescence decays due to the energy transfer to the surroundings (vibrational cooling). The slow vibrational cooling time was found to be 25 ps in the S_0 state of anthracene / CCl_4.

The other many researchers also studied on the non-radiative energy relaxation mechanism after photoexcitation. [1-3] Sukowski et al. investigated the vibrational relaxation process of azulene in various solvents. [17] The vibrationally hot S_0 state of azulene is generated by the very rapid internal conversion after photoexcitation to the S_1 state (1 ps). The subsequent vibrational relaxation process was monitored by the temperature dependent change of the $S_0 \rightarrow S_1$ absorption edge. The observed transient absorption signals rise within the experimental error (~2 ps). The decay of the signals reflect the vibrational cooling rates. They found that the vibrational cooling times in the S_0 state of azulene is 10~40 ps (e.g. 13 ps in methanol and 40 ps in CCl_4). A theoretical model was introduced to explain the experimental results. In this model, it is assumed that the excess energy of azulene is first transferred to a single solvent molecule by isolated binary collisions. The dissipation of the energy to the solvent molecules in the outer sphere is expressed by the macroscopic heat conduction. The calculated signals reproduced the experimentally observed signals very well.

To summarize the various results, it is revealed that the excess energy in large organic molecules is first redistributed within the intramolecular vibrational manifold. The time constant of this intramolecular energy transfer is believed to be very rapid, within a few ps. The subsequent energy flow process to solvent is considered to occur in 10~100 ps time scale.

However, recently, several researchers reported the results against the above energy relaxation scheme, i.e., the 'slow' intramolecular vibrational relaxation [18-26] and the 'fast' vibrational cooling have been observed in several systems. [15, 27-34] These experimental results were reviewed by Okamoto. [35]

Kruglik et al. reported that the 'slow' intramolecular vibrational relaxation of Ni^{2+} octaethylporphyrin (Ni(OEP)). [23] After the photoexcitation of Ni(OEP) by the UV pulse, the vibrationally excited S_0 state of OEP is produced. The rise profiles of the anti-Raman scattering signals from the vibrationally 'hot' OEP depend on the vibrational modes. This means that the

intramolecular vibrational relaxation of OEP does not complete within ~7 ps.

Iwata and Hamaguchi found the 'fast' vibrational cooling process in the S_1 state of *trans*-stilbene with the time resolved Raman spectroscopy. [29] The vibrational cooling process was monitored by monitoring the peak position change of the C=C stretching band which is very sensitive to the temperature of the surrounding solvents. The observed cooling kinetics were analyzed with a vibrational relaxation model. From the results, the excess energy is transferred to the solvent molecules in the first solvent shell within a few ps.

Mostly, the vibrational relaxation process has been studied in a view of the solute molecule: one photoexcite the solute molecule, then monitor the subsequent vibrational population change of the solute itself. Another approach is to study the vibrational relaxation process from the solvent side. In particular, if the thermalization process such as vibrational cooling is studied by detecting the temperature rise of the surrounding solvent, one can get the deep insight of the thermalization mechanism. In the present thesis, thermalization process is investigated from a solvent side by the new two methods: the transient grating acoustic method and the molecular heater-molecular thermometer integrated system.

One of the most powerful tool to detect the temperature is the photothermal spectroscopy which observe the deposited heat directly through the refractive index change of the surrounding solvent. However, the time resolution of the photothermal spectroscopies is rather slow for the thermalization process. [36, 37] The photoacoustic method cannot detect the heat releasing kinetics faster than the nanosecond order. The time resolution of the thermal lens method is recognized to be longer than 100 ns. The curve fitting method of the transient grating (TG) signal can provide ~50 ps time resolution.

Recently, new photothermal spectroscopies with a ps time resolution was developed mainly by Terazima and coworkers. [30-34] The thermalization process in the aqueous solutions were investigated by the temperature lens (Temp.L) method. [30] The Temp.L signal is originated from the refractive index change due to the temperature variation without the density change. The time resolution of this method is determined by a pulse width because the temperature change appears immediately after the heating. By analyzing the rise part of the Temp.L signal, the thermalization of Ni^{2+} in water completes within the response time (a few ps).

The vibrational cooling process was studied by the acoustic peak delay of the TG signal for *trans*-azobenzene in acetonitrile and ethanol. [33] In the both solvents, the thermalization rates are determined by the rate of the internal conversion from the S_1 state. This fact indicates that the rate of the temperature rise after the excited state relaxation could be very fast (a few ps). To reveal the thermalization mechanism in detailed, these new photothermal spectroscopies must be powerful tools.

In chapter 2, the thermalization process of the intramolecular proton transfer system is studied by the TG acoustic method. 2-(2'-Hydroxy-5'-methylphenyl)benzotriazole (HMPB) and 2-hydroxybenzophenone (HBP) were used as solute molecules. From the time profiles of the population grating (PG) signals, two distinct kinetics were observed for HMPB and HBP. For HMPB, the faster (600 fs) kinetics is attributed to the back proton transfer reaction in the ground state, and the faster process of HBP (400 fs) is attributed to the vibrational cooling in the S_1 state. The slower one (~30 ps) of both compounds is assigned to the vibrational cooling in the S_0 state. In ethanol (hydrogen bonding solvent), the PG signal originated from the T_1 state of HBP is apparent. However, the thermal energy from the T_1 state is negligibly small and the triplet quantum yield was found to be less than 0.05. The photoexcited HBP relaxes to the ground state by the internal conversion dominantly even in ethanol. The thermalization rates of these molecules were measured from a point of view of the translational energy of solvents by the acoustic peak delay method of the TG signal. The results show that in the early step of the thermalization, there is a very fast cooling process (less than a few ps) which is due to the energy transfer from the photoexcited solute to (several) effectively coupled solvent molecule(s), and then the heated solvent molecule becomes cool by the thermal diffusion to the bulk solvents. The thermalization processes depend on both of the solute and solvent properties. The time development of the temperature calculated based on this thermalization model explains the experimental observations.

A general spectroscopy does not have any spatial resolution. If we can monitor the transient temperature at the several distance from the photoexcited molecule, the heat flow mechanism as well as the thermalization process should be more clarified. In chapter 3, the vibrational cooling process of photoexcited azulene was studied by using a combined molecular thermometer (coumarin 151 (C151)). The transient absorption at the red edge of the absorption band of C151 detected after the photoexcitation of azulene is attributed to the hot band absorption of C151. The heating process of the first solvent shell around the photoexcited azulene was detected by using an azulene-coumarin

integrated system connected with a methylene group (Az-CH_2-C151) in several solvents. The time profiles of the transient absorption signals were analyzed by a thermalization model, which includes the intermolecular energy transfer from azulene to the solvents and the the thermal diffusion among the solvent. The cooling times of azulene in these solvents were found to be less than 2~5 ps. These results indicate that there is a very fast cooling process after the relaxation of the electronically excited state compared with that reported before. The transient absorption spectrum and its time profile of a compound with a longer chain (Az-$(CH_2)_3$-C151) are very similar to those of Az-CH_2-C151 except the much weaker intensity. These facts indicate that the molecular structure of Az-$(CH_2)_3$-C151 is flexible and the distance between the thermometer (C151) and the heater (azulene) is short.

2. Thermalization Process of Intramolecular Proton Transfer Systems Studied by the Transient Grating Method

2-1. Introduction

In this chapter, thermalization process of the intramolecular proton transfer system is studied by the transient grating (TG) method. To investigate the thermalization process in detail, it is preferable to use a molecule of which excited state lifetime is sufficiently short (less than a few ps). One of such molecules is an intramolecular proton transfer system (Fig. 2-1). For example, it is well known that the S_1 states of 2-(2'-hydroxy-5'-methylphenyl)benzotriazole (HMPB (commercial name: TINUVIN P or TIN)) and 2-hydroxybenzophenone (HBP) relax to the ground state very rapidly. [20, 38-55] The photophysical process as well as the thermalization processes after the internal conversion of HMPB and HBP are studied by the population grating (PG) and the acoustic peak delay method of the TG signal in several organic solvents.

HMPB performs an ultrafast proton transfer cycle and deposits the excess energy rapidly. [20, 38-46] Elsaesser and coworkers have studied the energy relaxation dynamics after photoexcitation of HMPB extensively. [20, 41-46] After the photoexcitation of the enol form of HMPB, the excited state proton transfer occurs in a 100 fs time scale, followed by the radiationless deactivation of the keto-type S_1 (S_1(keto)) state with a time constant of 150 fs. The keto-type ground (S_0(keto)) state molecule undergoes a proton back transfer to the enol geometry (S_0(enol)) with a time constant of 600 fs. In this chapter, we studied the thermalization process of HMPB after photoexcitation by the TG acoustic method and compared the results with the transient temperatures calculated by a simple thermalization model.

HBP has been used as a calorimetric reference and a polymer photostabilizer, because of the rapid dissipation of the energy of the photoexcitaion. [38, 47] It is believed that an efficient channel for the energy dissipation is provided by the intramolecular proton transfer in the photoexcited state. There are many researchers on the photoexcited state dynamics of HBP by time-resolved spectroscopies. [48-55] Hou et al. measured the ground state recovery time and the triplet state absorption using picosecond laser pulses. [49] In hexane, only a short-lived ground state repopulation signal was observed with a lifetime of ~35 ps, and no triplet-triplet (T-T) transient absorption signal

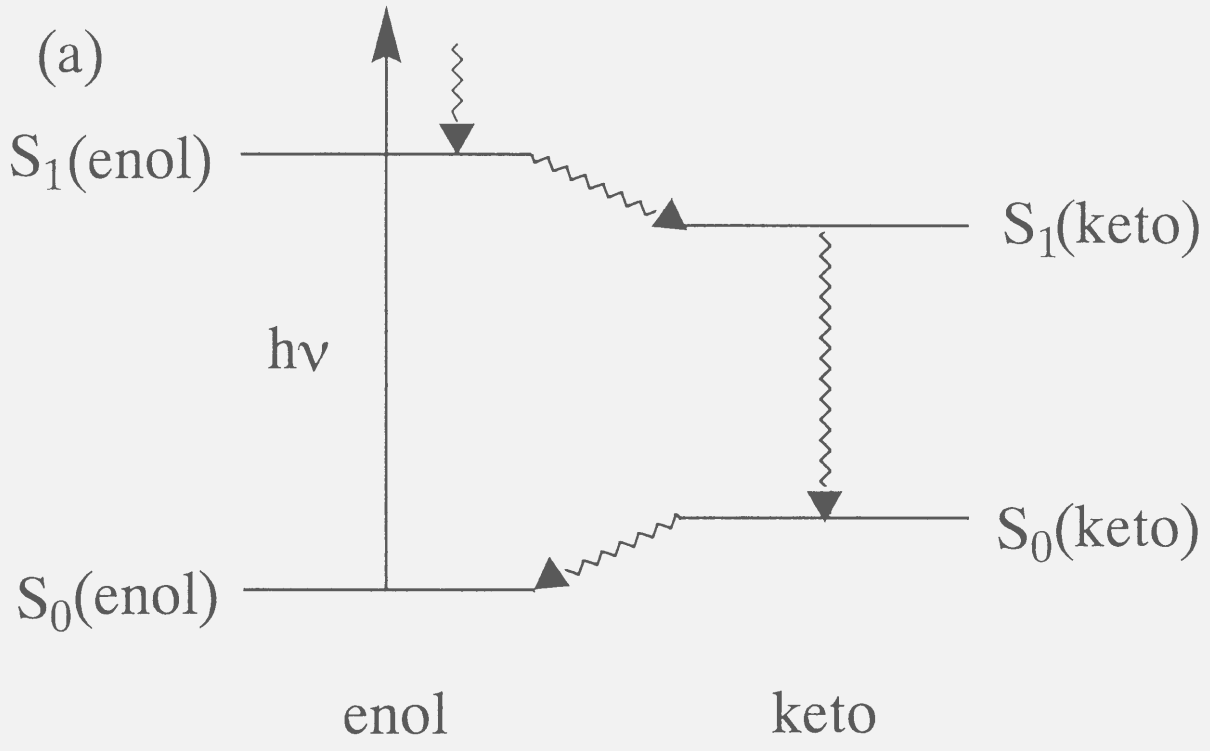

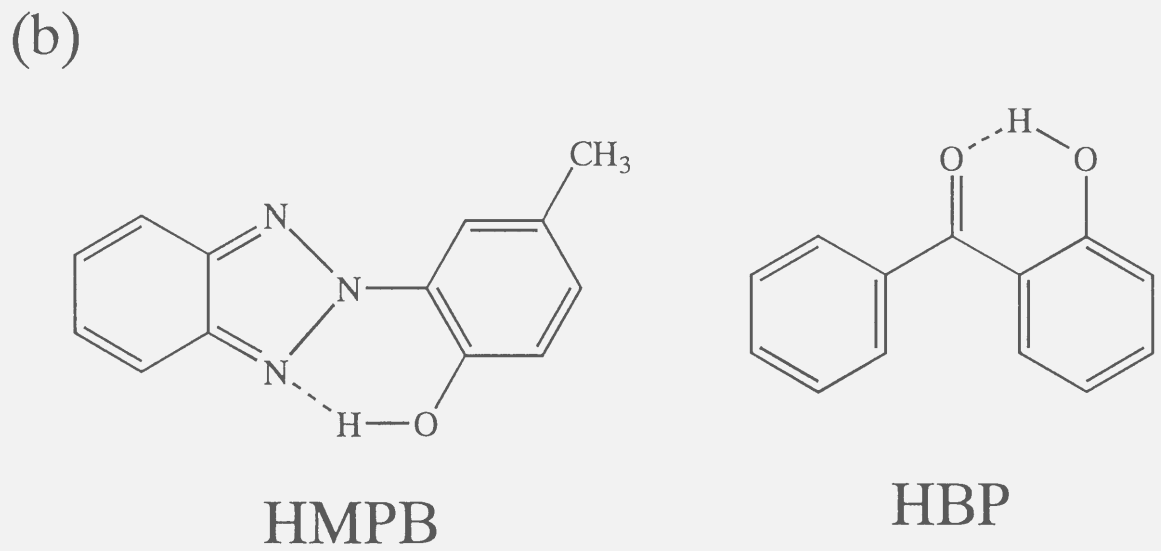

Fig. 2-1. (a) Schematic energy diagram of the proton transfer system. In the excited state, the enol form undergoes the proton transfer reaction to produce the keto from. After internal conversion, the back proton transfer occurs from the S_0 state keto form to the enol form. (b) Molecular structures of the enol forms of HBP and HMPB.

was detected. They attributed this lifetime to that of the S_1 state or a transient intramolecularly hydrogen bonded species in the S_0 state. In ethanol, short-lived (~30 ps) and long-lived ground state recovery signals and a T-T transient absorption signal were observed. The rise and decay times of the T-T absorption signal were <15 ps and 1.5 ns, respectively. They concluded that both of the intramolecularly (shorter component) and the intermolecularly (longer component) hydrogen bonded HBP exist in ethanol, while only the intramolecular hydrogen bonded HBP exists in hexane. The photoexcited intermolecularly hydrogen bonded HBP crosses over to the lowest triplet (T_1) state with a lifetime of <15 ps and backs to the S_0 state with 1.5 ns. Merritt et al. reported <10 ps as the lifetime of the S_1 state of the intramolecularly hydrogen bonded species in methylene chloride by the transient absorption measurement. [50] The lifetimes of the S_1 state were reported to be 6 ps in hexane and 30 ps in ethanol by Choi et al. with the two photon fluorescence excitation method, [51] and <4 ps in hexane and 7 ps in ethanol by Eisenthal with the fluorescence measurement. [53] Recently the quantum yields of the triplet formation were reported as 0.05-0.15 in several solvents. [55] In this chapter, we first characterize the photophysical processes of HBP by the population and acoustic grating method. The energies of the excited states are calculated by the *ab initio* molecular orbital calculations. Using these information, the thermalization process of HBP in solution is discussed.

2-2. Experimental

The experimental setup for the picosecond time-resolved transient grating experiment is similar to that reported previously (Fig. 2-2). [31--34, 56] A pulse of a Nd:YAG laser (Coherent Antares 76-S)-pumped dye laser (Coherent Satori 774; λ=640 nm), which was amplified with a dye amplifier system (Continuum PTA60 and Continuum RGA60) was split into three with two beam splitters. The frequency of the two beams was doubled to 320 nm by BBO crystals and used as excitation beams. The laser power was ~1μJ / pulse. These beams were focused by lenses (f=25 cm) and crossed at about 30° inside the quartz sample cell in order to generate an optical interference pattern. The other pulse was used as a probe beam. The probe beam passed through an optical delay line was focused by a lens (f= 20 cm) and brought into the sample cell by an angle that satisfied the Bragg condition. The diffracted TG signal was separated from other beams with a pin hole and a glass filter (Toshiba R-60) and detected by a photomultiplier. The detected TG signal was averaged with a

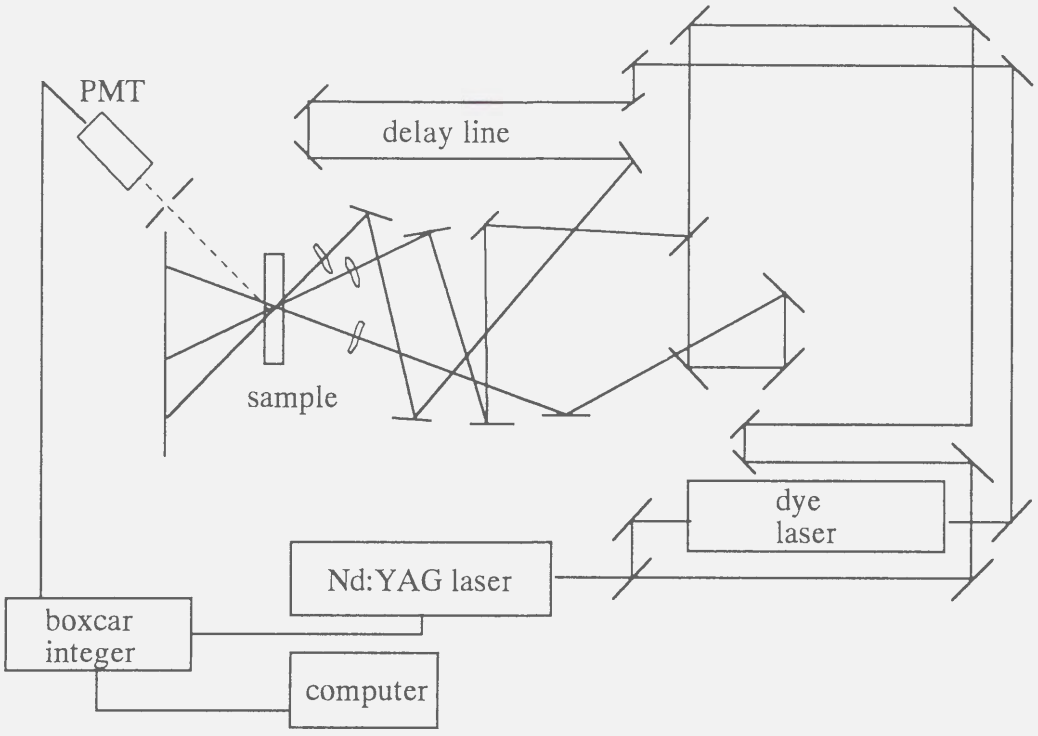

Fig. 2-2. The experimental set up for the TG measurements.

boxcar-integrator (EG&G Model 4400 Series) and with a personal computer. The pulse shape was monitored by the optical Kerr signal of a neat carbon tetrachloride solution. The pulse width was ~230 fs.

HMPB (Wako Pure Chemical Industries) and HBP (Tokyo Kasei) were used without further purification. The solvents, hexane, cyclohexane, acetonitrile, ethanol and carbon tetrachloride (Nacalai Tesque, Spectral grade) were used as received. The concentrations of the samples were ~20 mM.

The *ab initio* calculations of the energy diagram of HBP were performed with the GAMESS program package. [57] The heat capacities of the solute and solvent molecules were calculated by the MOPAC program package.

2-3. Analysis

According to the coupled wave theory, the intensity of the TG signal (I_{TG}) under the weak diffraction condition is given by [58]

$$I_{TG} = \alpha(\Delta n)^2 + \beta(\Delta k)^2 \qquad (2\text{-}1)$$

where α and β are constants which are determined by experimental conditions and Δn , Δk denote the peak-null differences in the refractive index and the absorbance, respectively. One of the dominant contributions to the TG signal comes from the change of the refractive index caused by the variation of the density. We consider that the thermal energy, Q, is deposited into the medium by the intermolecular energy transfer from the excited state i, that is,

$$\frac{dQ}{dt} = \sum_i \frac{Q_i}{\tau_i} \exp(-t/\tau_i)(1 + \cos qx) \qquad (2\text{-}2)$$

where τ_i is the thermalization rate from the excited state i to the medium, q is the magnitude of the wavevector of the grating, x denotes the coordinate along q and Q_i is the thermal energy from the

excited state i in unit volume. After the heat is released to the matrix, the medium expands periodically, which yields the variation of the refractive index (Δn_ρ). The signal due to this refractive index change oscillates sinusoidally (frequency ω=vq (v ; speed of sound in the solution)) because of the acoustic propagation (acoustic TG signal). The time profile of this TG signal is given by [31-34, 56, 59]

$$\begin{aligned}\Delta n_\rho(t) \simeq \left(\frac{\partial n}{\partial \rho}\right)_T \{ & \sum_i AQ_i \left(b^2+\omega^2\right)^{-1} \times \\ & \left[\frac{b}{\omega}\sin(\omega t)\exp(-d_a t) - \cos(\omega t)\exp(-d_a t) + \exp(-b t)\right] \\ & -AQ_i\left(\gamma_i{}^2+\omega^2\right)^{-1} \times \\ & \left[\frac{\gamma_i}{\omega}\sin(\omega t)\exp(-d_a t) - \cos(\omega t)\exp(-d_a t) + \exp(-\gamma_i t)\right] \ \}\end{aligned} \tag{2-3}$$

where d_a is the acoustic attenuation rate constant, $b=\lambda_w q^2/\rho_0 C_p$ (λ_w the thermal conductivity, C_p the specific heat at a constant pressure and ρ_0 the density of the solvent), $A=2q^2\alpha/\kappa\rho_0 C_p$ (α coefficient of thermal expansion and κ compressibility) and $\gamma_i=\tau_i^{-1}$. Because of the convolution effect, the acoustic oscillation is gradually distorted as the heat dissipation rate becomes slow. Even though the thermalization rate can be obtained from a fitting of the whole time profile of the acoustic signal, the time resolution of the curve fitting method is not high enough (~60 ps at best) [33] for studying the fast thermalization processes. On the other hand, by monitoring the peak delay time (Δt_{pd}) from the impulsive thermalization case, the time delay of the thermalization can be detected with a high time resolution. [33, 60] Previously, Terazima et al. have shown that Δt_{pd} is proportional to the thermalization time within $\tau_i \leq$ 40 ps. [33] When the acoustic damping is neglected, Δt_{pd} is almost the same as τ_i. If there are several thermalization processes, Δt_{pd} depends on the branching ratio of their releasing energies and their thermalization times. These calculations were performed based on the assumption that the excited state lifetime is short enough so that the heat releasing is determined only

by the thermalization rate.

In this chapter, we extend the calculation to show a relationship between Δt_{pd} and the thermalization rate when the lifetime of the excited state cannot be neglected. We consider the following scheme for the energy flow (Fig. 2-3). After photoexcitation to the zero vibrational level of the S_1 state, the S_1 state decays by the internal conversion with a lifetime of τ_{S1} to create vibrationally hot S_0 state (S_0*). The S_0* state returns to the equilibrium ground state by the vibrational cooling with a lifetime of τ_{temp}. In this case, dQ/dt is given by

$$\frac{dQ}{dt} = \frac{Q}{t_{S_1} - t_{temp}} \left\{ \exp(-t/t_{S_1}) - \exp(-t/t_{temp}) \right\} (1 + \cos qx) \quad . \qquad (2\text{-}4)$$

Figure 2-4 plots Δt_{pd} against τ_{temp} for τ_{S1}=7 ps under our experimental conditions (ω=1.02x10^{-10} s^{-1} and d_a=6x10^{-16} Np/cm s). This calculation indicates that the peak delay is almost equal to $\tau_{S1}+\tau_{temp}$ up to $\tau_{temp}\approx$30 ps under this condition. Hence τ_{temp} can be evaluated from Δt_{pd} using a relation of $\tau_{temp}=\Delta t_{pd}-\tau_{S1}$.

To determine Δt_{pd} experimentally, the acoustic frequency (ω) has to be measured. We measured ω from the time difference between the first (t_1) and the second (t_2) acoustic peaks. The temporal separation between the first and the second peaks ($\Delta t=t_2-t_1$) usually gives ω (= 2π / Δt) as long as τ_i varies in a fast rate region ($\tau_i \leq$ 60 ps under this experimental condition). Next, Δt_{pd} was calculated by a relation of $\Delta t_{pd}=t_1-\Delta t/2$.

Besides the acoustic TG signal, a PG signal was observed, which is due to the refractive index change (Δn_p) and/or the absorbance change (Δk_p) induced by the photoexcited species or photochemical products. These contributions can be expressed by

$$\Delta n_p = \sum_i R_i C_i(t) \qquad (2\text{-}5)$$

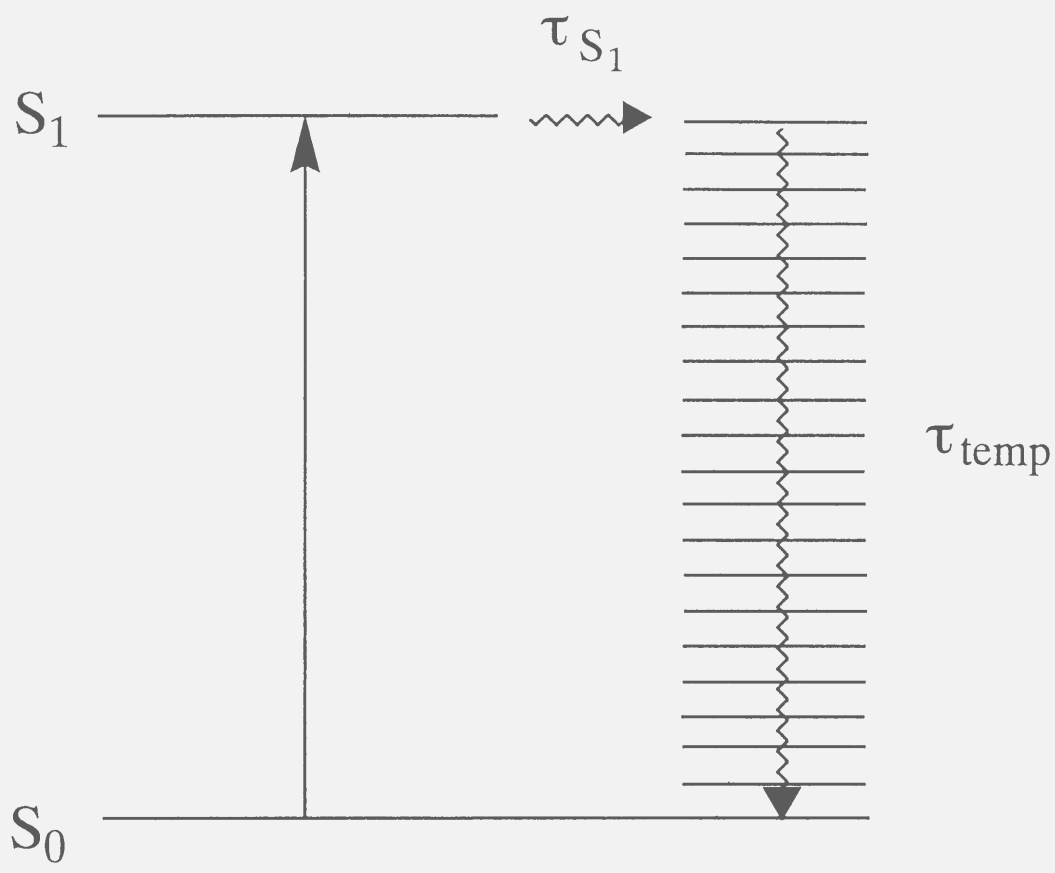

Fig. 2-3. Schematic thermalization process after photoexcitation to the bottom of the S_1 state. τ_{S1}: lifetime of the S_1 state and τ_{temp}: thermalization time.

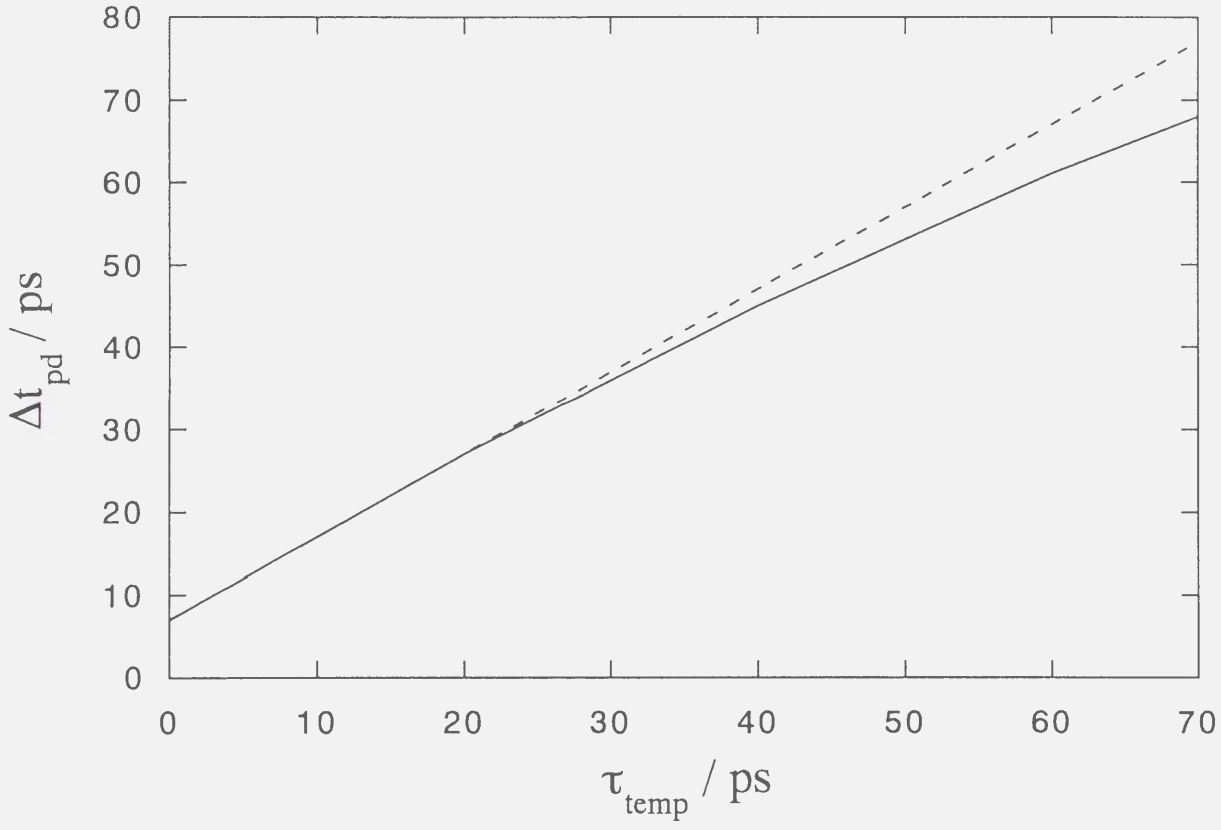

Fig. 2-4. Calculated acoustic peak delay (Δt_{pd}) against the thermalization time (τ_{temp}) under the condition of τ_{S1}=7 ps. The dashed line denotes the relationship of $\Delta t_{pd}=\tau_{temp}+\tau_{S1}$.

$$\Delta k_p = \sum_i R_i' C_i(t) \qquad (2\text{-}6)$$

where R_i and R'_i are constants which are determined by the refractive index and the absorbance changes by the presence of the transient species and $C_i(t)$ the concentration of the transient species.

2-4. Results

2-4-1. HMPB in cyclohexane

Figure 2-5 shows the TG signal of HMPB / cyclohexane in a picosecond time scale. We found that there is no contribution of non-resonant optical Kerr grating signal in the TG signal because any signal could not be detected from a neat cyclohexane solution. Obviously, this signal should be assigned to the PG signal of the photoexcited states of HMPB. This signal can be fitted well by

$$I_{TG} = \alpha \left\{ \delta n_f \exp(-t/\tau_f) + \delta n_s \exp(-t/\tau_s) + \Delta n_\rho \right\}^2 \qquad (2\text{-}7)$$

convoluted with the instrumental response function. The first and second terms represent the PG signal and the third term is the acoustic signal. The TG signal once reaches the baseline and rises again due to the acoustic signal. This fact indicates that the signs of (δn_f, δn_s) and Δn_ρ are opposite. Since Δn_ρ is generally negative, δn_f and δn_s are positive, which means that the creation of a new intermediate state (not the depletion of the S_0 state) contributes to the PG signal dominantly. The lifetimes of the PG signal are determined to be τ_f=600(±100) fs and τ_s≈30 ps. The lifetime τ_f=600 fs agrees well with the lifetime of S_0(keto) of HMPB that was measured by Elsaesser and coworkers. [43, 44] The very rapid rise of the PG signal (almost instantaneous within our laser pulse width) is also consistent with the ultrafast creation of the S_0(keto) state with a lifetime of 150 fs. [43, 44] Therefore we attribute the origin of the fast PG component to the S_0(keto) of HMPB. The origin of the ~30 ps component will be discussed later.

The acoustic TG signal of HMPB in cyclohexane is shown in Fig. 2-6(a). The solid curve represents the calculated signal with ω=1.14x10^{10} s^{-1}. To find the acoustic peak times (t_1 and t_2), the

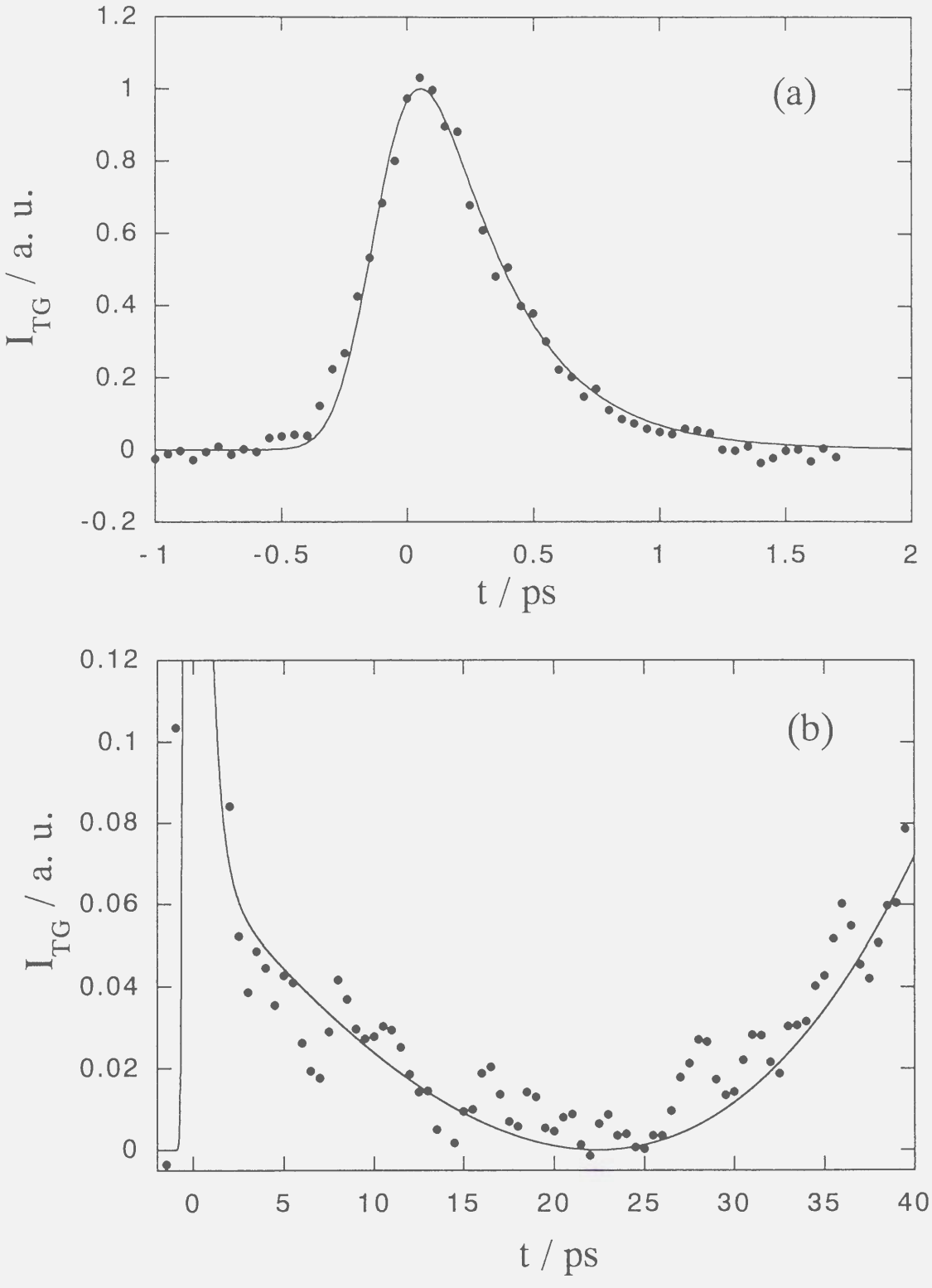

Fig. 2-5. The time profiles of the PG signals of HMPB / cyclohexane (circles). The solid lines denote the calculated curves (see text).

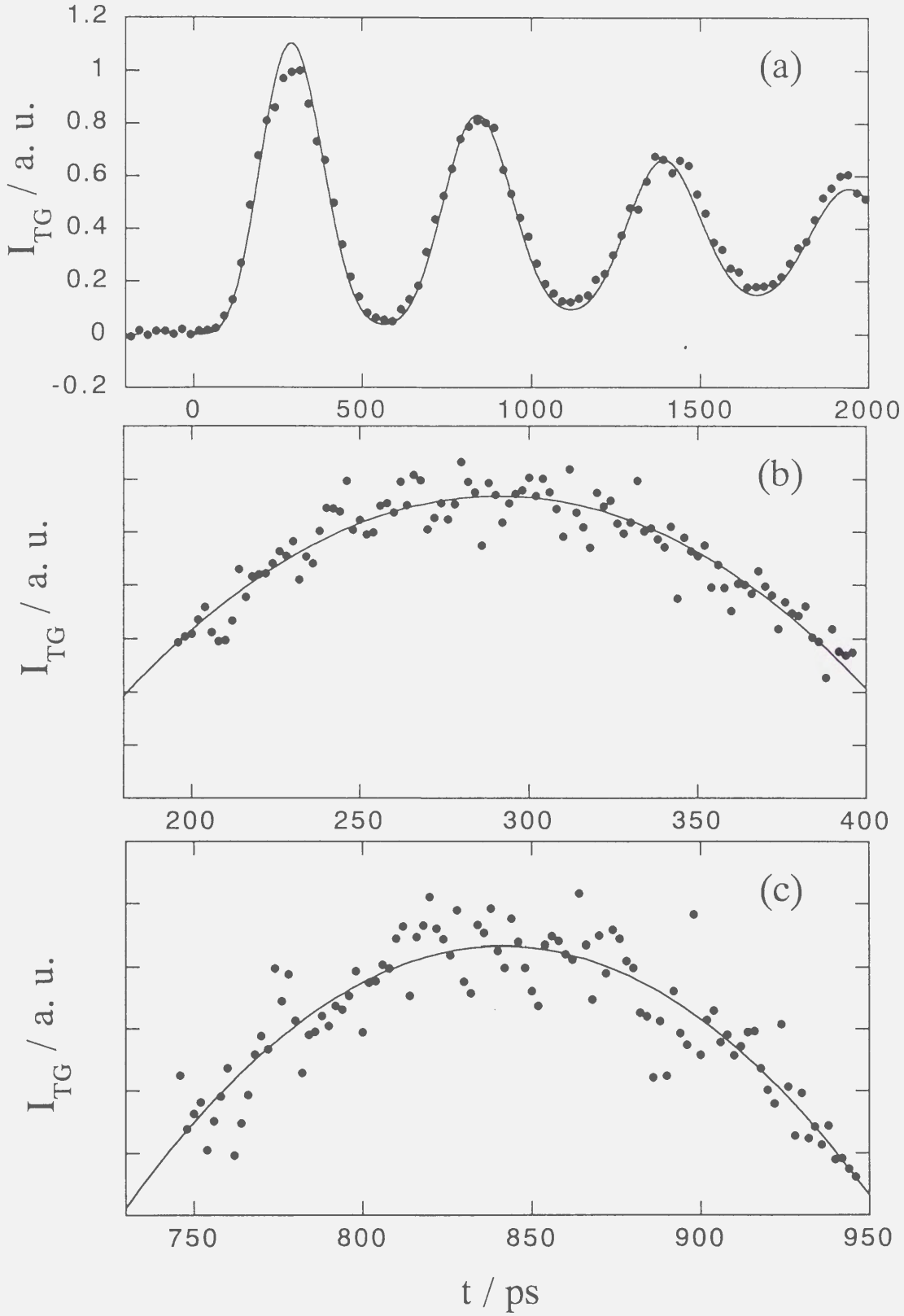

Fig. 2-6. The acoustic TG signals of HMPB / cyclohexane (circles). The solid lines denote the fitting curve as discussed in the text.

signals around the first two peaks were recorded in detail (Fig. 2-6(b), (c)). The time profiles around the peaks were fitted by the functions $A(t-t_i)^2+B$, where A and B are constants and i=1 and 2 for the first and second peaks, respectively. The acoustic frequency (ω) was calculated from these t_1 and t_2 as described in the previous section. The peak delay (Δt_{pd}) after the correction for the acoustic attenuation rate is found to be 20 ps.

2-4-2. HBP in non-hydrogen bonding solvents

Figure 2-7 shows the observed TG signal of HBP / hexane in a fast time scale. The time evolution of this signal can be fitted by eq. (2-7) convoluted with the instrumental response function of our experimental system. The lifetimes of faster and slower components are found to be τ_f=400 (±50) fs and τ_s=30(±5) ps, respectively.

The decay of this signal is not due to the rotational diffusion of the chemical species because of the following reason. If these lifetimes are the rotational diffusion times, they should be sensitive to the viscosity (η) of the solvents. However, the PG signals in cyclohexane was very similar to that in hexane, although the viscosity of hexane and cyclohexane are quite different (η=0.300 and 0.894 mPa s for hexane and cyclohexane, respectively at 25 °C). [61] Indeed, the lifetimes in both solvents are almost the same (Table 2-1). Therefore we conclude that the time evolutions of these signals reflect the population dynamics of the photoexcited HBP.

The TG acoustic signal in hexane is shown in Fig. 2-7(c). It is found that Δt_{pd} after correction for the acoustic attenuation rate is 10 ps using the same method as HMPB. In cyclohexane, Δt_{pd} is 13 ps. We also measured the TG signals in acetonitrile. The time profile of the TG signal is very similar to that in hexane and cyclohexane solutions. The obtained time constants are summarized in Table 2-1.

2-4-3. HBP in hydrogen bonding solvent

We also investigated the TG signals of HBP in ethanol (Fig. 2-8). In hydrogen bonding solvents such as ethanol, it was reported that intramolecularly as well as intermolecularly hydrogen bonded HBP exist. [49] After photoexcitation, the S_1 state of the intermolecularly hydrogen bonded HBP crosses over to the T_1 state, [49] and the T-T absorption spectrum was observed in the UV-visible

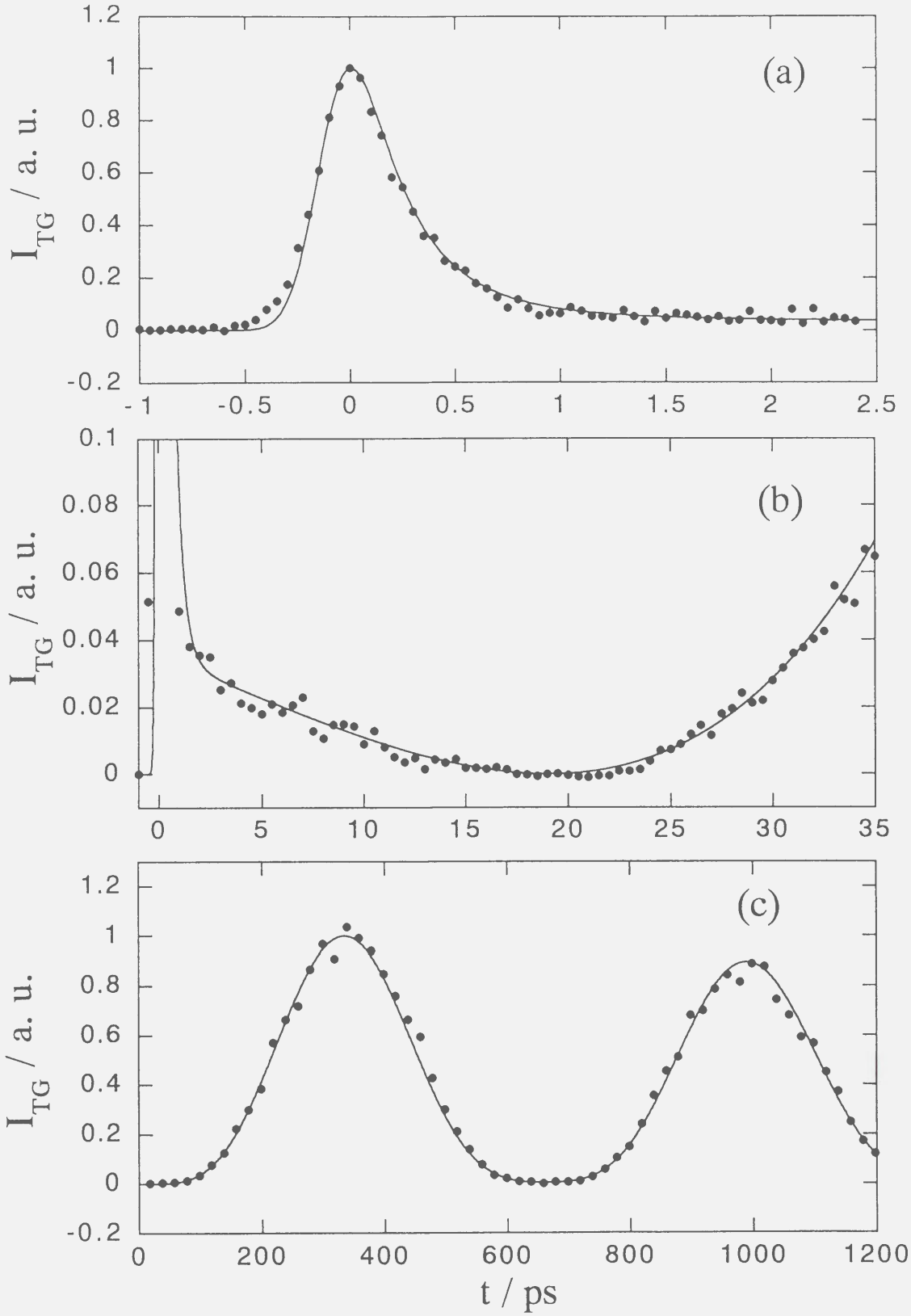

Fig. 2-7. The time profiles of the PG signals ((a), (b)) and the acoustic TG signals (c) of HBP in hexane (circles). The solid line denotes the calculated signal.

Table 2-1. The lifetimes (τ_f, τ_s) of the population grating signals, the peak delay (Δt_{pd}) of the acoustic TG signals and the calculated thermal energies (Q_f, Q_s) by assuming that the thermalization process takes place with lifetimes of 1 ps and 30 ps respectively.

	τ_f / fs	τ_s / ps	Δt_{pd} / ps [a]	Q_f / cm^{-1} [b]	Q_s / cm^{-1} [b]
HMPB / CH [c]	600±100	~30	20	10000	21000
HBP / hexane	400±50	30±5	10	20000	12000
HBP / CH	400±100	30±5	13	17000	14000
HBP / AcCN [d]	400±100	30±5	12	17000	14000
HBP / EtOH [e]	400±100	~30	7	24000	7200

a) The error of Δt_{pd} is ±3 ps. b) The errors of the Q_f and Q_s are ±2000 cm^{-1}. c) cyclohexane. d) acetonitrile. e) ethanol.

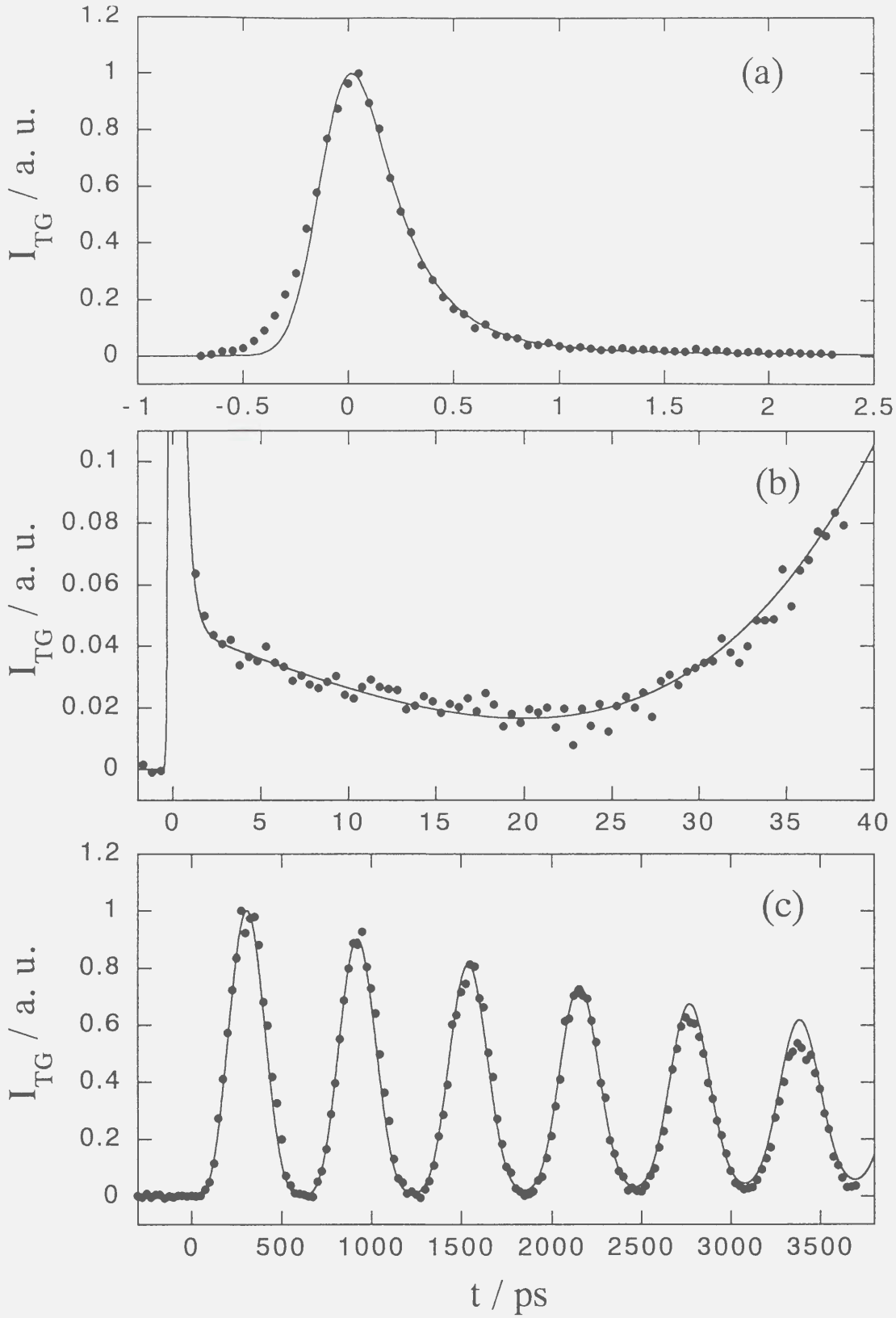

Fig. 2-8. The time profiles of the PG signals ((a), (b)) and the acoustic TG signals (c) of HBP in ethanol (circles). The solid line denotes the calculated curve with τ_f=400 fs and τ_s=30 ps.

region (c.a. 400~700 nm).[55] Indeed, the observed PG signal in ethanol does not reach the base line, which reflects the existence of an absorptive component due to the T_1 state of HBP. The time evolution of the signals can be fitted by the equation;

$$I_{TG} = \alpha \left\{ \delta n_f \exp(-t/\tau_f) + \delta n_s \exp(-t/\tau_s) + \delta n_T \exp(-t/\tau_T) + \Delta n_p \right\}^2 + \beta \left\{ \delta k_T \exp(-t/\tau_T) \right\}^2 \quad (2\text{-}8)$$

where τ_f, τ_s and τ_T are the lifetimes of the fastest, intermediate and slowest components, respectively. The first bracket in eq. (2-8) is due to the refractive index change and the second one due to the absorbance change. Since the slowest component is considered to be due to the T_1 state, τ_T was fixed to the reported lifetime of the T_1 state (1.5 ns) in the curve fitting by eq. (2-8).[49] The time profile of the PG signal can be reproduced with τ_f=400 (±100) fs and τ_s= 3~50 ps.

Figure 2-8(c) shows the acoustic signals of HBP in ethanol. If the quantum yield of the triplet formation is large, we have to take into account the heat releasing process by the deactivation from the T_1 state. In this case, the acoustic signal should increase gradually with a lifetime of 1.5 ns, which should be clearly distinct from the other fast heat releasing processes.[32, 56] From the curve fitting of the long time scale signal (Fig. 2-8(c)), we found that the triplet quantum efficiency is less than 0.05, which is consistent with the previously reported values (<0.03 in ethanol[48] and 0.07 in methanol[55]). Therefore we can neglect the intersystem crossing from the S_1 state to the T_1 state under our experimental condition and the dominate relaxation mechanism in ethanol should be similar to that in the non-hydrogen bonding solvents. The peak delay time is determined to be 7 ps.

2-5. Discussion

2-5-1. The excited state and thermalization dynamics of HMPB.

After photoexcitation to the S_1 state, HMPB shows a simple and fast photo cycle; HMPB returns to the ground state within 1 ps (see Introduction) and the temperature of HMPB is elevated.[43, 44] If all of the excess energy is dissipated to the solvents with one time constant, the thermalization time (τ_i) should be the same value as Δt_{pd}, which is 20 ps (Table 2-1). In this case,

photoexcited HMPB should relax to the thermally equilibrium state with a lifetime of 20 ps. However, it is clearly found that a 30 ps dynamics exists in the PG signals. Therefore it is unlikely that all of the excess energy is dissipated to the solvents with one time constant, that is, there are more than two thermalization kinetics. According to the above consideration, vibrational cooling time observed in the PG signal (30 ps) should be one of the thermalization times. However we do not have any information on the rate constant of the faster process. (Since the acoustic grating does not show slower heat releasing process, there is no slower process than 30 ps.) By assuming that the lifetime of the faster process (τ_f) is 1 ps (less than a few ps), the amount of the thermal energies associated with these two processes (Q_f and Q_s for τ_f=1 ps and τ_s=30 ps, respectively) can be calculated from the observed Δt_{pd} ($\Delta t_{pd} \simeq (Q_f/(Q_f+Q_s))\ \tau_f + (Q_s/(Q_f+Q_s))\ \tau_s$). (Since the uncertainty of Δt_{pd} is ±3 ps, the difference between τ_f=1 ps and τ_f < 3 ps is not important for further discussion.) In cyclohexane, an energy of about 10000 cm^{-1} is dissipated by the fast process and the remaining energy (21000 cm^{-1}) by the slower (30 ps) process.

2-5-2. The excited state and thermalization dynamics of HBP.

The kinetics of HBP is controversial and less clear. Hou et al. reported that only intramolecularly hydrogen bonded HBP exists in a non-hydrogen bonding solution and the S_1 state of this species relaxes to the S_0 state directly (no triplet formation). [49] The lifetime of the S_1 state was reported as <4 ps, [53] 6 ps [51] or <10 ps. [50] On the contrary, Bhasikuttan et al. observed the T-T absorption spectrum in a range of 400 - 700 nm in non-hydrogen bonding solvents (benzene, hexane and acetonitrile) as well as in hydrogen bonding solvents (methanol and DMSO). [55] In our TG experiments, however, the transient absorption component due to the T_1 state was observed only in ethanol, and not in the non-hydrogen bonding solvents (hexane, cyclohexane and acetonitrile). Therefore the intramolecularly hydrogen bonded species should be exclusively dominant in the non-hydrogen bonding solvents and the most part of the photoexcited HBP should relax directly to the ground state by the internal conversion from the S_1 state to the S_0 state. Furthermore, even in ethanol, we found that the amount of the thermal energy released by a species with a lifetime of 1.5 ns is very small. The quantum yield of the triplet formation in ethanol was determined to be smaller than 0.05. We conclude that the thermalization studied here reflects the relaxation dynamics of the

intramolecularly hydrogen bonded species.

The temporal profile of the PG signal shows two population dynamics besides the triplet state dynamics in ethanol (Table 2-1). Considering that the fluorescence and the transient absorption signals of HBP have been observed, we think that the lifetime of 400 fs of the PG signal is too short for the S_1 (keto) or S_0 (keto) lifetime. Hence this component should be attributed to the vibrational relaxation or the structural change in the S_1 state. Among the reported different lifetimes of the S_1 state, we believe that the lifetime measured by the fluorescence detection (<4ps in a non-hydrogen bonding solvent and 7 ps in ethanol) is most reliable because of the following reasons. First, since Δt_{pd} is found to be 7 ps in ethanol and it is highly unlikely that the lifetime of the S_1 state is slower than the heat releasing process, the lifetimes of 30 ps and >10 ps reported for the S_1 state in ethanol in other papers are probably not correct. [50, 51] Second, the fluorescence detection is the most direct measurement for the S_1 lifetime. Hot band absorption or some minor intermediate could contribute to the transient absorption signal.

Since the observed longer lifetime of 30 ps in the PG signals agrees well with the repopulation time of the S_0 (enol) state, this component should be attributed to the vibrational relaxation process in the S_0 state manifold. In ethanol, the lifetime of the intermediate component of the PG signal is less accurate because of the additional contribution from the T_1 state. However, since Hou et al. observed the repopulation kinetics with a lifetime of ~30 ps in the S_0 state of the intramolecularly hydrogen bonded HBP in ethanol, we attribute this intermediate component to the vibrational relaxation process in the S_0 state.

The photophysical process of HBP can be summarized as follows; the photoexcited S_1(enol) state relaxes to the S_1(keto) state with a lifetime of 400 fs. The S_1(keto) state decays to the S_0(keto) state with a lifetime of <4 ps in non-hydrogen bonding solvents and 7 ps in ethanol. The vibrational cooling process in the S_0 manifold takes place with a lifetime of ~30 ps. The thermalization process should reflect these excited state dynamics.

If we assume that the entire thermalization occurs with a lifetime of 30 ps, Δt_{pd} should be 30 ps, which is quite longer than the observed values, 7-13 ps in Table 2-1. Therefore similar to the case of HMPB, there are more than two thermalization kinetics. Let us assume that the thermalization process can be described by two (very fast and 30 ps) thermalization kinetics. The relative thermal energy from whole thermalization processes can be calculated from the observed Δt_{pd} as Q_f=20000

cm^{-1} and Q_s=12000 cm^{-1} in hexane. The estimated Q_f and Q_s in the other solvents are summarized in Table 2-1.

An important question is the physical origin of the fast and the slow thermalization processes. A simple and intuitive idea is that these kinetics could be related with the electronic structures of HBP; that is, the transition between different electronic states or geometrical transformation could determine the kinetics. First, we examine if the energies of Q_f and Q_s correspond to the vibrational relaxation in the S_1 state (S_1(enol)→S_1(keto)) and the other process (S_1(keto)→S_0(enol)), respectively. For that purpose, we evaluated the energies of these states. The geometries of the keto and enol forms in the S_1 state were optimized at the CI-singles (CIS) level with the STO-3G basis set. Using these geometries, the energies of the S_1(keto) and S_1(enol) states (E(S_1(keto)) and E(S_1(enol)), respectively) were calculated at the CIS level with the 6-31G basis set. However, we found that the energy of the S_1(keto) state is about 2000 cm^{-1} higher than that of the S_1(enol) state. We think that this E(S_1(keto))>E(S_1(enol)) is due to an insufficient electron correlation in our calculation. Indeed, it is currently accepted that the calculated energy levels of the proton transfer system are sensitive to the electron correlation used in the calculation. [62, 63]

Since this molecule is too large to calculate the energies with a more sophisticated method by our computer system, we estimated the energy gap between the S_1(keto) and S_1(enol) of HBP from the calculated and experimental data of analogous molecules. A number of *ab initio* calculations showed that the energies of the keto forms are roughly ~3000 cm^{-1} lower than those of the enol forms in the S_1 state for some 2-hydroxybenzoyl compounds (2-hydroxyacetophenone, methyl salicylate etc.) that undergo the proton transfer in the excited states. [64] The fluorescence spectra from the S_1(keto) states showed that the energy gaps (E(S_1(enol))-E(S_1(keto))) of methyl salicylate and related compounds are 3000-4500 cm^{-1}. [65] Considering the similar structure of HBP to these molecules, we can think E(S_1(enol))-E(S_1(keto))<4500 cm^{-1} for HBP. On the other hand, the lowest limit of the E(S_1(enol)) can be determined from the energy of the T_1(enol) state of HBP, which was obtained from a sharp phosphorescence spectrum at 77 K (24100 cm^{-1}). [48, 55] This energy is consistent with the energy of the S_1(enol) state estimated from the broad absorption spectrum previously (25600 cm^{-1}). [31] From these E(S_1(enol)) and E(S_1(enol))-E(S_1(keto)), the energy released by the vibrational

relaxation in the S_1 state is estimated to be less than 11700 cm^{-1} (= 31300 cm^{-1} - 24100 cm^{-1} + 4500 cm^{-1}). This energy is too low to account for the thermal energy from the faster process (Q_f= 17000~24000 cm^{-1}).

Figure 2-9 shows the potential energy curve of the ground state HBP at various O_{phenol}-H distances. Each state was calculated by the second-order Moller-Plesset perturbation theory (MP2) with 6-31G basis sets. The geometry at O_{phenol}-H=1.7 Å was used for the optimized keto form geometry in the S_1 state at CIS/STO-3G level. It should be noted that the calculated potential curve has no barrier along the back proton transfer coordinate. Therefore the keto form is not metastable in the S_0 state of HBP and the 30 ps dynamics can be considered rather as the vibrational relaxation process in the S_0 state than as the back proton transfer in the S_0 state (S_0(keto)→S_0(enol)).

We believe that the two distinct kinetics do not represent the relaxation processes in different electronic states. The faster process includes the vibrational relaxation in the S_1 state as well as in the S_0 state (Fig. 2-10) based on the above grounds. The two different kinetics will be discussed in the next section.

2-5-3. A thermalization model

In the previous sections, we found that the thermalization process takes place with two kinetics; the fast and slow (30 ps) ones, and the energies from these processes are given by Q_f and Q_s. These kinetics are not related to the intramolecular transition between different electronic states. The slow heat releasing process may suggest long lived vibrational modes which release the energy with the 30 ps lifetime. However, in this section, we show that these heat releasing can be explained well based on a simple model without considering any intramolecular vibrational modes for an energy reservoir.

Just after the relaxation of the excited state, only the excited solute molecule possesses the excess energy (Fig. 2-11(a)). The energy is first transferred to several solvent molecules that are effectively coupled to the solute (the directly energy accepting (DEA) solvents) (Fig. 2-11(b)). The rate is expected to be proportional to the strength of the intermolecular interaction and the temperature difference between the solute and the solvent. Here, the intramolecular vibrational redistribution within the solute and the solvent molecules is assumed to be very fast compared to the intermolecular energy transfer rate. The thermal energy of the DEA solvent diffuses to the outer shell by the thermal diffusion (Fig. 2-11(c)). This thermalization model is similar to previously proposed models of

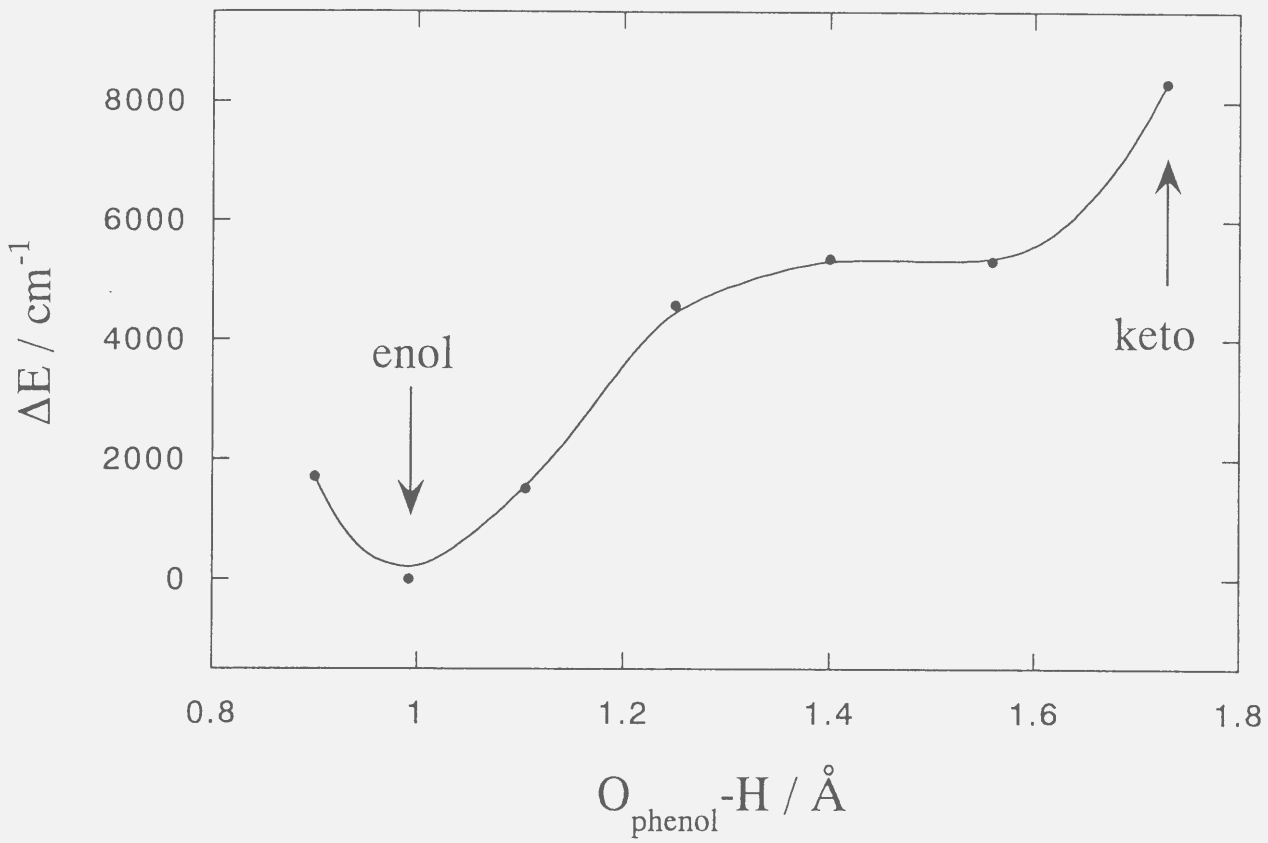

Fig. 2-9. The potential curve of the S_0 state of HBP calculated by the *ab initio* method along the back proton transfer coordinate. The optimized geometry of the keto form in the S_1 state and the enol form in the ground state are shown by 'keto' and 'enol'.

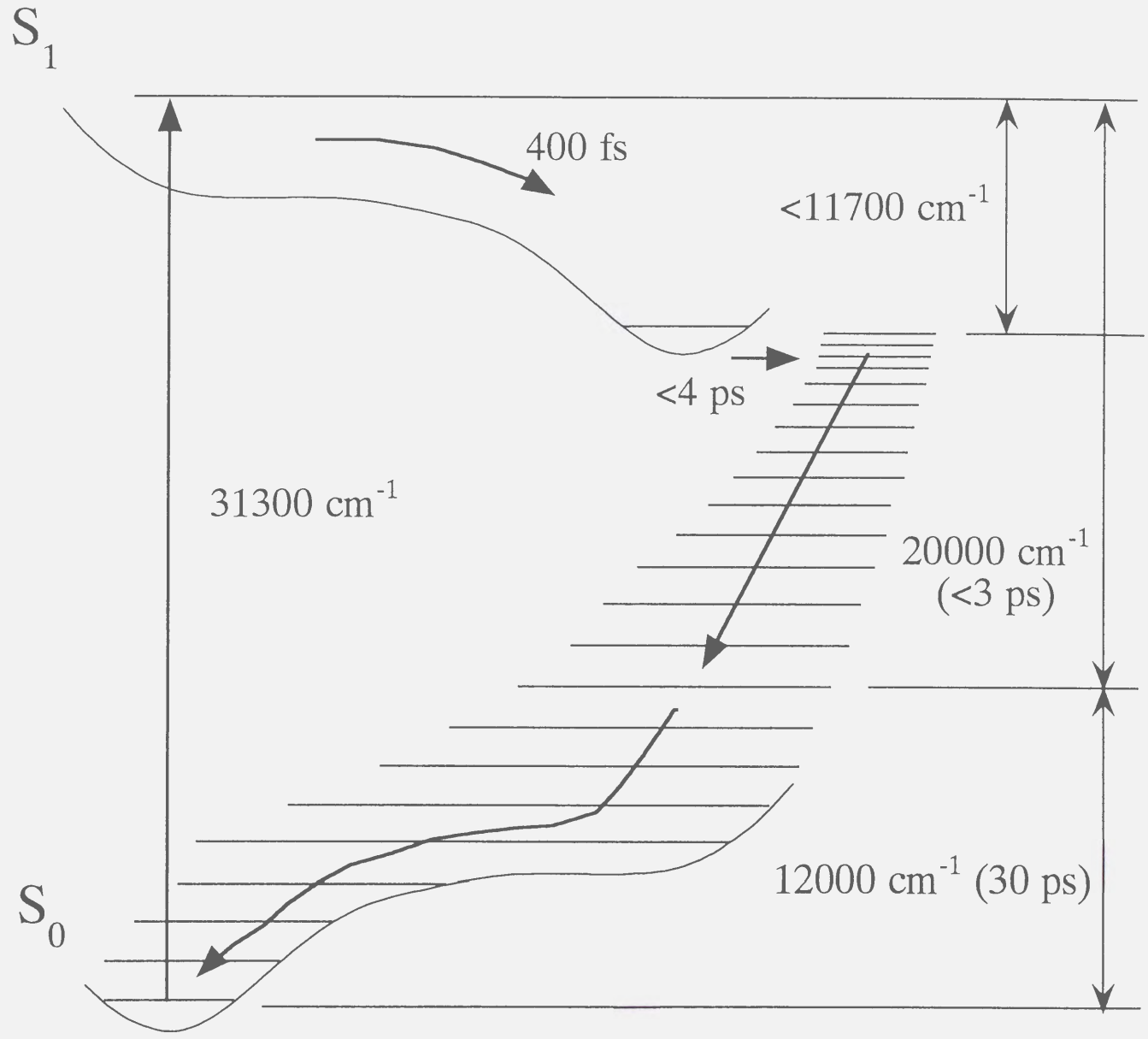

Fig. 2-10. Schematic energy diagram of HBP. After photoexcitation, the vibrational relaxation process in the S_1 state occurs with a lifetime of 400 fs, leading to the S_1(keto) state. By the internal conversion (<4 ps), the S_0* state is produced and then decays to the equilibrium ground state with 30 ps. The estimated released energies with <3 ps and 30 ps are 20000 cm^{-1} and 12000 cm^{-1}, respectively.

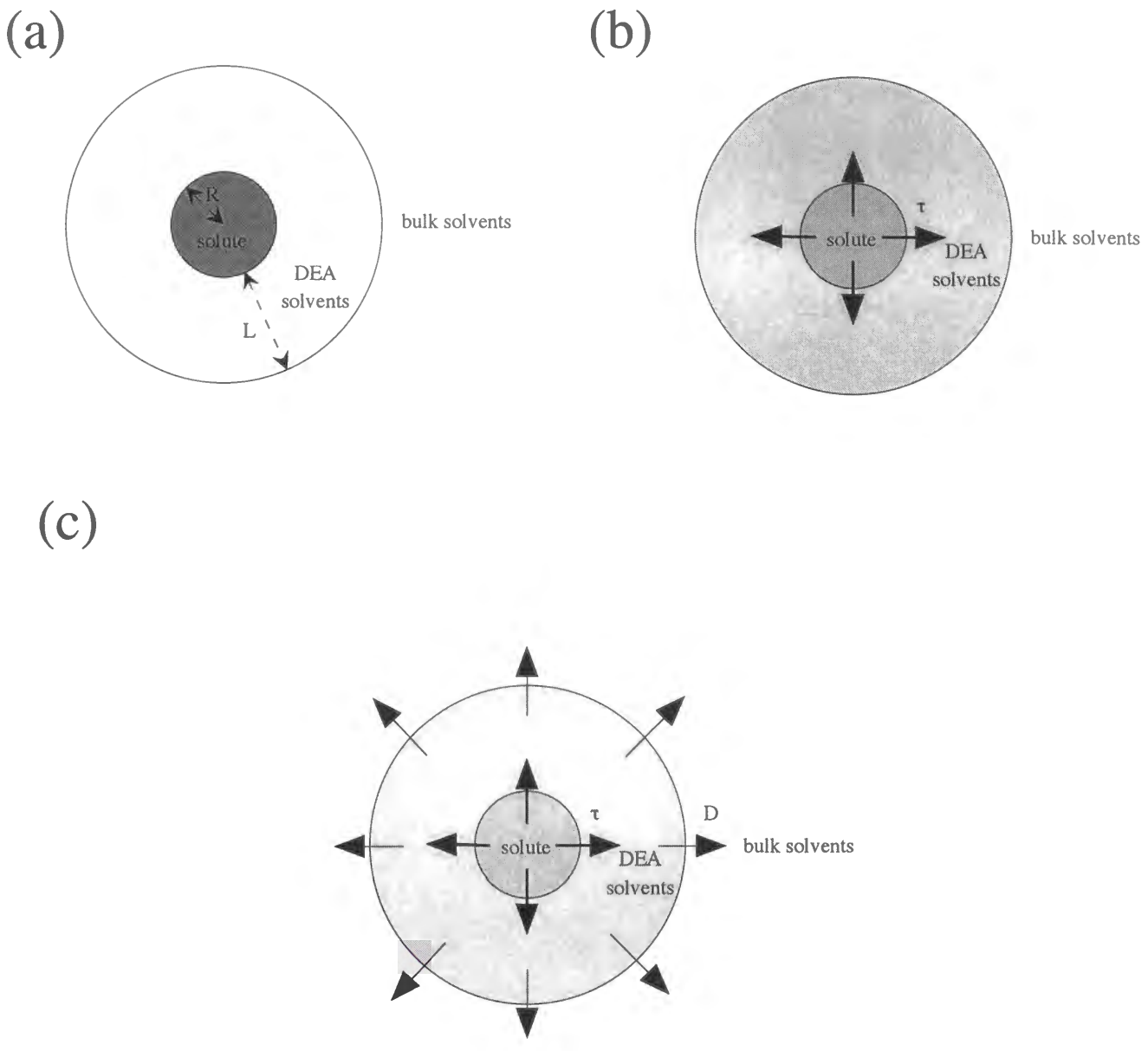

Fig. 2-11. Schematic illustration of the thermalization model. (a) After photoexcitation, hot solute molecule is produced. R is the radius of the solute molecule and L the thickness of the DEA solvent shell. (b) At first, the excess energy dissipates to the DEA solvents with a lifetime of τ. (c) Then the thermal energy diffuses to the bulk solvents with the thermal diffusivity D. The extent of the shading represents the temperature.

vibrational relaxation. [17, 29, 66] The temperatures of the solute and solvent molecules were calculated as follows based on this model.

The hot solute molecule dissipates the excess energy to the DEA solvent with a lifetime of τ that reflects the intermolecular interaction, and the rate is assumed to be proportional to the temperature difference between the solute (T_{solute}) and the DEA solvent ($T_{solvent}$) molecule(s). The energy of the solute increases with two steps; $S_1^* \rightarrow S_1$ (S_1^*: the Frank-Condon state from the ground state) and $S_1 \rightarrow S_0$ energy relaxation processes. For both HMPB and HBP, since the $S_1^* \rightarrow S_1$ process completes very fast (less than 1 ps), the time evolution of the solute energy from this process can be neglected. This contribution provides an initial condition of the solute temperature; $T_{solute}(t=0)=Q_0/C_{solute}$ ($Q_0=h\nu-E(S_1)$ and C_{solute}: heat capacity of the solute). T_{solute} is further elevated by the deactivation of the S_1 state with a lifetime of τ_{S1}. Therefore the time evolution of the solute energy can be given by

$$C_{solute}\frac{dT_{solute}(t)}{dt} = C_{solute}\left\{-\frac{T_{solute}(t)-T_{solvent}(t)}{\tau}\right\}+\frac{Q_1}{\tau_{S_1}}\exp(-t/\tau_{S_1}) \qquad (2\text{-}9)$$

where Q_1 is the released energy by the internal conversion from the S_1 state. The heat capacity is assumed to be independent of the temperature. This may not be correct, but for a qualitative discussion, this may be a reasonable approximation. This assumption will be examined later. The temperature change of the DEA solvent is given by

$$N_{solvent}C_{solvent}\frac{dT_{solvent}(t)}{dt} = C_{solute}\left\{\frac{T_{solute}(t)-T_{solvent}(t)}{\tau}\right\} \qquad (2\text{-}10)$$

where $N_{solvent}$ is the number of the DEA solvent(s) and $C_{solvent}$ is the heat capacity of the solvent.

The energy flow process from the DEA solvent(s) to the bulk solvent is assumed to be described by the classical heat conduction. Under the spherical symmetry condition, it is given by [67]

$$\frac{\partial (rT(t))}{\partial t} = D \frac{\partial^2 (rT(t))}{\partial r^2} \qquad (2\text{-}11)$$

where T is the temperature of the bulk solvent and D is the thermal diffusivity. In the above equations, τ and $N_{solvent}$ are only unknown quantities to calculate the transient temperature.

(a) HMPB

Since the lifetime of the S_1 state of HMPB is sufficiently short compared with the time resolution of the acoustic peak delay time, τ_{S1} can be assumed to be zero. Therefore the second term of eq. (2-9) can be neglected and the initial condition of T_{solute} is now $T_{solute}(t=0)=h\nu/C_{solute}$.

An initial guess of $N_{solvent}$ is given in the following way. Let us very simply assume that the temperature of the solute and the DEA solvent molecules become equal ($\Delta T_{solute}=\Delta T_{solvent}$) after Q_f is deposited to the DEA solvent. Physically, this assumption means that the fast process represents the energy equilibration between the solute and the DEA solvent, the slower process is due to the heat diffusion to the outer solvent shell and these processes are completely separated. $\Delta T_{solvent}$ and ΔT_{solute} are given by

$$\Delta T_{solvent} = \frac{Q_f}{N_{solvent} C_{solvent}} \qquad (2\text{-}12)$$

and

$$\Delta T_{solute} = \frac{Q_s}{C_{solute}} \quad . \qquad (2\text{-}13)$$

From these relations and $\Delta T_{solute} = \Delta T_{solvent}$, $N_{solvent}$ is given by

$$N_{solvent} = \frac{Q_f}{Q_s} \frac{C_{solute}}{C_{solvent}} \quad . \qquad (2\text{-}14)$$

The ratio $C_{solute}/C_{solvent}$ was calculated by the semi-empirical molecular orbital calculations (Table 2-2) and, using this value, $N_{solvent}$ was estimated to be 1.1 for HMPB / cyclohexane. The value of C_{solute} was obtained from the calculated $C_{solute}/C_{solvent}$ and literature values of the heat capacities of the solvents ($C_{solvent}$) [61] (Table 2-2). The time dependence of the temperatures of the solute and the solvents obtained by solving eq. (2-10) and (2-11) with this initial guess of $N_{solvent}$ is shown in Fig. 2-12(a). In this calculation, the thermalization rate from the solute to the DEA solvent (τ) is assumed to be 1 ps. The molecular size of the solvent (L) is estimated from the Lennard-Jones parameters. [68] The radius of HMPB (R=3.5 Å) is calculated from their van der Waals volume (V_w) which was estimated by the method of atom increment ($R=(3V_w/4\pi)^{1/3}$). [69] The other parameters used here are summarized in Table 2-2.

Interestingly, the time evolution of T_{solute} can be approximately fitted very well by a biexponential function;

$$T_{solute}(t) = A_f \exp(-t/\tau_f) + A_s \exp(-t/\tau_s) \quad . \qquad (2\text{-}15)$$

The lifetimes of the faster (τ_f) and slower (τ_s) components are 0.96 ps and 10.7 ps, respectively. As expected, the initial fast decrease of T_{solute} (Fig. 2-12(a)) is due to the heat releasing to the initially cold inner DEA solvent. $T_{solvent}$ rises because of this energy transport and decays by the diffusion of heat to the outer sphere. The ratio of the amplitudes of these components (A_s/A_f) is 0.80. Even using this initial guess of $N_{solvent}$, the qualitative features of this calculation explain the experimental observations.

In order to quantitatively adjust A_s/A_f to the experimentally observed Q_s/Q_f (=2.0), $N_{solvent}$ can be used as an adjustable parameter. The transient temperature can be fitted by a biexponential function with τ_f=1.4 ps, τ_s=20 ps, A_s/A_f=2.0 for $N_{solvent}$=0.4 (Fig. 2-12(b)). The physical meaning of $N_{solvent}$ less than 1 will be discussed in the next section.

(b) HBP

The time profile of the heat releasing from HBP will be more complex because the lifetime of

Table 2-2. The calculated ratio of the heat capacities of the solute and solvent molecules (C_{solute} / $C_{solvent}$), the literature values of the heat capacities of the solvents ($C_{solvent}$) taken from ref. 65, the estimated $N_{solvent}$ from eq. (2-14), the molecular diameters (L), the thermal diffusivity (D) and the calculated peak delay time (Δt_{pd}) by using the initial guess of $N_{solvent}$ for HBP.

	HMPB/CH[a)]	HBP/hexane	HBP/CH	HBP/AcCN[b)]	HBP/EtOH[c)]
$C_{solute}/C_{solvent}$	2.3	1.6	2.0	4.1	3.2
$C_{solvent}$ / J K^{-1} mol^{-1}	154.9	195.6	154.9	91.4	112.3
$N_{solvent}$	1.1	5.1	3.9	9.3	-
L / Å	6	6	6	4.5	4.5
D / $10^{-8}m^2s^{-1}$	8.49	8.30	8.49	10.9	8.79
Δt_{pd} / ps	-	4	5	3	-

a) cyclohexane. b) acetonitrile. c) ethanol.

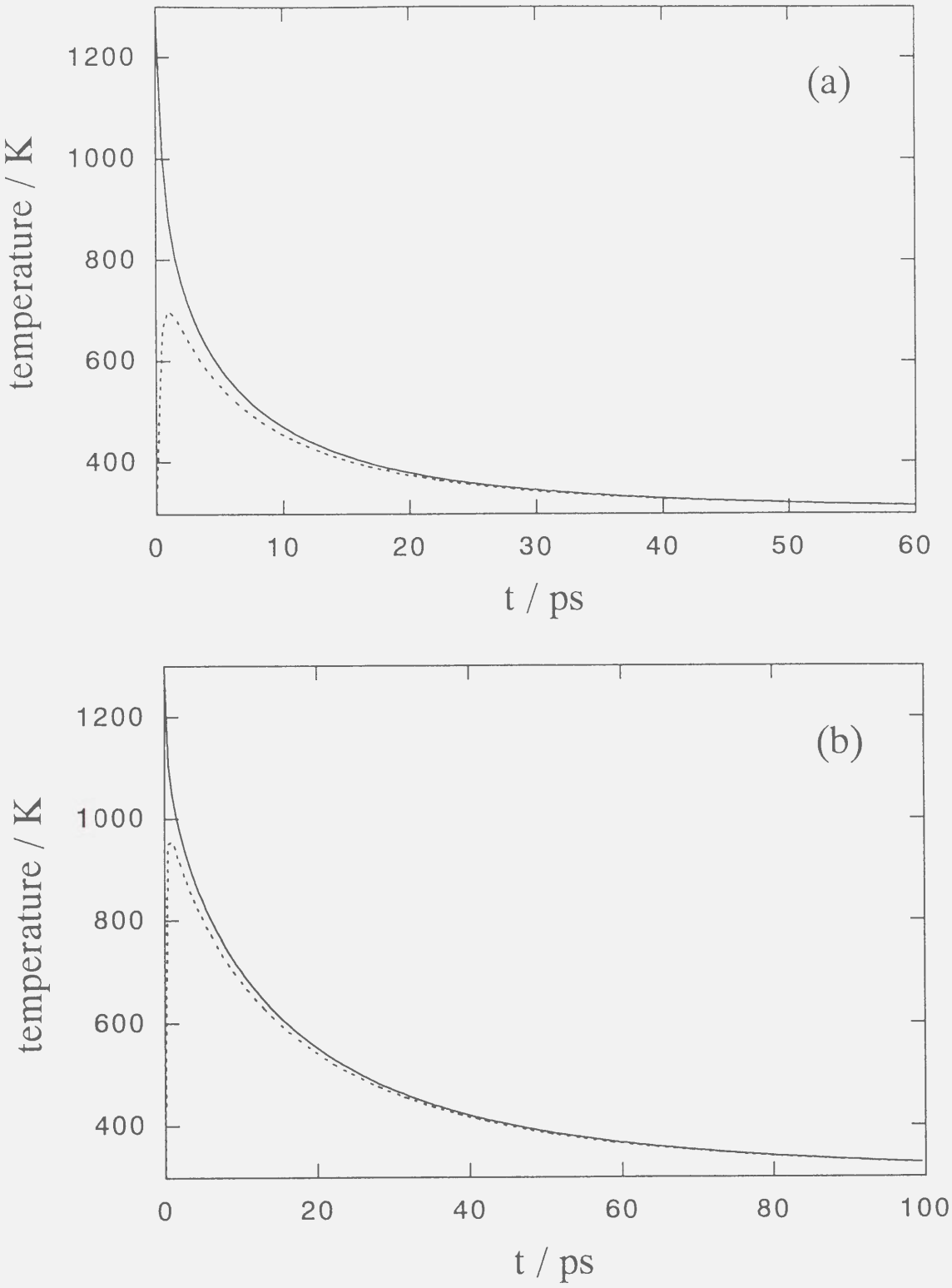

Fig. 2-12. The time evolution of the transient temperature of the photoexcited solute T_{solute} (solid line) and the DEA solvent $T_{solvent}$ (dashed line) of HMPB / cyclohexane. (a) $N_{solvent}$ is estimated from eq. (2-14) ($N_{solvent}$=1.1). (b) $N_{solvent}$ is 0.4.

the S_1 state cannot be neglected and the S_1 state acts as a time-delayed heat source. For evaluating the released energy, let us use a reasonable lifetime τ_{S1}=3 ps. (Using any lifetimes τ_{S1}<4 ps does not qualitatively change the main conclusion here.) Figure 2-13(a) shows a calculated T_{solute} and $T_{solvent}$ from eq. (2-9)-(2-11) with an initial guess of $N_{solvent}$=5.1 from eq. (2-14) for the hexane solution. The radius of HBP (R=3.5 Å) is calculated using the atom increment method [38] and the thermalization time (τ) is assumed to be 1 ps. The other parameters are listed in Table 2-2.

It should be noted that T_{solute} itself, in this case, does not represent the thermal energy released from the solute, because T_{solute} increases by the energy released from the internal conversion of the S_1 state. The thermalization rate and the experimentally observed acoustic peak delay are related to the time dependence of the energy coming out from the solute, Q(t), which is shown in Fig. 2-13(b). For a comparison with the experimental data, Δt_{pd} was calculated from the acoustic profile of the impulsive heating convoluted with dQ(t)/dt, numerically. By using the initial guess of $N_{solvent}$, Δt_{pd} is found to be 4 ps, which is shorter than the experimentally observed value. Using $N_{solvent}$ as a fitting parameter, we found that the experimental Δt_{pd} (=10 ps) was reproduced with $N_{solvent}\approx 0.5$ (Fig. 2-13(c)). dQ(t)/dt after 3 ps can be fitted by a biexponential function (eq. (2-15)) with lifetimes of 5.6 ps and 20 ps. In cyclohexane and acetonitrile, similar results were obtained. The obtained parameters are summarized in Table 2-3.

In ethanol, the lifetime of the S_1 state is very similar to Δt_{pd} (=7 ps) so that the observed Δt_{pd} can be reproduced with a large $N_{solvent}$ (>9). This result shows that the thermalization process should occur much more effectively in ethanol. The time profile of dQ(t)/dt in the slower time scale can be fitted well by a biexponential function with lifetimes of 6.6 ps and 11 ps.

By using this simple model, we can qualitatively explain the observed thermalization process. This model implies that the energy transfer from the solute to some solvent molecules is initially very fast, which is determined by the solute-solvent interaction. By this process, the temperature of the solute decreases, and that of the solvent increases. As the temperature difference becomes small, the energy transfer becomes inefficient. Subsequent energy flow from the solute to the solvent is determined by the thermal diffusion process to the outer solvents.

It is interesting to note that $N_{solvent}$ is much smaller than the number of the solvent molecules in the first solvation shell around the solute except for HBP / ethanol. This small number of $N_{solvent}$ could be due to the simplified thermalization model we used. However, we rather believe that

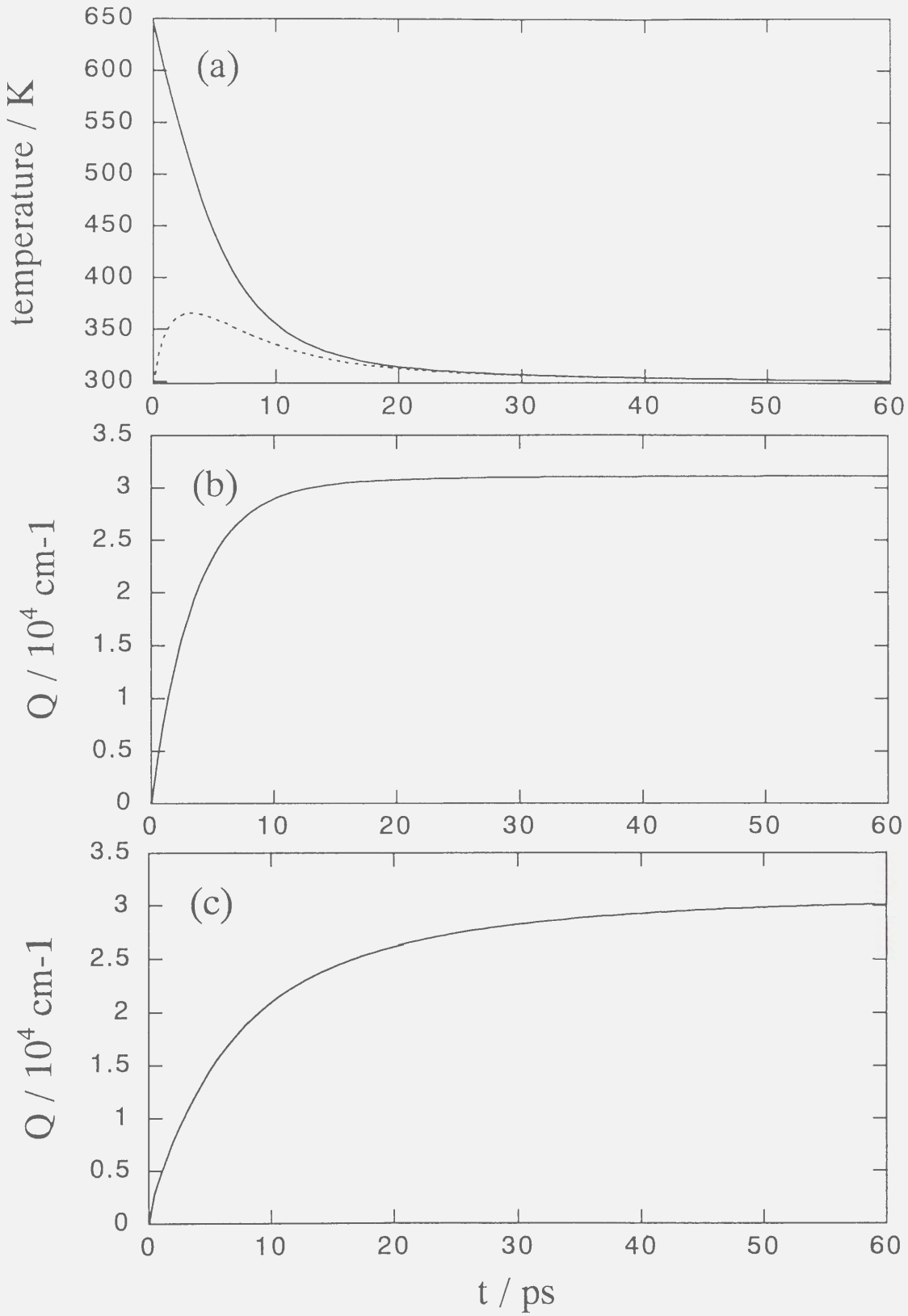

Fig. 2-13. The time evolution of (a) the transient temperature of the photoexcited solute T_{solute} (solid line) and $T_{solvent}$ (dashed line), (b) the released energy (Q(t)) of HBP / hexane ($N_{solvent}$=5.1) and (c) ($N_{solvent}$=0.5).

Table 2-3. $N_{solvent}$ is the calculated number of the DEA solvent to reproduce the experimentally observed Δt_{pd} of HBP. The time profile of Q(t) can be approximately fitted by the biexponential function (eq. (2-15)) with lifetimes of τ_f and τ_s.

	hexane	cyclohexane	acetonitrile
$N_{solvent}$	0.5	0.4	0.5
τ_f / ps	5.6	6.4	7.7
τ_s / ps	20	24	23

$N_{solvent}$ less than the number of the first solvent shell molecules is genuine because of the following consideration. If we assume that the energy of the solute flows into all the solvent molecules in the first solvent shell ($N_{solvent} \approx 14$), for example, in the HMPB case, the temperature of the solute drops quickly to $\Delta T_{solute} \approx 40$ K within 2 ps. After this significant temperature decrease, the temperature of only 40 K can drop with the 30 ps lifetime. Since most of the energy is released fast, the peak delay of the acoustic TG signal should be as fast as ~2 ps, which does not agree with the experimental observation. Hence as long as the energy of the solute is assumed to flow into all of the first solvent shell molecules, the observed Δt_{pd} cannot be explained regardless of the thermalization model. Probably, HMPB and HBP cannot interact strongly with all the solvent molecules that contact with the solute but can be efficiently coupled to only limited member of the contacted solvents.

For a quantitative discussion, we have to examine the heat capacities used in the calculation. Here we used the calculated C_{solute} and $C_{solvent}$ at room temperature under the equilibrium condition. At higher temperatures, C_{solute} and $C_{solvent}$ could be larger because much large number of vibrational states participate in the heat capacity. For example, using the semi-empirical molecular orbital calculation, the heat capacity of cyclohexane at 1000 K is estimated to be about 3 times larger than that at 300 K. On the other hand, since we are dealing with the temperature in a fast time scale, all vibrational freedoms may not be equilibrated. In this case, the heat capacity should be smaller than that under the equilibrium. For an extreme case, if all of the vibrational freedoms are completely neglected (i.e., only the translational and the rotational modes contribute to the heat capacity), the heat capacity of cyclohexane is 4 times smaller than $C_{solvent}$ we used. Since all vibrational modes cannot be neglected even for the calculation of the transient temperature, the difference between the heat capacities we used and that of the real system is much smaller and it will not change the qualitative feature described above. However, the difference will affect the quantitative value of $N_{solvent}$. For example, if the actual $C_{solvent}$ is 4 times smaller than $C_{solvent}$ we used, $N_{solvent}$ should be 4 times larger than listed in Table 2-2. $N_{solvent} < 1$ observed in many cases may be due to these effects.

An interesting energy releasing mechanism was proposed by Nagaoka et al. using the molecular dynamics calculation for a proton transfer reaction of formamidine in aqueous solution. [70] The reaction energy flows to or is donated from only a few water molecules. These molecules are located in regions effectively coupled to the solute; a reaction site as well as at a position where the water molecule can couple to the π electron of the solute. Experimentally, Terazima found that the

thermalization rate is enhanced by the hydrogen bonding between the solute and solvent. [34] Since only a few solvent molecules can participate in the hydrogen bonding to the solute, this result may indicate that these few molecules receive the thermal energy through the hydrogen bonding interaction. These theoretical and experimental studies indicate that the energy is initially released to not all but a few molecules around the solute. It may be reasonable to speculate that the effectively coupled solvent molecules (the DEA solvent molecules) are located close to a functional group (e.g. carboxyl group). A theoretical study using such as the molecular dynamics is required to further describe the thermalization process in detail.

In the above model, we assume that the intermolecular energy transfer from the solute to solvent is totally controlled by the simple kinetics (eq. (2-9) and (2-10)) and the thermal diffusion process (eq. (2-11)). The simple model can reproduce the experimentally observed two kinetic thermalization process. However, the calculated τ_s from the biexponential fitting (eq. (2-15)) of the transient temperature is slightly faster than the observed τ_s (30 ps). This discrepancy might be explained by the long lived vibrational modes of the solute. For example, the intermolecular energy transfer rates from vibrationally excited solvents to a molecular thermometer (oxazine-1) were reported and they depend on the vibrational mode of the solvent. [15] The CH stretching modes of acetone and ethanol dissipate their excess energies to the surroundings with lifetimes of 30 ps. On the contrary, the OH stretching mode of ethanol and the C=O overtone mode of acetone decay very rapidly (<2 ps and <5 ps, respectively). Similar to these cases, the vibrational energy from quickly relaxing modes heats up the solvent by the process described above, but there might be some other modes which can live long enough to provide the 30 ps cooling process.

6. Conclusion

The thermalization processes of HBP and HMPB after photoexcitation in several solvents were investigated by the transient grating (TG) method. The time evolution of the population grating (PG) signal of HMPB can be fitted by a double exponential function with lifetimes of 600 fs and 30 ps. The faster kinetics is attributed to the back proton transfer in the ground state (S_0(keto)→S_0(enol) in Fig. 2-1) and the slower one to the vibrational cooling process in the S_0 state. The PG signal of HBP in non-hydrogen bonding solvent can be also reproduced by a double exponential function with

lifetimes of 400 fs and 30 ps. Considering a previously reported fluorescence measurement of HBP, we assign the faster kinetics to the vibrational relaxation or the proton transfer reaction in the S_1 state (S_1(enol)→S_1(keto)) and the slower one to the vibrational cooling in the ground state. In ethanol (hydrogen bonding solvent), there is another component originated from the T_1 state of HBP besides above two components. The acoustic TG signal reveals that the triplet quantum yield of HBP in any solvents is less than 0.05. This result implies that the intermolecularly hydrogen bonded HBP is minor even in ethanol solution. The fast time constant (400 fs) should be attributed to the vibrational relaxation process in the S_1 state and the slow one (30 ps) to the vibrational cooling time in the S_0 state also in ethanol.

The thermalization rates of HMPB and HBP were obtained from the acoustic peak shift of the TG signal. The results show that there are very fast (less than a few ps) and slow (30 ps) vibrational cooling processes. The relative thermal energies for these processes depend on the solvents (Table 2-1). A thermalization model which represents the energy transfer from the solute to the solvent was presented. In this model, the energy of the solute is first transferred to some effectively coupled solvent and the temperature of the solute quickly decreases. The temperature of the effectively coupled solvent is elevated by the energy transport and the thermal energy is then diffused to the outer solvent molecules to establish the homogeneous distribution. This thermalization model explains the experimental observations: slow dynamics observed in the PG signal and the peak delay time of the acoustic signal. The fast heat releasing process results from the initial energy transfer to the effectively coupled solvent, and the slower one represents the cooling process by the thermal diffusion.

3. Spatially Resolved Thermalization Dynamics of Electronically Photoexcited Azulene Probed by a Molecular Integrated Thermometer

3-1. Introduction

The energy dissipation mechanisms by nonradiative transition from photoexcited states to the surroundings have been studied extensively. [1-3] Mostly, the energy dissipation has been discussed by associating it with the vibrational relaxation process. The vibrational cooling in the S_0 state of azulene is one of extensively studied systems in a wide density region experimentally and theoretically. [14, 17, 66, 71-80] After photoexcitation to the S_1 state, the vibrationally 'hot' azulene in the S_0 state is produced with a lifetime of 1ps, [81, 82] and a subsequent vibrational cooling is monitored via the hot band of azulene. [17, 66] The results showed that the vibrational cooling of azulene occurs around 10 ps. In *n*-alkanes, the cooling times decrease with increasing the chain length from 12.5 ps in pentane to 10.8 ps in hexadecane. The hydrogen bond formation has a strong influence on this thermalization process. With increasing the hydrogen bond density, the vibrational cooling time decreases from 9 ps in ethanol to 3.3 ps in 3:1 mixture of water and methanol. In these studies, azulene itself acts a role of a molecular thermometer to monitor the molecular energy.

On the other hand, studies of the thermalization process by monitoring the temperature rise of the surrounding matrix could be another important approach. [83] This approach has been mainly used by our group using several photothermal spectroscopies. [30-34] A fast temperature rise of the surrounding solvents with a few ps time resolution was monitored after photoexcitaion of solute molecules in water [30-32] and organic solvents. [33, 34]

One of important parameters, which has not been detected so far is the spatial resolution. If we can detect the transient temperature of the solvent as a function of the distance from the solute, the thermalization process as well as the heat flow mechanism will be more clear (Fig. 3-1). In this chapter, we carried out the first attempt to detect the thermalization process with a high spatial resolution by using a molecular heater and a molecular thermometer integrated system (Fig. 3-2). After photoexcitation of azulene that is used as a heater molecule, the excess energy is dissipated to the surroundings. This energy flow is monitored via a hot band absorption change of a thermometer (coumarin 151 (C151)) combined with a methylene group.

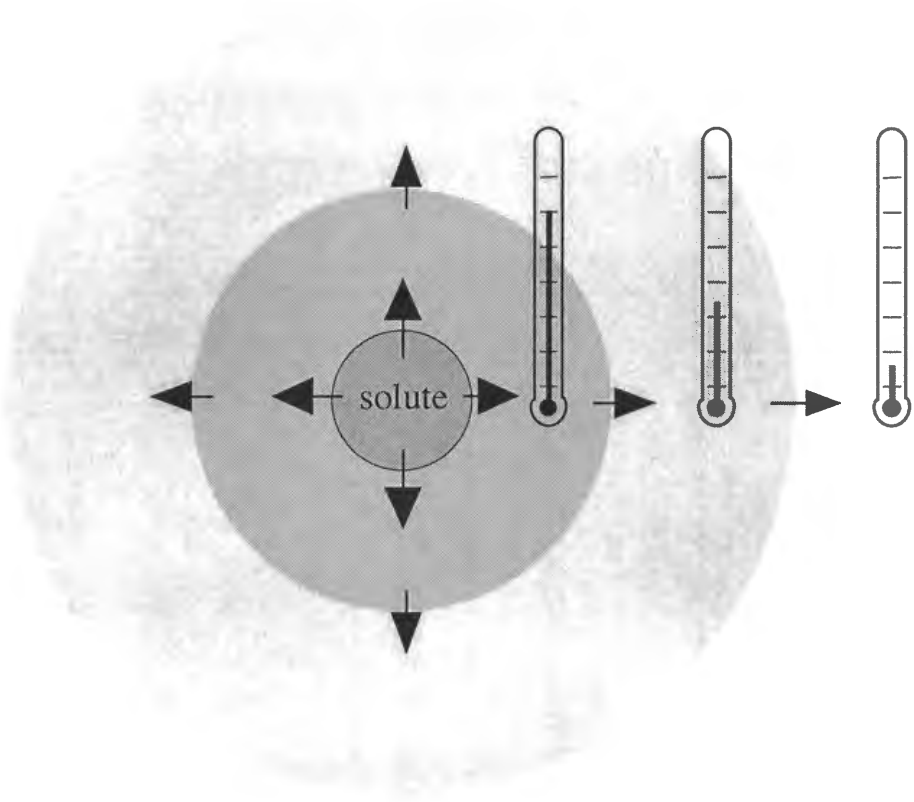

Fig. 3-1. Schematic showing how the transient temperature can be monitored with a high spatial resolution.

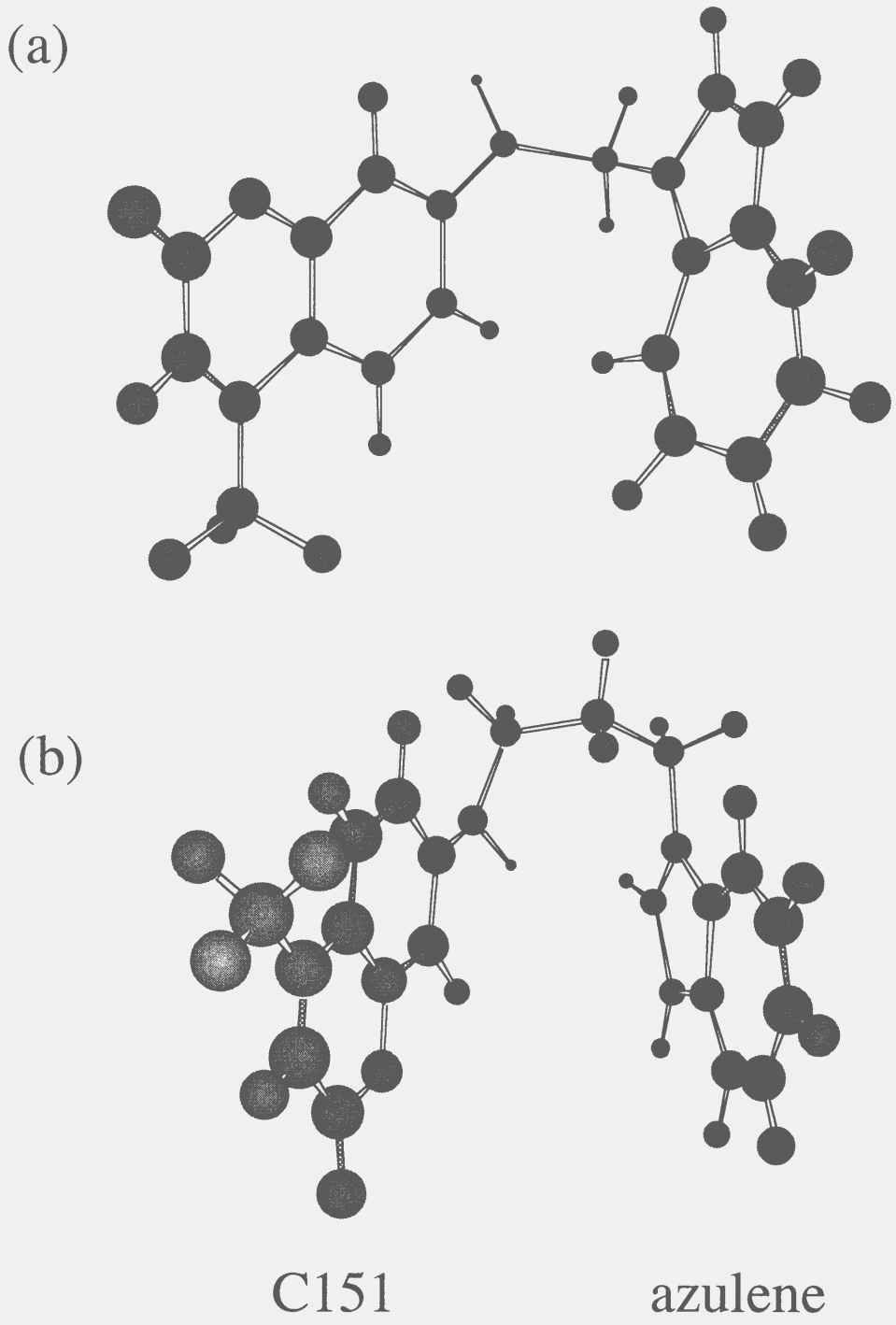

Fig. 3-2. The optimized molecular structure of (a) Az-CH_2-C151 and (b) Az-$(CH_2)_3$-C151 by the semi-empirical molecular orbital calculations (AM1 method).

For a heater molecule, it is preferable that the photoexcited state relax quickly to generate large excess energy instantaneously in the lower state. We chose azulene for heater because the lifetime of the S_1 state is as short as 1 ps [81, 82] and the vibrational relaxation in the ground state has been extensively studied already. [14, 17, 66, 71-80]

The molecular thermometer should possess several properties to be used as a thermometer in this system. (1) The absorption band should not overlap with that of azulene. (2) The energy of the S_1 state of the thermometer should be higher than that of azulene to prevent direct electronic energy transfer from azulene to thermometer. (3) To be a thermometer, the absorption spectrum should be sensitive to (local) temperature. One of molecules which satisfies these demands is coumarin 151 (C151).

Using Az-CH_2-C151, the thermometer is expected to detect the temperature of the solvent in the first solvent shell because of the short distance between the heater and the thermometer. The observed results are analyzed by a simple thermalization model proposed in chapter 2 and compared with the vibrational cooling rate measured via the hot band detection of azulene itself. Then the transient temperature detected by a compound in which azulene and C151 is combined with a longer chain (propylene group) (Az-$(CH_2)_3$-C151) is discussed.

3-2. Experimental

3-2-1. The transient absorption measurements

The transient absorption spectra were measured by a standard pump-probe technique using an amplified picosecond pulsed dye laser (Fig. 3-3). [84] A pulse of a Nd:YAG laser (Coherent Antares 76-S)-pumped dye laser (Coherent 700; λ=590 nm), which was amplified with a dye amplifier system (Continuum PTA60 and Continuum RGA60) was split by a 50-50 beam splitter for the pump and probe beams. The laser power was ~0.5 mJ / pulse at 50 Hz. The probe beam was focused by a lens (f=15 cm) and brought into a 1 cm cell of flowing water to generate white light continuum. The white light continuum then passed thorough a polarizer to select a vertically polarized light, and was split into two (sample and reference beams) with a beam splitter. The sample beam was focused by a concave mirror (R=50 cm) and brought into a sample cell. The optical path length was 3 mm. The pump beam was focused into the sample cell with a lens (f=50 cm). The polarization of the pump

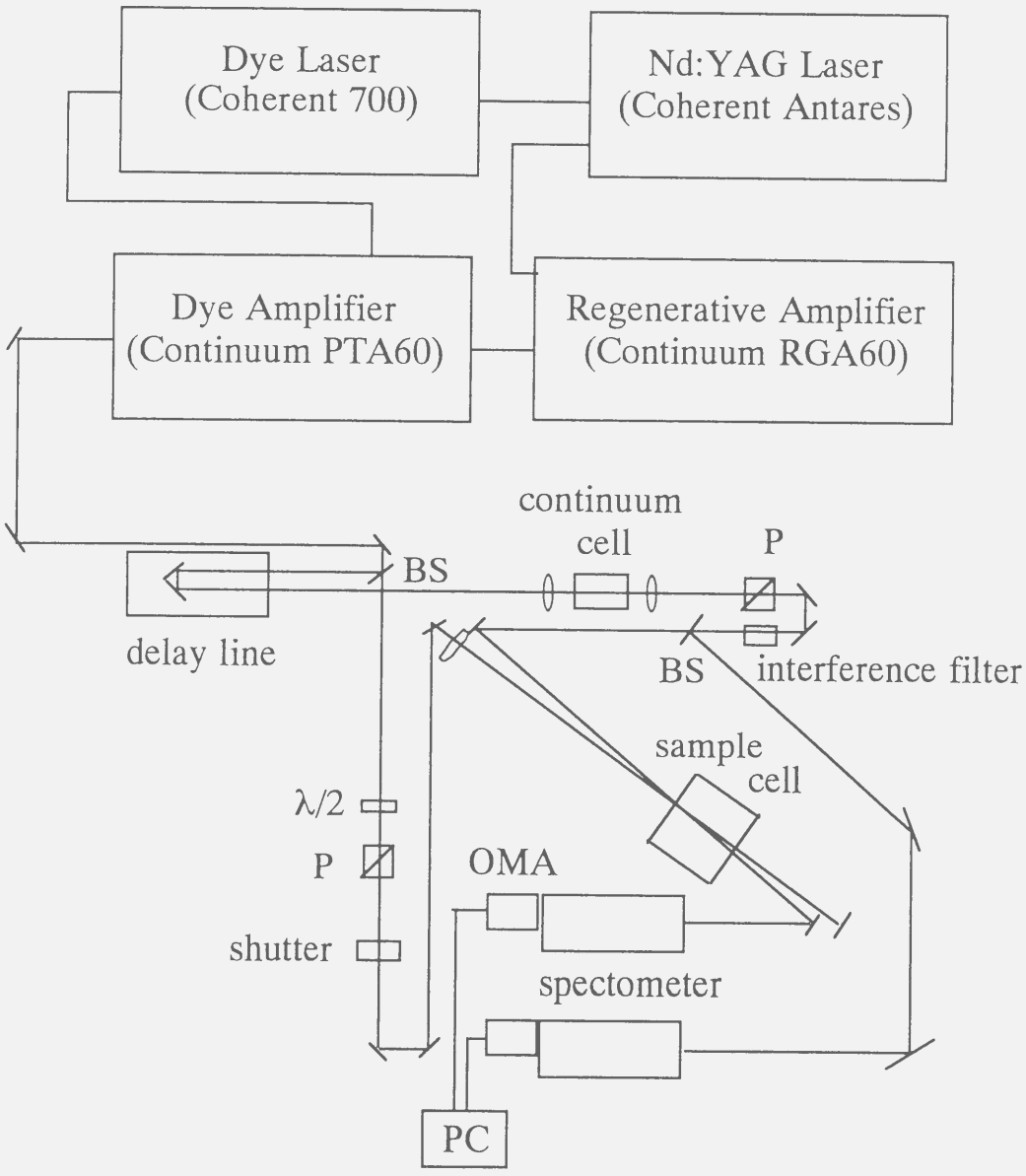

Fig. 3-3. The experimental set up for the transient absorption measurements.

beam was adjusted to the magic angle (54.7 °). The probe beam after a sample cell and the reference beam were collected to an optical fiber connected to a spectrometer (Chromex 250IS) and detected by an intensified silicon photodiode array (EG&G, OMA1421). The signal was normalized by the reference, and the difference of the optical density (ΔOD) with and without pump beam was measured at each delay time. The pulse shape was monitored by the optical Kerr signal of the neat carbon tetrachloride solution. The pulse width was typically 4 ps. The concentration of the sample was ~5 mM in ethanol and 2-propanol for Az-CH_2-C151, and ~10 mM in acetone and benzene for Az-CH_2-C151 and Az-$(CH_2)_3$-C151. From the intensity of the pump pulse and the pumped area (~$2x10^{-3}$ cm), we calculated that ~8% of the solute molecules were photoexcited in a typical case. All the solvents (ethanol, 2-propanol, acetone, benzene and carbon tetrachloride (Nacalai Tesque, Spectral grade)) were used without further purification.

3-2-2. The steady-state absorption measurement under a constant density

The set up for the steady-state absorption measurement under a high pressure condition is reported elsewhere. [85] Briefly, the absorption spectra were recorded with a spectrometer (Shimadzu UV-240). A high pressure optical cell was used at elevated pressures. [84, 85] The stability of the temperature was ±0.2 °C. The pressure was measured by a Heise Bourdon gage with a ±0.2 MPa accuracy. The densities of the solution were calculated from the PVT data of ethanol [86] and benzene. [87]

3-3. Results

3-3-1. Az-CH_2-C151

The absorption spectrum of Az-CH_2-C151 (Fig. 3-4) is almost the same as the sum of the absorption spectra of azulene and of C151 except for slight red shifts (~10 nm). Hence, the intermolecular interaction between azulene and C151 in the ground state appears to be weak. The absorption band from 500 nm to 700 nm is mainly the $S_0 \rightarrow S_1$ transition band of the azulene moiety, and does not overlap with the long wavelength edge of the 0-0 transition of the C151 moiety. Therefore we can photoexcite only azulene to the S_1 state using the laser light centered at 590 nm.

The observed transient absorption spectrum of Az-CH_2-C151 / ethanol is shown in Fig. 3-5(a).

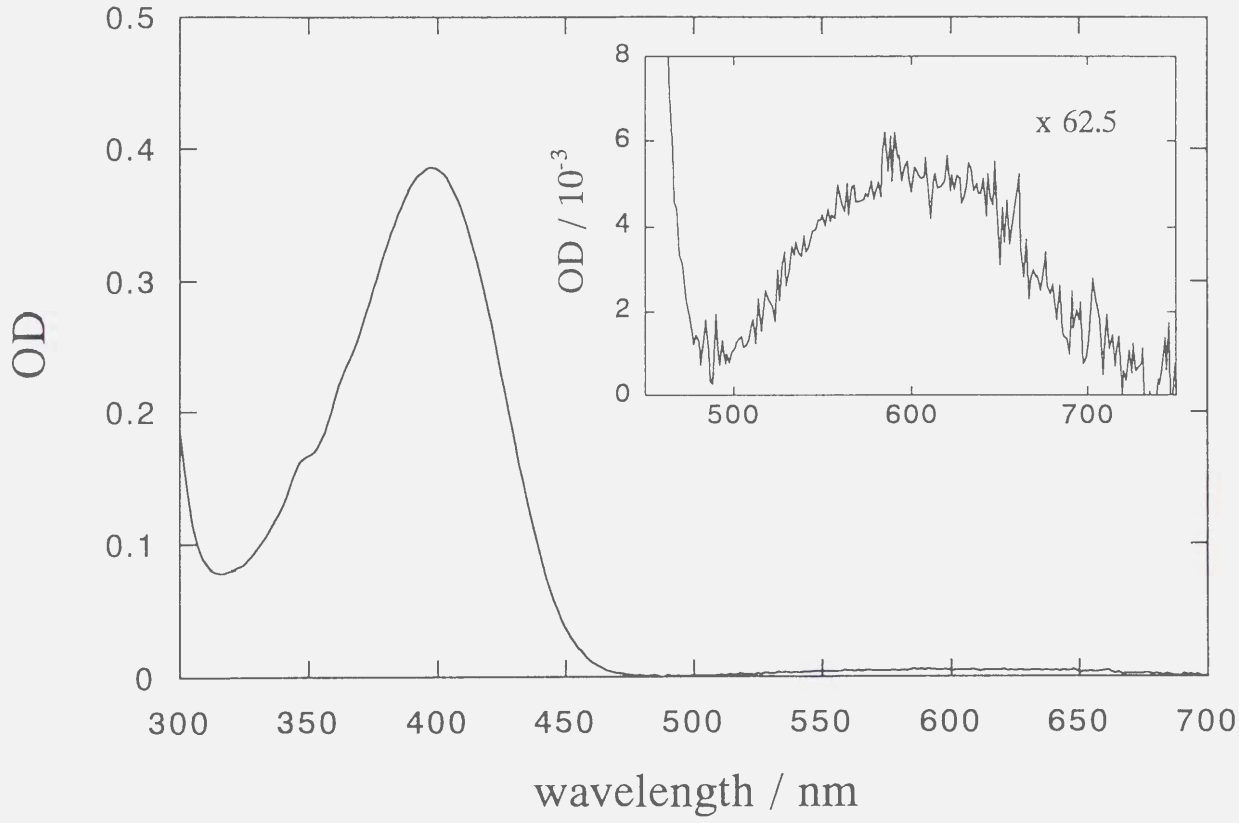

Fig. 3-4. The absorption spectrum of Az-CH_2-C151 / ethanol.

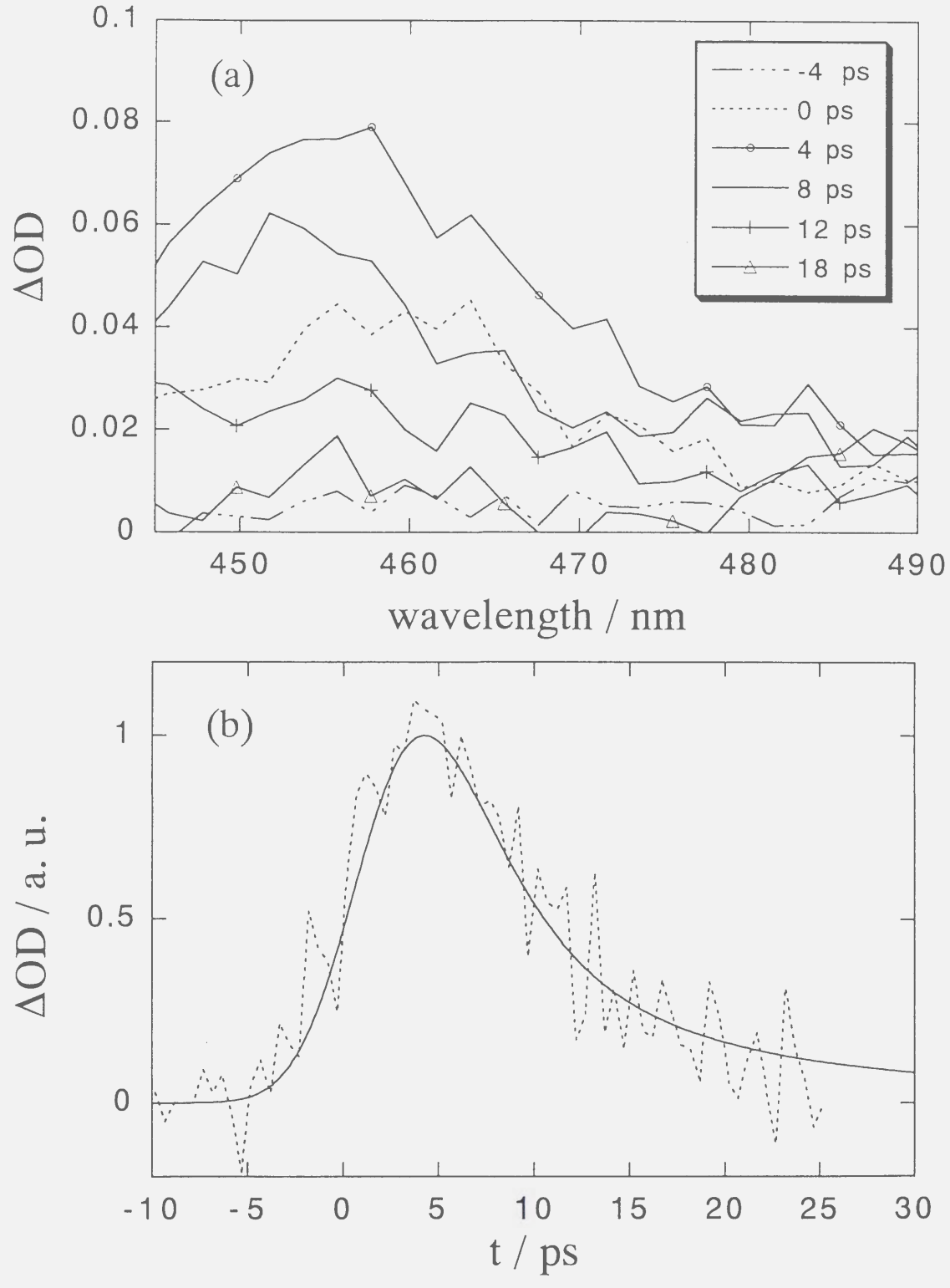

Fig. 3-5. (a) The transient absorption spectrum of Az-CH_2-C151 in ethanol. (b) The time profile of the transient absorption signal probed at 450 nm. The solid line represents the calculated signal based on the thermalization model (τ_{sum}=2 ps).

The signal appears just on the red edge region of the C151 absorption band (Fig. 3-6). The time evolution of the transient absorption signal probed at 450 nm is shown in Figure 3-5(b). The time profile of the transient absorption signal is almost identical at all the wavelengths in which the transient absorption signal appears. The transient absorption spectra were also measured in acetone (Fig. 3-7), 2-propanol and benzene (Fig. 3-8). The spectra are very much similar.

These transient absorption signals are attributed to the hot band of the C151 absorption based on the following reasons. First of all, any signal was not observed from the sample which contained only azulene or C151 under the same experimental condition. Hence the observed transient absorption signal is not the absorption of the excited states of azulene or C151. Second, the wavelength in which the transient signal appears is on the red edge of the absorption band of C151. It could be possible that the signals come from the hot band of azulene. However, this contribution may be minor because the absorption coefficient of azulene is much smaller than that of C151. Indeed when the observed transient absorption signal is converted to the absorption coefficient (ε), the frequency dependence of ε shows the characteristic feature of the hot band of C151 (Fig. 3-6). Moreover, the wavelength region in which the transient absorption signal appears depends on the solvent and this dependence can be reasonably explained by the solvatochromic shift of the C151 absorption band. [88] Therefore we conclude that the observed transient absorption signal is due to the hot band signal of C151.

Besides the hot band signal, when the excitation laser power was strong, another component of the transient absorption signal was observed in a longer wavelength region. This component is particularly clear in benzene at a wavelength around 455 nm (Fig. 3-8(a)). This signal quickly rises and the decay is very fast (<1 ps). The time profile of this component is about the same as the instrumental response function. The origin of this component is not clear at present but could be a transient absorption from higher excited states produced by the multiphoton absorption. This contribution can be minimized by using a weak pump laser power. This component is not seen in the signals of the ethanol, 2-propanol and acetone solutions. The amplitudes of the hot band signals were proportional to the pump laser power. Hence we believe that this contribution does not participate in the hot band signals we are studying.

3-3-2. Az-$(CH_2)_3$-C151

The hot band spectrum of Az-$(CH_2)_3$-C151 in acetone is shown in Fig. 3-9(a). The fast rising

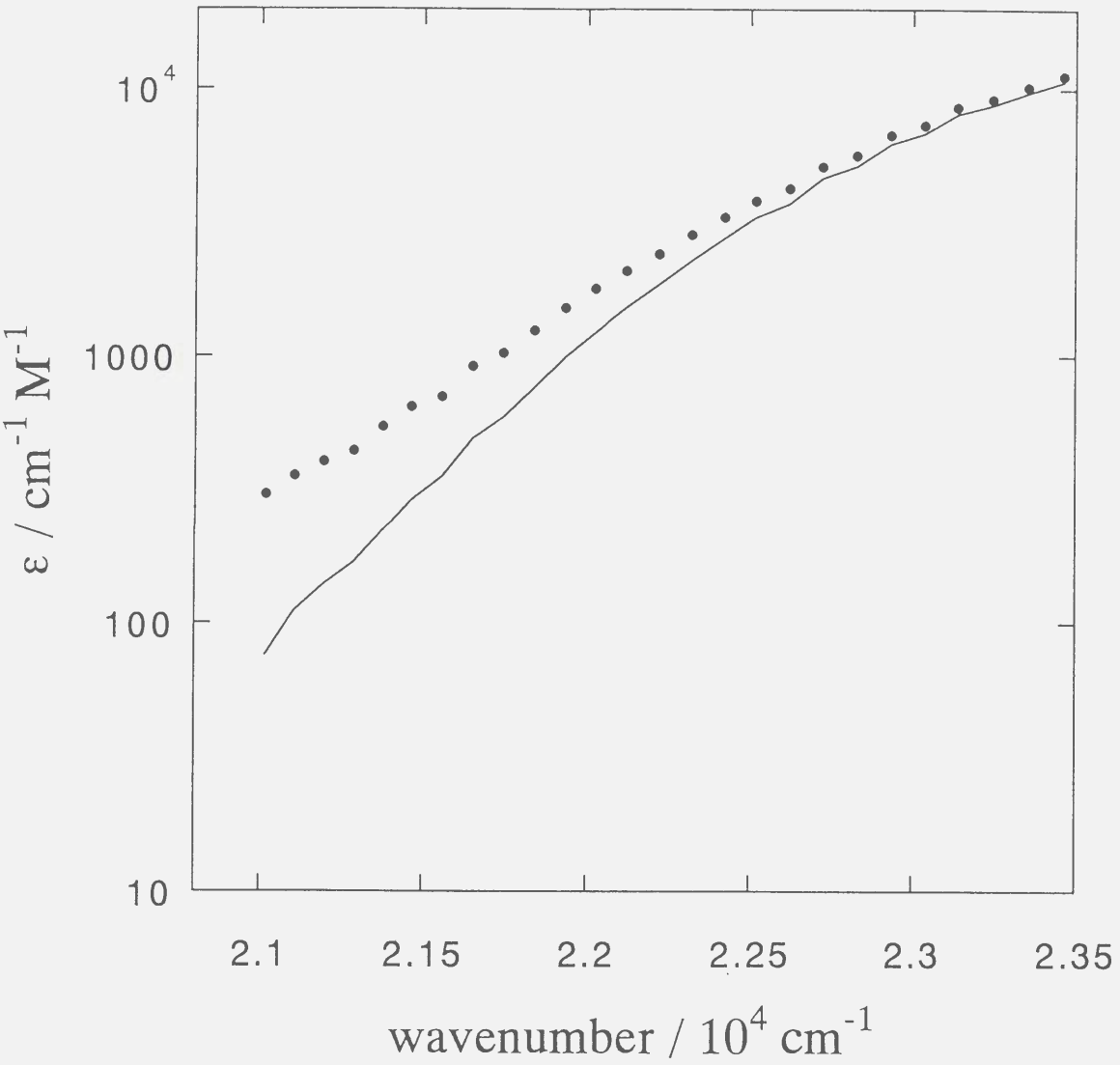

Fig. 3-6. The solid line shows the red edge of the C151 absorption spectrum at room temperature and the solid circle the absorption coefficient at 4 ps after photoexcitation of azulene moiety in ethanol.

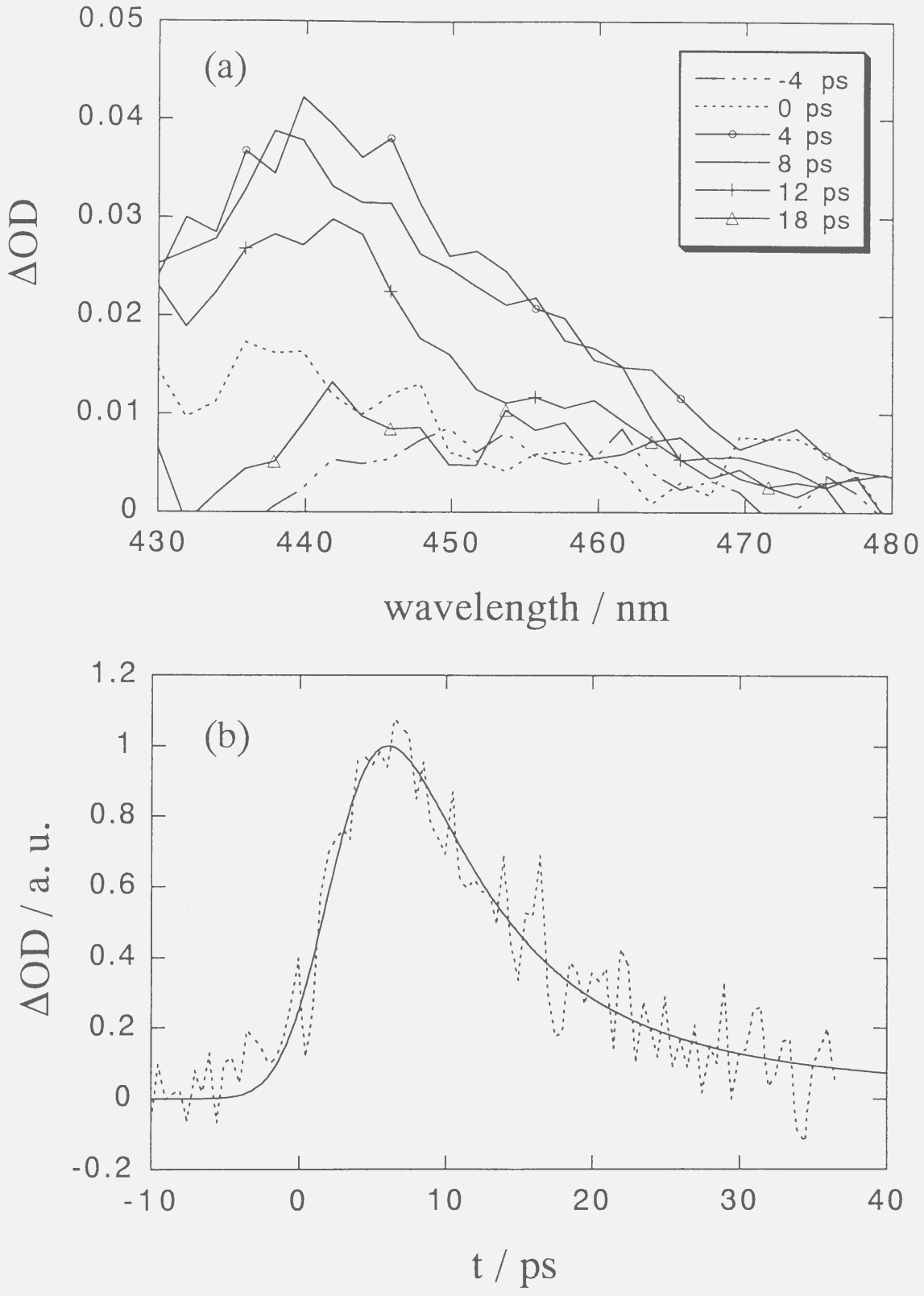

Fig. 3-7. (a) The transient absorption spectrum of Az-CH_2-C151 in acetone. (b) The time profile of the transient absorption signal probed at 440 nm. The solid line represents the calculated signal based on the thermalization model (τ_{sum}=5 ps).

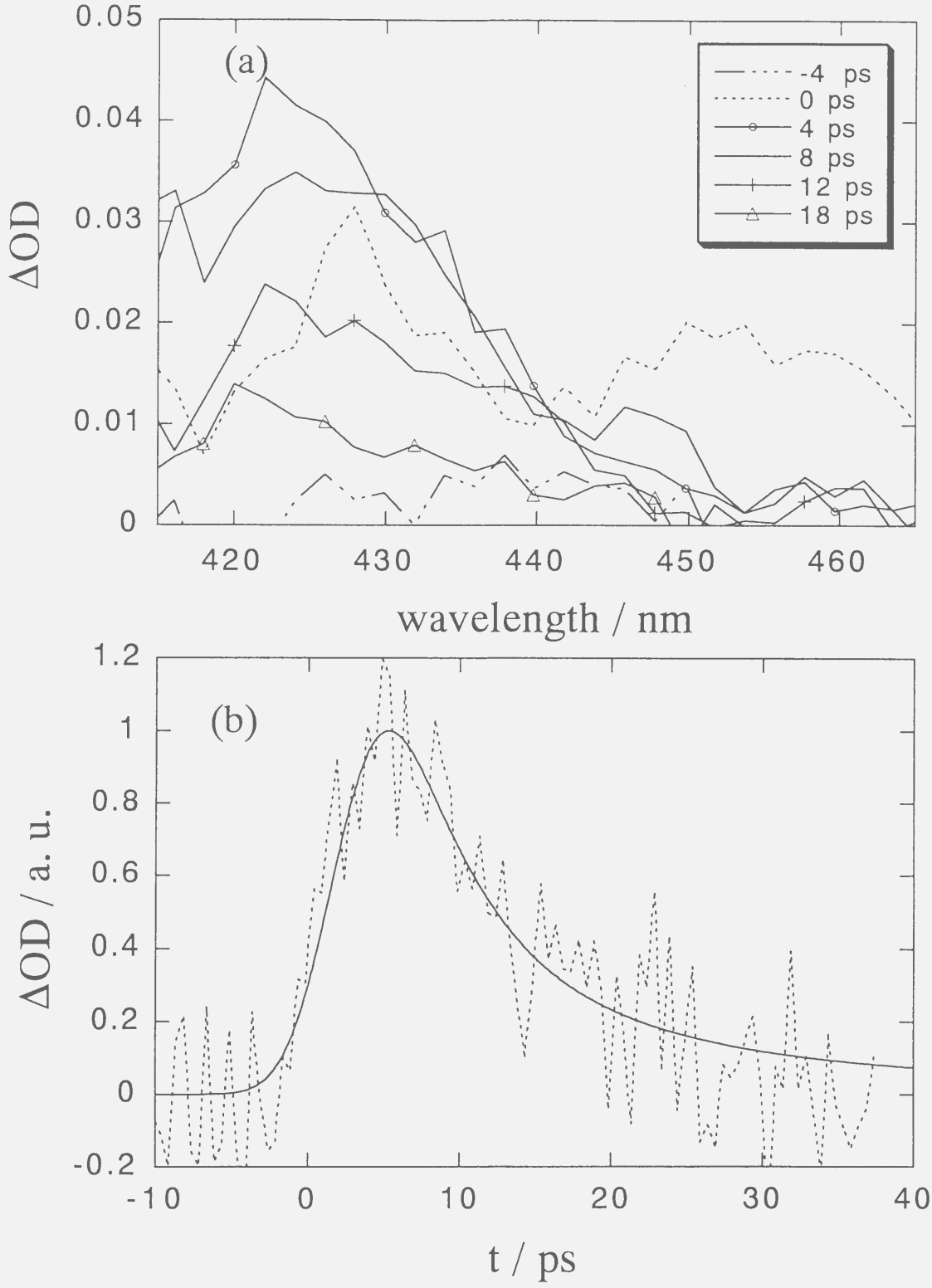

Fig. 3-8. (a) The transient absorption spectrum of Az-CH_2-C151 in benzene. (b) The time profile of the transient absorption signal probed at 420 nm. The solid line represents the calculated signal based on the thermalization model (τ_{sum}=3 ps).

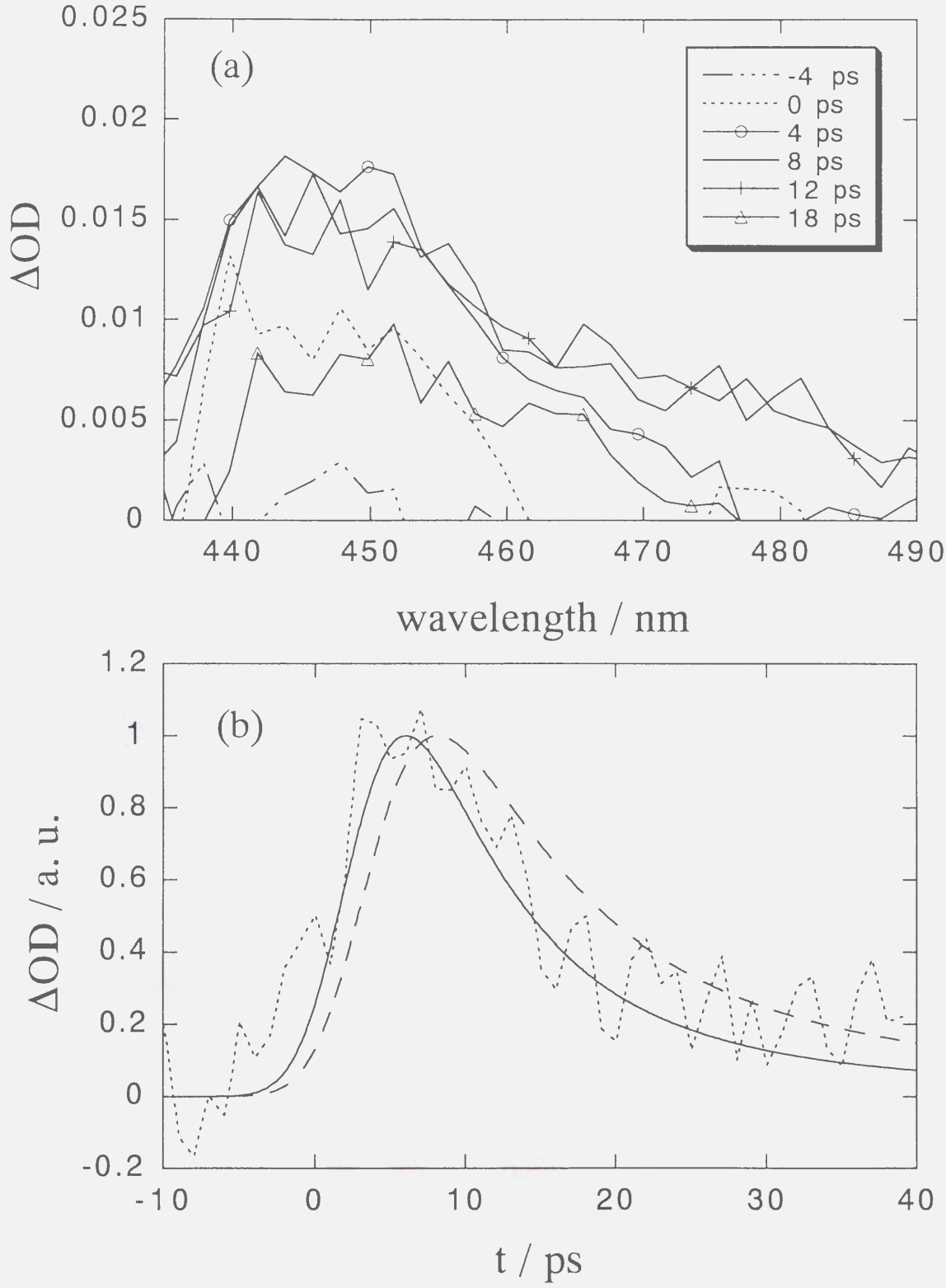

Fig. 3-9. (a) The transient absorption spectrum of Az-$(CH_2)_3$-C151 in acetone. (b) The time profile of the transient absorption signal probed at 450 nm. The solid lines represent the calculated signal when the thermometer monitors the temperature of the DEA solvent (τ_{sum}=5 ps). The broken line denotes the time profile of the transient temperature of the thermometer when the propylene chain is stretched out (~11 Å).

signal observed in Az-CH_2-C151 / benzene was also observed in this system when the pump laser power was strong. The spectrum of this component was estimated from the transient absorption spectra of Az-CH_2-C151 in acetone recorded at a stronger pump laser power. The hot band spectrum (Fig. 3-9(a)) is obtained by subtracting the estimated spectrum of this component from the raw data. The time profile of the transient absorption signal probed at 450 nm is shown in Fig. 3-9(b). The time evolution of this signal is very similar to that of Az-CH_2-C151 except for the long time behavior and a weaker intensity.

The transient absorption signal was observed also in benzene. The spectrum and the time profile of the signal are similar to those of Az-CH_2-C151 in benzene. We could not observe any signal in ethanol and 2-propanol because of the low solubilities of Az-$(CH_2)_3$-C151.

3-4. Discussion

A simple interpretation of the observed transient spectra is that the signal directly reflects the temperature rise of C151 due to the thermal energy dissipation from azulene. However, we must consider that the absorption coefficient (ε) is not generally proportional to the temperature. First, we examine the relationship between ε and T at the probe wavelength. The hot band absorption appears due to the thermal excitation of higher vibrational levels in the ground state. Kaiser and coworkers introduced the following model for analyzing the temperature dependent electronic absorption spectrum, which has been used in many systems. [2, 3, 12, 13, 89] In this model, ε at a wavenumber ν and at a temperature T is expressed by

$$\varepsilon(\nu, T) \propto S(\nu) \exp\left\{-h(\nu - \nu_{00})/kT\right\} \qquad (3\text{-}1)$$

where ν_{00} is the wavenumber of the 0-0 transition and k is the Boltzmann constant. $S(\nu)$ is determined by the density of the vibrational states and the Frank-Condon factors. If we assume that the temperature dependence of ε is expressed by eq. (3-1), the ratio of $\varepsilon(\nu,T)$ to that at room temperature (T_{rt}=298 K) is given by

$$\frac{\varepsilon(\nu, T)}{\varepsilon(\nu, T_{rt})} = \exp\left\{h(\nu - \nu_{00})(1/kT - 1/kT_{rt})\right\} \quad . \qquad (3\text{-}2)$$

Let us examine eq. (3-2) for the transient absorption signal of Az-CH_2-C151 / ethanol. The ratio of $\varepsilon(T)$ measured at 4 ps after photoexcitation to $\varepsilon(T_{rt})$ is shown in Fig. 3-10(a). If the above analysis is appropriate, the plot of $\ln\{\varepsilon(T)/\varepsilon(T_{rt})\}$ vs. ν should be linear. However the plot deviates from the linear relation at a higher wavenumber region. Probably this deviation is due to the contributions from the vibronic bands in the excited state. We fitted the data points in the red edge region by a linear function of ν with a parameter of ν_{00} and T (solid line in Fig. 3-10(a)). From the fitting, we determined $\Delta T = T - T_{rt} \approx 66$ K and $\nu_{00} \approx 22400$ cm^{-1}. The frequency of the 0-0 transition is reasonably close to that estimated from the absorption and the fluorescence spectra of Az-CH_2-C151 / ethanol (22500 cm^{-1}, Fig. 3-11). This agreement supports our interpretation that the induced absorption in this region comes from the thermal broadening of the 0-0 transition band of C151. Later we will show that the estimated temperature rise here is consistent with the estimated ΔT from a theoretical analysis based on the thermalization model. The same analysis was carried out in the other solvents. The obtained ΔT and ν_{00} are listed in Table 3-1.

By using the determined ν_{00} (=22400 cm^{-1}), the temperature dependence of $\varepsilon(T)$ at the probe wavelength of 450 nm can be calculated from eq. (3-1) (Fig. 3-10(b)). The plot of ε vs. T shows that ε is almost proportional to T in this temperature range. Therefore we conclude that the observed transient absorption signal intensity at 450 nm is directly proportional to the temperature change of the molecular thermometer. In the other solvents used here, this linear relationship is valid, too. Based on these results, hereafter, we analyze the temperature change of the molecular thermometer (C151) from the time profile of the transient absorption signal.

To calibrate the temperature rise from the transient absorption intensity by another method, the temperature dependence of the steady-state absorption spectra of Az-CH_2-C151 was measured at several temperatures under an ambient pressure. Generally, with increasing the temperature, the absorption spectrum is thermally broadened due to the population increase of the higher vibrational

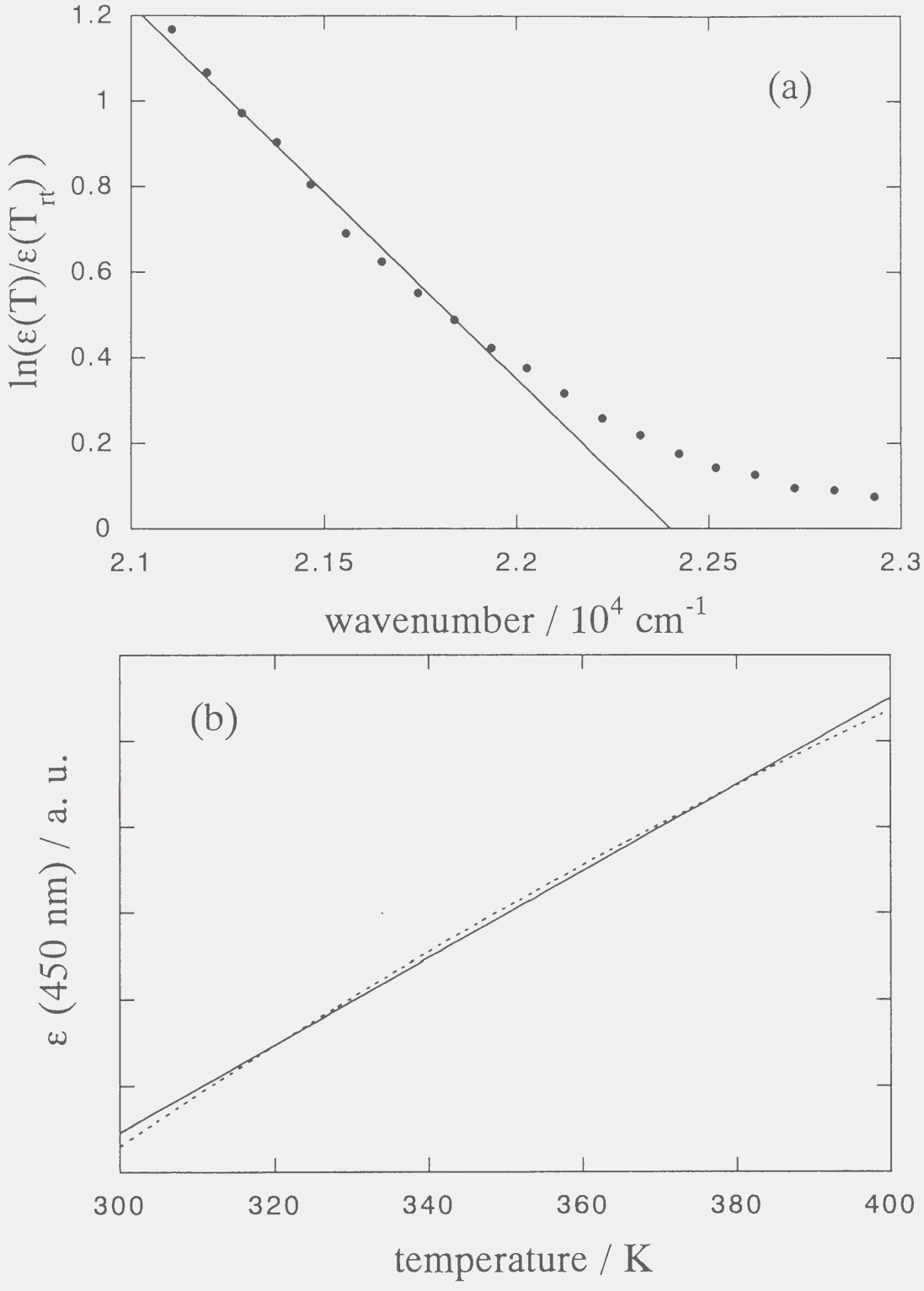

Fig. 3-10. (a) The ratio of ε(T) at 4 ps after the photoexcitation to ε(T_{rt}) of Az-CH_2-C151 / ethanol. The solid line denotes the fitting line by using eq. (3-2). (b) Relation between the absorption coefficient at 450 nm (ε(450 nm)) and the temperature (dotted line). The solid line denotes the best fitted line by a linear function.

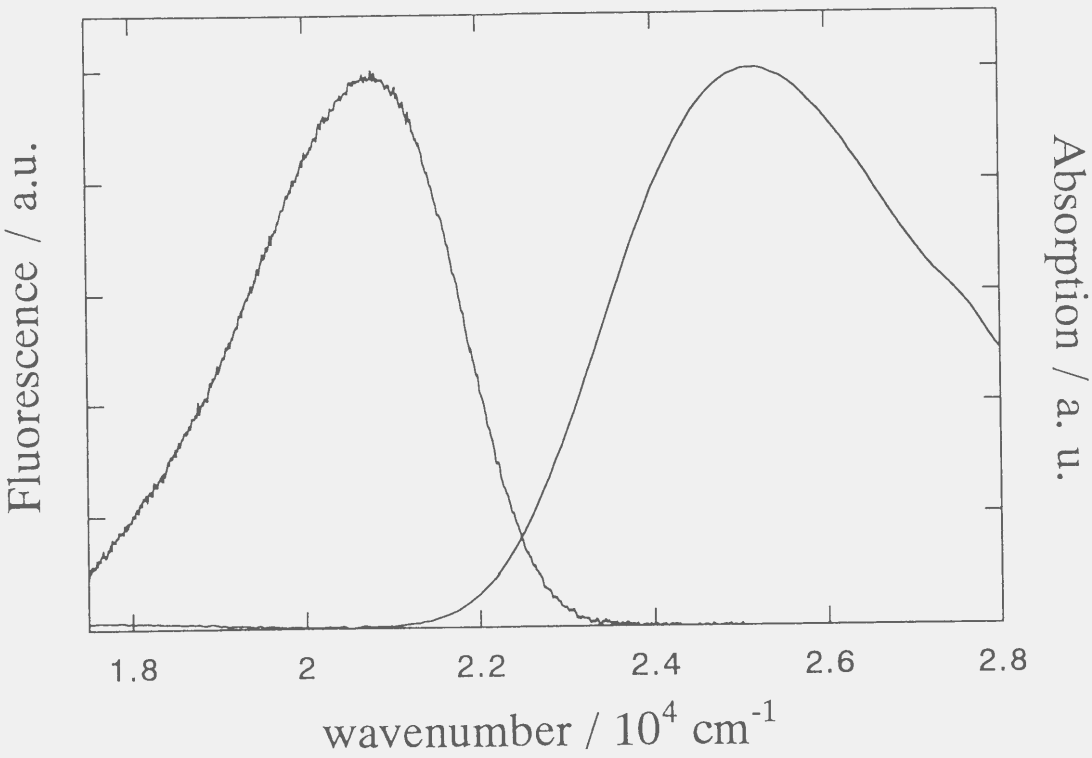

Fig. 3-11. The absorption and the fluorescence spectra of Az-CH_2-C151 / ethanol.

levels. The observed $S_0 \rightarrow S_1$ absorption band of C151 at higher temperature is thermally broadened as expected. However the entire absorption band shifts to the blue side with increasing the temperature and the hot band did not appear in the red edge. This was totally unexpected. This spectral shift at a higher temperature, however, has been observed for many molecules and is known as "thermochromism". [90, 91] This observation is inconsistent with the hot band observation in the transient absorption spectrum.

A similar phenomenon in studies of the transient temperature has been sometimes reported so far. For example, Scherer et al. tried to calibrate the transient temperature of the molecular thermometer (oxazine-1) in a ps time scale by using the steady-state absorption spectrum. [15] In this case, the hot band signal could be fitted not by a spectrum expected at a high temperature but by a spectrum after a correction of the thermochromic shift. In their analysis, the origins of the temperature dependence of the steady-state spectrum were divided to three components. The first, the absorption change of optically active modes with large Frank-Condon factors induced by the increase in thermal population, the second, the line broadening due to the population change of low frequency modes and the modes with small Frank-Condon factors, and the third, the temperature dependent shift of the absorption spectrum. They found that the observed transient spectrum should be fitted by the former two components. They concluded that the steady-state absorption spectrum cannot be compared with the transient absorption spectrum in a ps time scale probably because the thermochromic shift takes place slowly by the change of the dielectric constant and the refractive index of the solvent.

The thermochromism results from the temperature dependence of the orientational and the isotropic polarization of the solvent. [90, 91] The time responses of these contributions are unclear because systematic time resolved studies of the thermochromism are quite limited. The orientational response of the solvent may be very fast because a large part of the dynamic Stokes shift occurs in the very short time scale, which is induced by the oriental redistribution of the surrounding solvents. [93-98] On the other hand, the temperature dependence of the isotropic contribution comes from the density variation, which could take place slowly. We measured the absorption spectrum at a constant density (ρ) to subtract the isotropic contribution. The temperature dependence of the absorption coefficient $\Delta\varepsilon/\Delta T$ was determined from the absorption spectrum of Az-CH_2-C151 in ethanol under

ρ=0.81 g cm^{-3} at 25 °C and 50 °C (Fig. 3-12). Assuming $\Delta\varepsilon \propto \Delta T$, $\Delta\varepsilon/\Delta T$ was found to be 1.7 cm^{-1} M^{-1} K^{-1} at 455 nm in ethanol. By using this value, a temperature rise of ~290 K at the maximum is calculated from the transient absorption intensity of Az-CH_2-C151 / ethanol. This temperature rise of ~290 K is inconsistent with the estimated ΔT from the red-edge analysis of the absorption spectrum presented before (~66 K) and also from the analysis based on the thermalization model (~30 K).

Next we subtract the temperature dependent blue shift from the observed temperature dependence of the absorption spectrum, that is, the observed absorption spectrum at 50 °C is shifted so that the peak of the absorption spectrum at 50 °C matches to that at 25 °C (broken line in Fig. 3-12). If we use this spectral correction, $\Delta\varepsilon/\Delta T$=6.4 cm^{-1} M^{-1} K^{-1} is obtained at 455 nm, which leads to $\Delta T \approx$78 K at the peak of the transient absorption intensity.

We also measured the steady-state absorption spectrum in benzene. In the case of benzene, the dipole moment is zero and the thermochromic shift results only from the isotropic contribution. But, the hot band was not appeared in the red edge of C151 under an ambient pressure. The absorption spectra at 20, 50 and 75 °C under the same density (ρ=0.88 g cm^{-1}) are shown in Fig. 3-13. The absorption spectra are not shifted because of the no orientational contribution due to the dipolemoment. In this temperature range, $\Delta\varepsilon \propto \Delta T$ was almost valid and $\Delta\varepsilon/\Delta T$ was estimated to be 5.5 cm^{-1} M^{-1} T^{-1} at 425 nm, which leads $\Delta T \approx$120 K.

It is surprising that this temperature rise is almost identical to the estimated ΔT from the analysis of the red edge broadening of the absorption spectrum. This coincidence may indicate that the absorption spectrum shift due to the temperature rise occurs slowly, and the transient broadening should be analyzed without taking into account the frequency shift of the spectrum. However, the detailed mechanism about the thermochromism including its time response is still unclear and further studies are needed to reveal the relationship between the transient and the steady-state absorption spectra.

The hot band absorption appears because the vibrational levels of the thermometer are thermally excited and it should require a certain time delay after the heating. The time evolution of the signal, therefore, should include the vibrational cooling process of azulene, the thermal conduction to the thermometer and the thermally vibrational excitation process of the thermometer. Taking into account these rates, we calculated the time profile of the transient temperature using a thermalization model

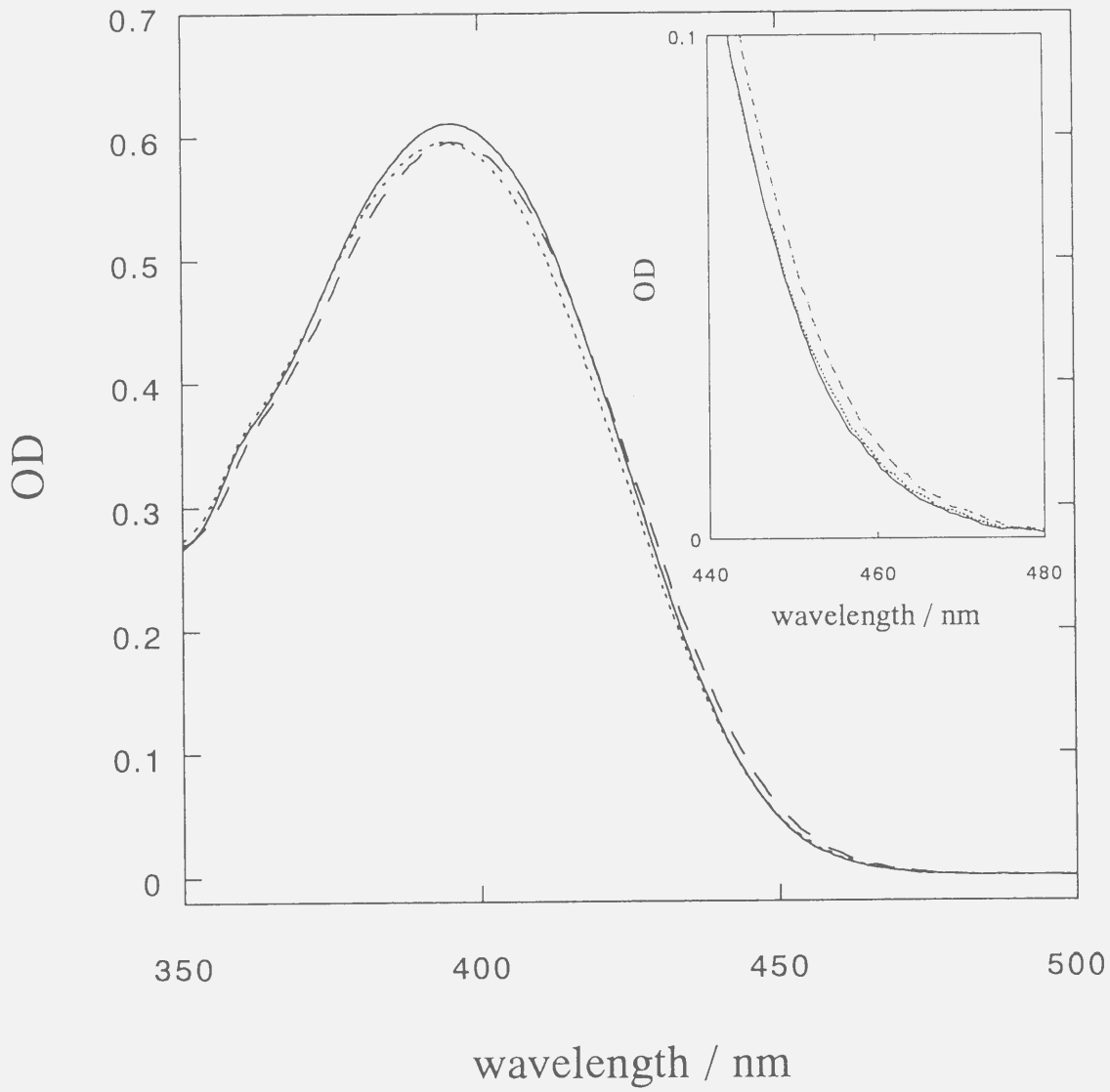

Fig. 3-12. The absorption spectrum of C151 under ρ=0.81 g cm^{-3} in ethanol. The solid and dotted lines denote the observed spectra at 25 °C and 50 °C, respectively. The spectrum corrected for the thermochromism is shown by the broken line.

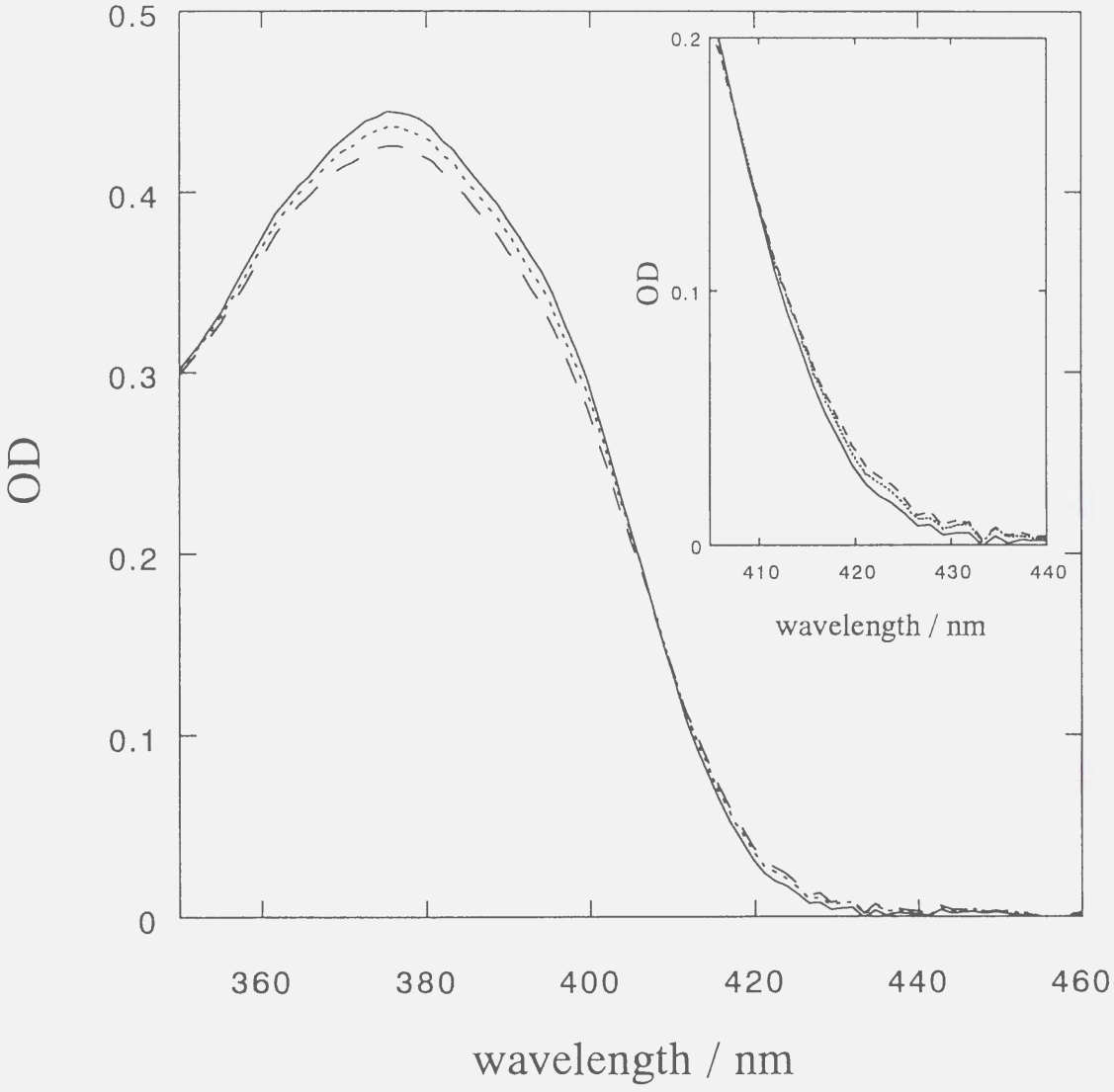

Fig. 3-13. The absorption spectrum of C151 under ρ=0.88 g cm^{-3} in benzene. The solid, dotted and broken lines denote the observed spectra at 20 , 50 and 75 °C, respectively.

proposed in chapter 2. In this calculation, we assume that the possibility of the through-bond vibrational energy transfer from the heater to the thermometer is quite low because of the following reasons. [24] (1) The time profile of the transient absorption signal of Az-$(CH_2)_3$-C151 is very similar to that of Az-CH_2-C151. If the energy transfer occurs through the σ-bond, the transfer rate may strongly depend on the number of the σ-bonds between the two chromospheres. [98-102] For example, the triplet-triplet energy transfer of a compound, 2-naphthyl group (accepter) connected via a spacer with 4-benzophenoneyl group (donor), was studied by Closs et al. [98] In this case, the energy transfer process can be explained by the through bond mechanism. The observed triplet-triplet energy transfer rate of the compound with three σ-bonds separating between the donor and the accepter is ~10 times larger than that of the four σ-bond separating compound. In the present case, we did not observe such a delay in the time profile on going from Az-CH_2-C151 to Az-$(CH_2)_3$-C151. (2) If the solvent reorganization process controls the energy transfer kinetics, the rate should depend on the solvent regardless of the energy transfer mechanism: through σ-bonds or through space. Indeed, the solvent dependent rates were observed in the electron transfer process by the through bond mechanism. [98, 100] However, in this case, the vibrational excitation is hardly affected by the solvent reorganization. Hence the solvent dependence is not expected for the direct energy transfer through the σ-bond. The observed solvent dependent rates, that will be described later may be evidence for the thermal energy transfer trough the medium of solvent molecules. This solvent mediated energy transfer will be treated later by a thermalization model. (3) The direct energy transfer from the S_1 state of azulene to the S_1 state of C151 cannot occur because the energy of the S_1 state of C151 locates above that of azulene. (4) The vibrational temperature rise of azulene just after the relaxation from the Frank-Condon state to the S_0 state is calculated to be up to ~1100 K. If all the photon energy absorbed by azulene transfers to C151 directly, the temperature of C151 should rise to 500~600 K. This is inconsistent with the estimated temperature rise (~66 K). (5) The time profile of the observed transient absorption signal can be fitted well by the thermalization model in which the heat transfer from azulene to C151 through the solvent is assumed as shown later. Therefore we conclude that the excess energy of azulene first transfers to the solvent which locates in the vicinity of azulene, then the temperature of C151 rises by the thermal energy transfer from the solvent.

Previously we have proposed a simple model for the energy transfer from a photoexcited solute to the surrounding solvent molecules. In that model, we assumed that the excess energy of photoexcited solute is first transferred to several solvent molecules that are effectively coupled to the solute (the directly energy accepting (DEA) solvents). We also assumed that the rate is proportional to a rate (τ^{-1}) determined by the intermolecular interaction and the temperature difference between the solute (T_{solute}) and the DEA solvent (T_{DEA}). The thermal energy of the DEA solvent diffuses to the outer solvents (which is assumed to be continuous) by the thermal diffusion. Using this thermalization model, we calculate the temperature change of the molecular thermometer. The internal excess energy of the solute increases with two steps; $S_1^* \rightarrow S_1$ (S_1^*: the Frank-Condon state from the ground state) and $S_1 \rightarrow S_0$ processes (1 ps). Since the $S_1^* \rightarrow S_1$ process of azulene completes very fast (less than 1 ps), [82] the time evolution of the solute energy from this process can be neglected. This contribution provides an initial condition of the solute temperature; $T_{solute}(t=0)=Q_0/C_{solute}$ ($Q_0=h\nu-E(S_1)$ and C_{solute}: heat capacity of the solute). T_{solute} is further elevated by the energy from the deactivation of the S_1 state with a lifetime of τ_{S1} (=1 ps). Therefore the time evolution of the solute energy can be given by

$$C_{solute}\frac{dT_{solute}(t)}{dt} = C_{solute}\left\{-\frac{T_{solute}(t)-T_{DEA}(t)}{\tau}\right\}+\frac{E(S_1)}{\tau_{S_1}}\exp(-t/\tau_{S_1}) \quad . \qquad (3\text{-}3)$$

The temperature change of the DEA solvent is given by

$$N_{DEA}C_{solvent}\frac{dT_{DEA}(t)}{dt} = C_{solute}\left\{\frac{T_{solute}(t)-T_{DEA}(t)}{\tau}\right\} \qquad (3\text{-}4)$$

where N_{DEA} is the number of the DEA solvent(s) and $C_{solvent}$ is the heat capacity of the solvent.

The thermal diffusion process to the outer sphere under the spherical symmetry condition may be described by [67]

$$\frac{\partial (rT(t))}{\partial t} = D \frac{\partial^2 (rT(t))}{\partial r^2} \qquad (3\text{-}5)$$

where T is the temperature of the bulk solvent, r is the distance from the center of the heater and D is the thermal diffusivity.

The molecular thermometer (C151) should detect the energy flow from the inner solvent to the outer solvent. As regarding the distance between the heater and the thermometer, we should take a distance between a point where the energy is released and a point where the temperature is detected in the molecular structures. However, we do not know which part of azulene releases the heat and which part of C151 is sensitive to the temperature. Hence, considering the expected fast intramolecular vibrational redistribution, we take the center-to-center distance between the chromophores to represent the distance between heater and the thermometer. The uncertainty of the spatial resolution in this system, therefore, is around 0.3 nm, which is the molecular size of azulene and C151. The center-to-center distance between azulene and C151 moiety of Az-CH_2-C151 is estimated to be 0.65 nm from the optimized geometry (Fig. 3-2(a)) by a semi-empirical molecular orbital calculation (AM1 method, MOPAC program package). The radius of azulene is 0.33 nm [17] and the diameters of solvents used here are 0.43~0.55 nm. [68] We assume that the molecular thermometer locates between the DEA solvents and the outer continuum medium. The temperature of C151 increases by the energy flow from the DEA solvents and decreases by the the energy transfer to the continuum.

The response time of the temperature elevation and the temperature decrease of C151 could be different. However, using two different response times adds a complexity and more parameters to the model and we will not gain much insight into the thermalization process. Hence we assume that the rate constants of the energy transfer to C151 and from C151 are identical ($1/\tau_{vib}$). Under this assumption, the response function of C151 (g(t)) after impulsive heating is given by

$$g(t) = \frac{C_{solvent}}{C_{C151}} \frac{t}{\tau_{vib}} \exp(-t/\tau_{vib}) \qquad (3\text{-}6)$$

where C_{C151} is the heat capacity of C151. Therefore the experimentally observed $\Delta T_{C151}(t)$ is expressed by

$$\Delta T_{C151}(t) = \int_{-\infty}^{t} \Delta T_{DEA}(t-t')\, g(t')\, dt' \,. \qquad (3\text{-}7)$$

In this calculation, we assumed N_{DEA}=2. Although ~10 solvent molecules should exist in the first solvent shell, a small N_{DEA} was used for the following reasons. (1) If we use a large N_{DEA}, the calculated temperature rise becomes rather low (e.g., $\Delta T \approx 7$ K for N_{DEA}=10). This low temperature rise is inconsistent with the estimated ΔT from the broadening of the absorption edge (~66 K) and may not be detected as the hot band absorption. (2) Sukowski et al. fitted the experimentally observed energy loss curve of azulene successfully by a similar model. They assumed that one solvent molecule accept the excess energy from azulene in the first step of the vibrational cooling. [17] (3) Schultz et al. speculated that azulene can strongly couple to the solvents above and below the azulene plane from the molecular dynamics simulation. [75] (4) Schwarzer et al. assumed two solvent molecules form the first solvent shell around azulene in a similar calculation. [66]

The S_1-S_0 energy spacing ($E(S_1)$) is estimated to be ~14500 cm^{-1}. [75, 82] The molecular size of the solvent (L) is estimated from the Lennard-Jones parameters. [68] The radius (R=3.5 Å) and the heat capacity (C_{solute}=186 J mol^{-1} K^{-1}) of azulene were estimated from Ref. 17. The literature values were used for the heat capacities of the solvents. [61] The ratio of $C_{C151}/C_{solvent}$ was obtained by a semi-empirical molecular orbital calculation by AM1 method with MOPAC program package. The other parameters used in the calculation are listed in Table 3-1.

Even using this simple model, the energy transfer rate from azulene to solvent ($1/\tau$) and the thermal excitation rate of C151 ($1/\tau_{vib}$) could not be determined independently by the fitting of the observed transient temperature under our signal to noise ratio. After calculating the temporal profile of the transient temperature of C151 using various parameters, it was found that the profiles calculated with the same $\tau_{sum}=\tau+2.5\ \tau_{vib}$ give very similar curves. Hence we can determine only

Table 3-1. ΔT and ν_{00} obtained from the broadening of the $S_0 \rightarrow S_1$ absorption tail of C151, τ_{sum} to reproduce the observed time profile of the hot band signal from Az-CH_2-C151, and the parameters used in the calculations.

	ethanol	2-propanol	acetone	benzene
ΔT / K	66	17	26	68
ν_{00} / cm^{-1}	22400	22800	23400	24200
τ_{sum} / ps [a)]	2	2	5	3
$C_{solvent}$ / J K^{-1} mol^{-1}	112	157	136	126
L / Å	4	4.5	4	5.5
D / 10^{-8} m^2 s^{-1}	8.6	6.9	9.3	9.4

a) Uncertainty of τ_{sum} is ±1 ps.

τ_{sum} from the fitting of the observed profile. The best fit of the experimentally observed profile is obtained by using τ_{sum}=2 ps in ethanol. The calculated temperature rise was ~30 K. This value is close to that obtained from absorption broadening (~ 66 K) as stated before.

The calculated temperature profile reproduces the observed one well (solid line in Fig. 3-4(b)). Therefore the vibrational cooling time of azulene should be shorter than 2 ps, which is much shorter than the vibrational relaxation time obtained by monitoring the vibrational temperature of azulene itself. [17, 66] Similar short cooling times were observed also in the other solvents (Table 3-1).

What is the origin of the difference between the thermalization times determined here and those reported previously? We may think the following two possibilities. First, by combining the methylene group and C151, the density of state around azulene should be increased. As a result, the coupling between the vibrational modes of azulene and the translational mode of the DEA solvents becomes strong and the cooling time of azulene could be faster than the isolated azulene case. Second, the non-uniform intramolecular vibrational relaxation may participate in the difference. If the intramolecular vibrational redistribution is fast enough compared with the vibrational cooling process, the temperature decrease monitored from the solute temperature should be the same as the temperature increase monitored outside of the solute. However, if the intramolecular vibrational relaxation is not fast enough compared with the thermalization process, we should observe several kinetics in the thermalization process. For example, it could be possible that the hot band detection method in the previous studies monitored the population of the vibrational levels with low vibrational quantum numbers, while the transient temperature detection in this study monitors overall energy transfer from azulene to the solvent. If most of the vibrational populations dissipate their excess energy to the solvents very fast, the temperature of the solvent rises very fast and the minor part of the temperature rise could not be detected. On the other hand, the hot band detection of azulene is sensitive to the population dynamics of the vibrational levels with relatively large Frank-Condon factors to the S_1 state and the relaxation of these states could be slow.

A typical time scale of the intramolecular vibrational relaxation has been believed to be in a range of sub-ps for large molecules. [1-3] If this is the case for azulene, the second explanation is unrealistic. Recently, however, slow intramolecular relaxation processes (several ps) have been observed in the several large molecules. [18-26] For example, Nakabayashi et al. studied the intramolecular vibrational relaxation of *trans*-stilbene by the picosecond time resolved anti-Stokes

Raman spectroscopy. [25, 26] They found that the non-equilibrium S_1 state persists for several ps after photoexcitation. The intramolecular vibrational relaxation time of azulene may be in a ps time scale. Schwarzer et al. considered that 3ps may be a reasonable intramolecular relaxation time for azulene when they found that the cooling rates were deviated from the isolated binary collision model in a higher density region. [66] The deviation started from the density in which the time between collisions by the solvent molecules was estimated to be 3 ps. To clarify the existence of the fast energy dissipation process, a photothermal spectroscopic study on the vibrational cooling of azulene is required.

The determined τ_{sum} depends on the solvent (Table 3-1). The thermalization (and the thermal excitation) occurs faster in the alcoholic solution. We believe that the short thermalization time in the alcoholic solvent is due to the hydrogen bonding between azulene and the solvent. It was already reported that the hydrogen bond formation has a strong influence on the vibrational cooling rate of azulene. [66] The same tendency has been reported in other systems. [30, 34, 103, 104] Recently, McDowell studied the collisional deactivation of the triplet pyrazine in the gas phase. [103] They found that water is an unusually strong vibrational relaxer. Terazima reported that the thermalization rate of Betaine-30 has a good correlation with the hydrogen bond density. [34] The thermalization time in a mixture of water and ethanol becomes shorter with increasing the mole fraction of water. The importance of the hydrogen bonding was suggested theoretically by the molecular dynamics simulation, too. [104] In non-alcohol solvents, τ_{sum} in acetone is longer than that in benzene. This result implies that the polarity of the solvent is not important for determining the rate of the thermalization process. This is consistent with the previous observation of the vibrational cooling of azulene. [17, 66]

The time profile of the transient absorption of Az-$(CH_2)_3$-C151 (Fig. 3-9(b)) is very similar to that of Az-CH_2-C151 except for the signal intensity. Naturally the profile can be fitted by the same model presented for Az-CH_2-C151 (solid line in Fig. 3-7(b)). If the propylene chain is stretched out, the distance between azulene and C151 is estimated to be ~11 Å from the semi-empirical molecular orbital calculation. In this case, the time profile of the transient temperature is clearly delayed and does not reproduce the observed signal (broken line in Fig. 3-9(b)). This result indicates that the C151 moiety should locate near the azulene moiety due to the flexibility of the propylene chain. One

of notable differences is that the signal intensity of Az-$(CH_2)_3$-C151 is ~3 times weaker than that of Az-CH_2-C151. The weaker intensity may come from two factors. First, the distance between azulene and C151 could be rather broadly distributed. From the signal intensity, we think that about ~1/3 of C151 locates in the vicinity of azulene. It was reported that the chromophores connected with a flexible spacer can be close to each other. [101, 102, 105, 106] Second, since the thermal energy is conducted uniformly in space, the temperature rise at a far distance from the molecular heater should be smaller than that at a closer distance. Hence, the compound that has a long distance between azulene and C151 cannot contribute to the transient temperature signal significantly. We think that these two factors make the time profile of the transient temperature of Az-$(CH_2)_3$-C151 similar to that of Az-CH_2-C151.

It may be interesting to note that the deviation of the calculated temperature rise from the observed signal can be seen in the long time delay. This feature was always observed also in benzene although the signal to noise ratio is not good. This long tail may represent the time development of the temperature at the outer sphere, which was monitored by the lengthened form of Az-$(CH_2)_3$-C151. It may be very interesting to study the transient temperature from compounds with a rigid spacer between the two chromophores to fix the distance between the heater and the thermometer. Such molecular integrated systems will provide ideal systems for revealing the thermalization process with a high spatial resolution. A study along this line will be conducted in this group in future.

3-5. Conclusion

A very fast vibrational cooling process of azulene was studied by the transient absorption method using molecular integrated systems with a molecular thermometer (C151). Vibrationally highly excited azulene (molecular heater) is formed by the light absorption into the S_1 state and the subsequent relaxation to the ground state by the internal conversion with a lifetime of 1 ps. After the azulene moiety was photoexcited, the transient absorption signal was observed at the red edge of the $S_0 \rightarrow S_1$ absorption band of the C151 moiety. This is explained by the heating of the surrounding solvent, which changes the temperature of the C151 moiety. The rise rate of this signal should be determined by the cooling rate of azulene, the heat conduction from azulene to C151, and the thermal excitation rate of C151 through the solvents. First, a compound combined with the methylene chain between the heater and the thermometer (Az-CH_2-C151) was examined. From the optimized

structure, we think that the thermometer should monitor the transient temperature of the solvent in the first solvent shell. The cooling time of azulene was found to be less than 2~5 ps. This result indicates that there is a very fast thermalization process of hot azulene than that reported from the hot band detection of azulene itself. This vibrational cooling rate depends on the solvent. It was found that the hydrogen bonding strongly affects the thermalization time. The transient absorption spectrum as well as the time profile of a compound with a longer chain (Az-$(CH_2)_3$-C151) are very similar to those of Az-CH_2-C151 except for the signal intensity. This fact indicates that about ~1/3 of C151 moiety locates in the vicinity of azulene moiety because of the flexibility of the propylene chain. The deviation from the calculated signal was observed in the long time delay, which may reflect the temperature of the solvent in the outer shell.

3-6. Synthesis

3-6-1. Az-CH_2-C151

7-((Azulene-1-yl) methylideneamino)-4-trifluoromethylcoumarin (Az-CH=C151)

A 50-ml flask equipped with a Dien-Stark trap, a magnetic stirrer and a reflux condenser was charged with 0.458 g (2 mmol) of 7-amino-4-trifluoromethylcoumarin (C151), 1-azulenecarboxaldeh yde (0.312 g, 2 mmol), *p*-toluenesulfonic acid (0.0380 g, 0.2 mmol) and toluene (25 ml). 1-azulenecarboxaldehyde was prepared from azulene by the previously reported method. [107, 108] This mixture was heated to reflux in an oil bath under nitrogen with stirring for 2 days. The mixture was cooled to room temperature and the orange-red solid was collected by filtration. The solid was washed twice with benzene and dried *in vacuo* to give 0.530 g (1.4 mmol, 70%) of pure Az-CH=N-C490. ^{1}H NMR (δ in $CDCl_3$) 9.49 (d, 1H, *J*=9.5 Hz, azulene ring), 8.99 (s, 1H, -CH=N-), 8.47 (d, 1H, *J*=9.5 Hz, azulene ring), 8.34 (d, 1H, *J*=4.0 Hz, azulene ring), 7.82 (t, 1H, *J*=9.8 Hz, azulene ring), 7.75 (dd, 1H, *J*=8.5 Hz, 1.3 Hz, coumarin ring), 7.55 (t, 1H, *J*=9.8 Hz, azulene ring), 7.46 (t, 1H, *J*=10 Hz, azulene ring), 7.44 (d, 1H, *J*=4.5 Hz, azulene ring), 7.29 (d, 1H, *J*=8.5 Hz, coumarin ring), 7.28 (d, 1H, *J*=9.0 Hz, coumarin ring), 6.72 (s, 1H, coumarin ring). Mass spectrum 368 (calcd for $M+H^+$: 368).

7-((Azulene-1-yl) methylamino)-4-trifluoromethylcoumarin (Az-CH_2-C151)

Az-CH=C151 (0.25 g, 0.7 mmol) was dissolved in 10 ml ethanol, and sodium borohydride (0.0265 g, 0.7 mmol) was added to the solution. In the dark, the solution was stirred for 2 days at

room temperature under nitrogen. Water (~0.5 ml) was added to the reaction mixture, allowed to stand for ~5 min, and evaporated. The crude product was dissolved in 20 ml of benzene and the dark purple solid was removed by filtration. The filtrate was chromatographed first on alumina (SUMITOMO KAGAKU KCG-1525, 2 cm in diameter and 3 cm height) with 1% methanol/benzene (v/v), and then on size-extrication column (BIO-RAD BIO-BEANS S-X1, 5 cm diameter and 50 cm height) with benzene. The first green fraction was collected and evaporated, to yield 0.0574 g (0.16 mmol, 22%) of Az-CH_2-C151. ^{1}H NMR (δ in $CDCl_3$) 8.37 (d, 2H, *J*=9.5 Hz, azulene ring), 7.92 (d, 1H, *J*=3.5 Hz, azulene ring), 7.67 (t, 1H, *J*=9.8 Hz, azulene ring), 7.49 (dd, 1H, *J*=8.5 Hz, 2.0 Hz, coumarin ring), 7.37 (t, 1H, *J*=4.5 Hz, azulene ring), 7.24 (td, 1H, *J*=10 Hz, 2.0 Hz, azulene ring), 6.61 (m, 2H, coumarin ring), 6.44 (s, 1H, coumarin ring), 4.83 (d, 2H, *J*=4.0 Hz, -CH_2-), 4.64 (s, 1H, -NH-). Mass spectrum 370 (calcd for M+H^+: 370).

3-6-2. Az-$(CH_2)_3$-C151

Ethyl 3-(azulene-1-yl)-2-propenate (Az-CH=$CHCO_2C_2H_5$)

Triethyl phosphonoacetate (0.432 g, 1.92 mmol) was dissolved in 3 ml benzene, and was slowly added to sodium hydride (60 % oil suspension) (0.0846 g, 2.12 mmol) under nitrogen. This mixture was stirred for 1 hour. A solution of 1-azulenecarboxaldehyde (0.1 g, 0.641 mmol) in benzene (7 ml) was added under nitrogen, and the solution was heated to 60-65 °C with stirring for 5 hours. The mixture was washed with water and extracted with benzene then evaporated. The resulting solid was chromatographed on silica gel with 10% ethyl acetate/hexane (v/v). The third dark blue fraction was collected and evaporated, to yield 0.111 g (0.491 mmol, 77 %) of Az-CH=$CHCO_2C_2H_5$. ^{1}H NMR (δ in $CDCl_3$) 8.60 (d, 1H, *J*=10.5 Hz, azulene ring), 8.32 (d, 1H, *J*=15.5 Hz, -CH=), 8.31 (d, 1H, *J*=10.5 Hz, azulene ring), 8.20 (d, 1H, *J*=4.0 Hz, azulene ring), 7.67 (t, 1H, *J*=10 Hz, azulene ring), 7.41 (d, 1H, *J*=4.5 Hz, azulene ring), 7.32 (t, 1H, *J*=10 Hz, azulene ring), 7.26 (t, 1H, *J*=10 Hz, azulene ring), 6.47 (d, 1H, *J*=15.5 Hz, =CH-), 4.30 (q, 2H, *J*=7.0 Hz, -CH_2-), 1.37 (t, 3H, *J*=7.5 Hz, -CH_3).

Ethyl 3-(azulene-1-yl)-2-propanate (Az-$CH_2CH_2CO_2C_2H_5$)

A mixture of Az-CH=$CHCO_2C_2H_5$ (0.402 g, 1.78 mmol), nickel(II) chloride hexahydrate (0.127 g, 0.534 mmol) and sodium borohydride (0.404 g, 10.7 mmol) was dissolved in methanol (20 ml), and stirred under nitrogen for 2 hours. The mixture was washed with water, extracted with

dichloromethane then evaporated, to yield 0.333 g (1.46 mmol, 82 %) of Az-$CH_2CH_2CO_2C_2H_5$. ^{1}H NMR (δ in $CDCl_3$) 8.31 (d, 1H, *J*=9.5 Hz, azulene ring), 8.26 (d, 1H, *J*=9 Hz, azulene ring), 7.79 (d, 1H, *J*=4.0 Hz, azulene ring), 7.55 (t, 1H, *J*=10.5 Hz, azulene ring), 7.33 (d, 1H, *J*=4.0 Hz, azulene ring), 7.12 (t, 1H, *J*=10 Hz, azulene ring), 7.09 (t, 1H, *J*=9.5 Hz, azulene ring), 4.13 (q, 2H, *J*=7.0 Hz, -CH_2-), 3.42 (t, 2H, *J*=8.0 Hz, -CH_2-), 2.76 (t, 2H,*J*=8.0 Hz, -CH_2-), 1.22 (t, 3H, *J*=7.0 Hz, -CH_3).

3-(Azulene-1-yl)-1-hydroxypropane (Az-$(CH_2)_3OH$)

Lithium aluminum hydride (0.222 g, 5.84 mmol) was added to a solution of Az-$CH_2CH_2CO_2C_2H_5$ (0.333 g, 1.46 mmol) in dry dimethyl ether (20 ml). The solution was immersed in an ice bath and stirred under nitrogen for 3 hours. The mixture was washed with water and extracted with diethyl ether then evaporated. The resulting solid was chromatographed on silica gel with 50% ethyl acetate/hexane (v/v). The second blue fraction was collected and evaporated, to yield 0.0639 g (0.351 mmol, 24 %) of Az-$(CH_2)_3OH$. ^{1}H NMR (δ in $CDCl_3$) 8.30 (d, 1H, *J*=9 Hz, azulene ring), 8.25 (d, 1H, *J*=9 Hz, azulene ring), 7.80 (d, 1H, *J*=4.0 Hz, azulene ring), 7.54 (t, 1H, *J*=10 Hz, azulene ring), 7.34 (d, 1H, *J*=3.5 Hz, azulene ring), 7.09 (t, 1H, *J*=10 Hz, azulene ring), 7.07 (t, 1H, *J*=10 Hz, azulene ring), 3.72 (dt, 2H, *J*=6.0 Hz, -CH_2-), 3.18 (t, 2H, *J*=7.5 Hz, -CH_2-), 2.04 (tt, 2H, *J*=7.0 Hz,.-CH_2-).

3-(Azulene-1-yl)-1-propyl-methylsulfonate (Az-$(CH_2)_3OSO_2CH_3$)

A mixture of Az-$(CH_2)_3OH$ (0.0243 g, 0.134 mmol) and methanesulfonyl chloride (0.0460 g, 0.402 mmol) was dissolved in dry pyridine (10 ml). The mixture was stirred under nitrogen for 30 minutes, then washed with 1N HCl, extracted with dichloromethane and evaporated, yield to 0.0326 g (0.116 mmol, 87 %) of Az-$(CH_2)_3OSO_2CH_3$. ^{1}H NMR (δ in $CDCl_3$) 8.27 (d, 2H, *J*=9.5 Hz, azulene ring), 7.79 (d, 1H, *J*=4.0 Hz, azulene ring), 7.56 (t, 1H, *J*=10 Hz, azulene ring), 7.35 (d, 1H, *J*=3.5 Hz, azulene ring), 7.13 (t, 1H, *J*=9.5 Hz, azulene ring), 7.10 (t, 1H, *J*=9.5 Hz, azulene ring), 4.24 (t, 2H, *J*=6.5 Hz, Az-CH_2-), 3.23 (t, 2H, *J*=8.0 Hz, -CH_2-OSO_2-), 2.96 (s, 3H, -CH_3), 2.22 (tt, 2H, *J*=7.0 Hz,.-CH_2-).

1-(Azulene-1-yl)-3-idopropane (Az-$(CH_2)_3I$)

Az-$(CH_2)_3OSO_2CH_3$ (0.0326 g, 0.116 mmol) was added to the saturated sodium iodide / acetone solution (10 ml). This mixture was heated to reflux in an oil bath under nitrogen with stirring for 2 hours. The mixture was washed with water, extracted with dichloromethane and evaporated,

yield to 0.0283 g (0.0956 mmol, 82%) of Az-$(CH_2)_3$I. ^{1}H NMR (δ in $CDCl_3$) 8.32 (d, 1H, *J*=9.5 Hz, azulene ring), 8.26 (d, 1H, *J*=9 Hz, azulene ring), 7.79 (d, 1H, *J*=3.5 Hz, azulene ring), 7.55 (t, 1H, *J*=10 Hz, azulene ring), 7.34 (d, 1H, *J*=4.5 Hz, azulene ring), 7.12 (t, 1H, *J*=9.5 Hz, azulene ring), 7.09 (t, 1H, *J*=10 Hz, azulene ring), 3.20 (t, 4H, *J*=7.0 Hz, Az-CH_2- and -CH_2I), 2.27 (tt, 2H, *J*=7.0 Hz,.-CH_2-). Mass spectrum 296 (calcd for M^+: 296).

7-((Azulene-1-yl) propylamino)-4-trifluoromethylcoumarin (Az-$(CH_2)_3$-C151)

A mixture of Az-$(CH_2)_3$I (0.0283 g, 0.0956 mmol), C151 (0.0219 g, 0.0956 mmol) and potassium carbonate (0.0264g, 0.191 mmol) was dissolved in butylnitrile(10 ml). The mixture was heated to reflux under nitrogen for 1.5 days. The crude product was dissolved in benzene and the dark solid was removed by filtration. The filtrate was chromatographed on silica gel with dichloromethane. The green fraction was collected and evaporated, to yield 0.0015 g (0.0038 mmol, 4.0%) of Az-$(CH_2)_3$-C151. ^{1}H NMR (δ in $CDCl_3$) 8.28 (d, 1H, *J*=9.0 Hz, azulene ring), 8.25 (d, 1H, *J*=10 Hz, azulene ring), 7.78 (d, 1H, *J*=3.5 Hz, azulene ring), 7.55 (t, 1H, *J*=10 Hz, azulene ring), 7.40 (dd, 1H, *J*=9.0 Hz, 2.0 Hz, coumarin ring), 7.36 (d, 1H, *J*=4.0 Hz, azulene ring), 7.10 (t, 1H, *J*=9.5 Hz, azulene ring), 7.08 (t, 1H, *J*=10.5 Hz, azulene ring), 6.40 (m, 3H, coumarin ring), 5.27 (s, 1H,-NH-), 4.30 (d, 2H, *J*=7.0 Hz, Az-CH_2-), 3.24 (dt, 2H, -CH_2-), 2.14 (tt, 2H, *J*=7.0 Hz, -CH_2-). Mass spectrum 397 (calcd for M^+: 397).

All ^{1}H NMR spectra were recorded on a JEOL alpha-500 (operating at 500 MHz), and FAB-MS spectra were recorded on a JEOL HX-110 with 3-nitrobenzyl alcohol matrix. Azulene (Lancaster) and C151 (SIGMA) were used as received.

4. Summary

The thermalization processes in the several systems were studied by detecting the temperature rise of the surrounding solvent. At first, photophysical and thermalization processes after photoexcitation of 2-(2'-hydroxy-5'-methylphenyl)benzotriazole (HMPB) in cyclohexane and 2-hydroxybenzophenone (HBP) in various solvents were investigated by the transient grating (TG) method. These molecules undergo the proton transfer reaction in the excited states. The rapid energy dissipation of HMPB and HBP are resulted from these proton transfer processes. In the time profiles of the population grating (PG) signals, two distinct kinetics were observed for HMPB and HBP. For HMPB, the faster (600 fs) kinetics is attributed to the back proton transfer reaction in the ground state, and the faster process of HBP (400 fs) is attributed to the vibrational cooling in the S_1 state. The slower one (~30 ps) of both compounds is assigned to the vibrational cooling in the S_0 state. In ethanol (hydrogen bonding solvent), the PG signal originated from the T_1 state of HBP is apparent. However, the dissipated heat from the T_1 state is negligibly small and the triplet quantum yield was found to be less than 0.05. The photoexcited HBP relaxes to the ground state by the internal conversion dominantly even in ethanol. The thermalization rates of these molecules were measured from a point of view of the translational energy of solvents by the acoustic peak delay method of the TG signal. The observed delay times of the acoustic peak position are shorter than 30 ps (cooling time in the S_0 state) in all solvents used here (10 ps in hexane, 13 ps in cyclohexane, 12 ps in acetonitrile and 7 ps in ethanol). The results show that there are, at least, two cooling kinetics in these systems. Then we introduced a simple thermalization model. In this model, first, the hot solute transfers its excess energy to strongly coupled surrounding solvent molecules in the first solvent shell, then the excess energy of the solvent diffuse to the bulk medium by the thermal diffusion. The time development of the temperature calculated based on this thermalization model explains the experimental observations. From these analyses, it is revealed that in the early step of the thermalization, there is a very fast cooling process (less than a few ps) and then the heated solvent molecule becomes cool by the thermal diffusion to the bulk solvents. The thermalization processes depend on both of the solute and solvent properties.

Second, the vibrational cooling process of photoexcited azulene was studied by using a combined molecular thermometer (coumarin 151 (C151)). The transient absorption at the red edge of

the absorption band of C151 detected after the photoexcitation of azulene is attributed to the hot band absorption of C151 for following reasons. (1) Any signal was not observed from the sample which contained only azulene or C151 under the same experimental condition. (2) The wavelength in which the transient signal appears is on the red edge of the absorption band of C151. (3) The wavelength region in which the transient absorption signal appears depends on the solvent and this dependence can be reasonably explained by the solvatochromic shift of the C151 absorption band. The heating process of the first solvent shell around the photoexcited azulene was detected by using an azulene-coumarin integrated system connected with a methylene group (Az-CH_2-C151) in several solvents. The time profiles of the transient absorption signals were analyzed by a thermalization model, which includes the intermolecular energy transfer from azulene to the solvents and the thermal diffusion among the solvent. The cooling times of azulene in these solvents were found to be less than 2~5 ps. These results indicate that there is a very fast cooling process after the relaxation of the electronically excited state compared with that reported before. The observed thermalization time depends on the solvent. In particular, the excess energy dissipates effectively in the hydrogen bonding solvents (ethanol and 2-propanol). The transient absorption spectrum and its time profile of a compound with a longer chain (Az-$(CH_2)_3$-C151) are very similar to those of Az-CH_2-C151 except the much weaker intensity. These facts indicate that the molecular structure of Az-$(CH_2)_3$-C151 is flexible and the distance between the thermometer (C151) and the heater (azulene) has a distribution. The compounds in that C151 locates in vicinity of azulene mainly participate in the transient absorption signal.

References

1. G. R. Fleming, *Chemical Applications of Ultrafast Spectroscopy*, Oxford University Press, 1986, New York.
2. W. Kaiser, *Ultrashort laser pulses and applications*, 2nd ed., Springer-Verlag, 1993, New York.
3. T. Elsaesser, W. Kaiser, *Annu. Rev. Phys. Chem.*, **42**, 83 (1991).
4. A. Laubereau, A. Seilmeier, W. Kaiser, *Chem. Phys. Lett.*, **36**, 232 (1975).
5. A. Penzkofer, W. Falkenstein, W. Kaiser, *Chem. Phys. Lett.*, **44**, 82 (1976).
6. K. Spanner, A. Laubereau, W. Kaiser, *Chem. Phys. Lett.*, **44**, 88 (1976).
7. A. Fendt, S. F. Fischer, W. Kaiser, *Chem. Phys. Lett.*, **82**, 350 (1981).
8. C. Kolmeder, W. Zinth, W. Kaiser, *Chem. Phys. Lett.*, **91**, 323 (1982).
9. W. Zinth, C. Kolmeder, B. Benna, A. Irgens-Defregger, S. F. Fischer, W. Kaiser, *J. Chem. Phys.*, **78**, 3916 (1983).
10. N. H. Gottfried, W. Kaiser, *Chem. Phys. Lett.*, **101**, 331 (1983).
11. F. Wondrazek, A. Seilmeier, W. Kaiser, *Chem. Phys. Lett.*, **104**, 121 (1984).
12. A. Seilmeier, P. O. J. Scherer, W. Kaiser, *Chem. Phys. Lett.*, **105**, 140 (1984).
13. N. H. Gottfried, A. Seilmeier, W. Kaiser, *Chem. Phys. Lett.*, **111**, 326 (1984).
14. W. Wild, A. Seilmeier, N. H. Gottfried, W. Kaiser, *Chem. Phys. Lett.*, **119**, 259 (1985).
15. P. O. J. Scherer, A. Seilmeier, W. Kaiser, *J. Chem. Phys.*, **83**, 3948 (1985).
16. H.-J. Hübner, M. Wörner, W. Kaiser, A. Seilmeier, *Chem. Phys. Lett.*, **182**, 315 (1991).
17. U. Sukowski, A. Seilmeier, T. Elsaesser, and S. F. Fischer, *J. Chem. Phys.*, **93**, 4094 (1990).
18. R. J. Sension; A. Z. Szarka, R.M. Hochstrasser, *J. Chem. Phys.*, **97**, 5239 (1992).
19. M. C. Schneebeck, L. E. Vigil, M. R. Ondrias, *Chem. Phys. Lett.*, **215**, 251 (1993).
20. K. Lenz, M. Pfeiffer, A. Lau, T. Elsaesser, *Chem. Phys. Lett.*, **229**, 340 (1994).
21. J. Qian, S. L. Schultz, J. M. Jean, *Chem. Phys. Lett.*, **233**, 9 (1995).
22. A. P. Shreve, R. A. Mathies, *J. Phys. Chem.*, **99**, 7285 (1995).
23. S. G. Kruglik, Y. Mizutani, T. Kitagawa, *Chem. Phys. Lett.*, **266**, 283 (1997).
24. Y. Mizutani, T. Kitagawa, *Science*, **278**, 443 (1997).
25. T. Nakabayashi, H. Okamoto, M. Tasumi, *J. Phys. Chem. A*, **101**, 7189 (1997).
26. T. Nakabayashi, H. Okamoto, M. Tasumi, *J. Phys. Chem. A*, **102**, 9686 (1998).
27. L. Nikowa, D. Schwarzer, J. Troe, *Ber. Bunsenges. Phys. Chem.*, **98**, 262 (1994).

28. L. Nikowa, D. Schwarzer, J. Troe, *Chem. Phys. Lett.*, **233**, 303 (1995).
29. K. Iwata, H. Hamaguchi, *J. Phys. Chem. A*, **101**, 632 (1997).
30. M. Terazima, *J. Chem. Phys.* **105**, 6587 (1996).
31. T. Okazaki, N. Hirota, M. Terazima, *J. Phys. Chem. A*, **101**, 650 (1997).
32. M. Takezaki, N. Hirota, M. Terazima, *J. Phys. Chem. A*, **101**, 3443 (1997).
33. M. Terazima, M. Takezaki, S. Yamaguchi, N. Hirota, *J. Chem. Phys.*, **109**, 603 (1998).
34. M. Terazima, *Chem. Phys. Lett.*, in press.
35. 岡本裕巳, 分光研究, **47**, 209 (1998).
36. M. Terazima, *Adv. Photochem.*, **24**, 255 (1998).
37. 寺嶋正秀, 分光研究, **47**, 230 (1998).
38. D. Bailey, O. Vogl, *J. Macromol. Sci.-Rev. Macromol. Chem.*, **14**, 267 (1976).
39. K. P. Ghiggino, A. D. Scully, I. H. Leaver, *J. Phys. Chem.*, **90**, 5089 (1986).
40. Y. R. Kim, J. T. Yardley, R. M. Hochstrasser, *Chem. Phys.*, **136**, 311 (1989).
41. M. Wiechmann, H. Port, F. Laermer, W. Frey, T. Elsaesser, *Chem. Phys. Lett.*, **165**, 28 (1990).
42. M. Wiechmann, H. Port, F. Lärmer, W. Frey, T. Elsaesser, *J. Phys. Chem.*, **95**, 1918 (1991).
43. W. Frey, T. Elsaesser, *Chem. Phys. Lett.*, **189**, 565 (1992).
44. C. Chudoba, S. Lutgen, T. Jentzsch, E. Riedle, M. Woerner, T. Elsaesser, *Chem. Phys. Lett.*, **240**, 35 (1995).
45. C. Chudoba, E. Riedle, M. Pfeiffer, T. Elsaesser, *Chem. Phys. Lett.*, **263**, 622 (1996).
46. M. Pfeiffer, A. Lau, K. Lenz, T. Elsaesser, *Chem. Phys. Lett.*, **268**, 258 (1997).
47. S. E. Braslavsky, G. E. Heibel, *Chem. Rev.*, **92**, 1381 (1992).
48. A. A. Lamola, L. J. Sharp, *J. Phys. Chem.*, **70**, 2634 (1966).
49. S. Y. Hou, W. M. Hetherington III; G. M. Korenowski, K. B. Eisenthal, *Chem. Phys. Lett.*, **68**, 282 (1979).
50. C. Merritt, G. W. Scott, A. Gupta, A. Yavrouian, *Chem. Phys. Lett.*, **69**, 169 (1980).
51. K. J. Choi, L. A. Hallidy, and M. R. Topp, in *Picosecond Phenomena II*, edited by R. Hochstrasser, W. Kaiser, and C. V. Shank, (Springer-Verlag, Berlin, 1980).
52. J. C. Scaiano, *Chem. Phys. Lett.*, **92**, 97 (1982).
53. K. B. Eisenthal, *Ultrafast Chemical Reactions in the Liquid State*, in *Ultrashort laser pulses and applications*, 2nd ed. by W. Kaiser, (Springer-Verlag, New York, 1993).
54. P. F. McGarry, S. Jockusch, Y. Fujiwara, N. A. Kaprinidis, N. J. Turro, *J. Phys. Chem. A*,

101, 764 (1997).

55. A. C. Bhasikuttan, A. K. Singh, D. K. Palit, A. V. Sapre, J. P. Mittal, *J. Phys. Chem. A*, **102**, 3470 (1998).

56. M. Takezaki, N. Hirota, M. Terazima, *J. Phys. Chem.*, **100**, 10015 (1996).

57. M. W. Schmidt, K. K. Baldridge, J. A. Boatz, S. T. Elbert, M. S. Gordon, J. H. Jensen, S. Koseki, N. Matsunaga, K. A. Nguyen, S. Su, T. L. Windus, M. Dupuis, J. A. Montgomery,Jr., *J. Comput. Chem.*, **14**, 1347 (1993).

58. H. J. Eichler, P. Günter, and D. W. Pohl, *Laser-Induced Dynamic Gratings* ; (Springer-Verlag, Berlin, 1986).

59. L. Genberg; Q. Bao, S. Gracewski, R. J. D. Miller, *Chem. Phys.* **131**, 81 (1989).

60. J. Deàk, H. Chiu, C. M. Lewis, R. J. D. Miller, *J. Phys. Chem. B*, **102**, 6621 (1998).

61. *Handbook of Chemistry and Physics,* 73rd ed., (CRC press, Boca Raton, 1992).

62. A. L. Sobolewski,W. Domcke, *Chem. Phys.*, **184**, 115 (1994).

63. M. V. Verner, S. Scheiner, *J. Phys. Chem.*, **99**, 642 (1995).

64. J. Catalán, J. Palomar, J. L. G. De Paz, *J. Phys. Chem. A*, **101**, 7914 (1997).

65. T. Nishiya, S. Yamauchi, N. Hirota, M. Baba, I. Hanazaki, *J. Phys. Chem.*, **90**, 5730 (1986).

66. D. Schwarzer, J. Troe, M. Votsmeier, M. Zerezke, *J. Chem. Phys.*, **105**, 3121 (1996).

67. H. S. Carslaw, J. C. Jaeger, *Conduction of Heat in Solids*, 2nd ed., (Oxford University, Oxford, 1959).

68. F. M. Mourits, F. H. A. Rummens, *Can. J. Chem.*, **55**, 3010 (1979).

69. J. T. Edward, *J. Chem. Edc.*, **47**, 261 (1970).

70. M. Nagaoka, Y. Okuno, T. Yamabe, *J. Phys. Chem.*, **98**, 12506 (1994).

71 J. R. Baker, *J. Phys. Chem.,* **88**, 11 (1984).

72. H. Hippler, L. Lindemann, J. Troe, *J. Chem. Phys.*, **83**, 3906 (1985).

73. L. Brouwer, H. Hippler, L. Lindemann, J. Troe, *J. Phys. Chem.*, **89**, 4608 (1985).

74. U. Hold, T. Lenzer, K. Luther, K. Reihs, A. Symonds, *Ber. Bunsenges. Phys. Chem.*, **101**, 552 (1997).

75. K. E. Schultz, D. J. Russell, C. B. Harris, *J. Chem. Phys.*, **97**, 5431 (1992).

76. D. Schwarzer, J. Troe, M. Votsmeier, M. Zerezke, *Ber. Bunsenges. Phys. Chem.*, **101**, 595 (1997).

77. D. Schwarzer, J. Troe, M. Zerezke, *J. Chem. Phys.*, **107**, 8380 (1997).

78. D. Schwarzer, J. Troe, M. Zerezke, *J. Phys. Chem. A*, **102**, 4207 (1998).

79. C. Hidelbach, I. I. Fedchenia, D. Schwarzer, J. Schroeder, *J. Chem. Phys.*, **108**, 10152 (1998).

80. C. Hidelbach, J. Schroeder, D. Schwarzer, V. S. Vikhrenko, *Chem. Phys. Lett.*, **291**, 333 (1998).

81. D. Schwarzer, J. Troe, J. Schroeder, *Ber. Bunsenges. Phys. Chem.*, **95**, 933 (1991).

82. B. D. Wagner, M. Szymanski, R. P. Steer, *J. Chem. Phys.*, **98**, 301 (1993).

83. Proceedings of the international conference on photoacoustic and photothermal phenomena such as *J. de Phys.*, vol. 4, C7 (1994); *Progress in Natural Science*, vol. 6, China (1996).

84. Y. Kimura, Y. Takebayashi, N. Hirota, *J. Chem. Phys.*, **108**, 1485 (1998).

85. Y. Yoshimura, J. Osugi, M. Nakahara, *J. Am. Chem. Soc.*, **105**, 5414 (1983).

86. Y. Tanaka, T. Yamamoto, Y. Satomi, H. Kubota, T. Makita, *Rev. Phys. Chem. Japan*, **47**, 12 (1977).

87. J. H. Dymond, N. Glen, J. Robertson, J. D. Isdale, *J. Chem. Thermodynamics*, **14**, 1149 (1982).

88. T. Gustavsson, L. Cassara, V. Gulbinas, G. Gurzadyan, J.-C. Mialocq, S. Pommeret, M. Sorgius, P. van der Meulen, *J. Phys. Chem. A*, **102**, 4229 (1998).

89. R. J. Sension, S. T. Repinec, R. M. Hochstrasser, *J. Chem. Phys.*, **93**, 9185 (1990).

90. T. Hagan, D. Pilloud, P. Suppan, *Chem. Phys. Lett.*, **139**, 499 (1987).

91. P. Suppan, *J. Photochem. Photobio. A: Chem.*, **50**, 293 (1990).

92. S. J. Rosenthal, X. Xie, M. Du, G. R. Fleming, *J. Chem. Phys.*, **95**, 4715 (1991).

93. M. Cho, S. J. Rosenthal, N. F. Scherer, L. D. Ziegler, G. R. Fleming, *J. Chem. Phys.*, **96**, 5033 (1992).

94. R. Jimenez, G. R. Fleming, P. V. Kumar, M. Maroncelli, *Nature*, **369**, 471 (1994).

95. P. V. Kumar, M. Maroncelli, *J.Chem.Phys.*, **103**, 3038 (1995).

96. J. Gardecki, M. L. Horng, A. Papazyan, M. Maroncelli, *J. Mol. Liq.*, **65/66**, 49 (1995).

97. M. L. Horng, J. A. Gardecki, A. Papazyan, M. Maroncelli, *J. Phys. Chem.*, **99**, 17311 (1995).

98. G. L. Closs, P. Piotriwiak, J. M. MacInnis, G. R. Fleming, *J. Am. Chem. Soc.*, **110**, 2652 (1988).

99. G. L. Closs, M. D. Johnson, J. R. Miller, P. Piotriwiak, *J. Am. Chem. Soc.*, **111**, 3751 (1989).

100. M. E. Sigman, G. L. Closs, *J. Phys. Chem.*, **95**, 5012 (1991).

101. P. Klán, P. J. Wagner, *J. Am. Chem. Soc.*, **120**, 2198 (1998).

102. K. Hisada, A. Tsuchida, S. Ito, M. Yamamoto, *J. Chem. Phys. B*, **102**, 2640 (1998).
103. D. R. McDowell, F. Wu, R. B. Weisman, *J. Chem. Phys.*, **108**, 9404 (1998).
104. I. Ohmine, *J. Chem. Phys.*, **85**, 3342 (1986).
105. P. J. Wagner, G. M. El-Taliawi, *J. Am. Chem. Soc.*, **114**, 8325 (1992).
106. F. D. Lewis, J. M. Wagner-Brennan, J. M. Denari, *J. Phys. Chem. A*, **102**, 519 (1998).
107. K. Hafner, C. Bernhard, *Ann.*, **625**, 108 (1959).
108. 日本化学会編　新実験化学法講座１４　有機化合物の合成と反応（II）P. 691　丸善 (1977).

Acknowledgements

I would like to thank Professor Noboru Hirota for his advice and encouragement. I am deeply grateful to my advisor, Professor Masahide Terazima. I'd like to thank Dr. Yoshifumi Kimura for fruitful discussions and his kind help of the transient absorption measurements and the experiments with the high pressure cell. I also thank those persons for their kind help of the organic synthesis. Namely, Professor Atsuhiro Osuka, Professor Toshi Nagata and Professor Hiroyuki Furuta. I would like to thank Mr. Fujitsugu Amita for his kind help of the metal working. I also thank Dr. Sigehiko Hayashi, Mr. Takeki Ishida and Dr. Hirofumi Sato for their kind help of the *ab initio* calculations. I wish to thank the Japan Society for the Promotion of Science. Finally, I am specially grateful to my parents.